REACTIVE COMPATIBILIZATION IN IMMISCIBLE POLYMER BLENDS

by

Nora Colleen Beck Tan

Dissertation submitted to the Faculty of the Graduate School
of The University of Maryland in partial fulfillment
of the requirements for the degree of
Doctor of Philosophy
1994

Advisory Committee:

Assistant Professor R. M. Briber, Advisor
Associate Professor D. I. Bigio
Assistant Professor I. Lloyd
Dr. D. G. Peiffer
Professor T. G. Smith
Professor M. Wuttig

REPORT DOCUMENTATION PAGE

Form Approved
OMB No. 0704-0188

1. AGENCY USE ONLY (Leave Blank)	2. REPORT DATE	3. REPORT TYPE AND DATES COVERED
	1994	Final

4. TITLE AND SUBTITLE
Reactive Compatibilization in Immiscible Polymer Blends

5. FUNDING NUMBERS

AFRL-SR-BL-TR-98-
0001

6. AUTHORS
Nora Colleen Beck Tan

7. PERFORMING ORGANIZATION NAME(S) AND ADDRESS(ES)
The University of Maryland

9. SPONSORING/MONITORING AGENCY NAME(S) AND ADDRESS(ES)
AFOSR/NI
110 Duncan Avenue, Room B-115
Bolling Air Force Base, DC 20332-8080

10. SPONSORING/MONITORING AGENCY REPORT NUMBER

11. SUPPLEMENTARY NOTES

12a. DISTRIBUTION AVAILABILITY STATEMENT
Approved for Public Release

12b. DISTRIBUTION CODE

13. ABSTRACT *(Maximum 200 words)*
See attached.

14. SUBJECT TERMS

15. NUMBER OF PAGES

16. PRICE CODE

17. SECURITY CLASSIFICATION OF REPORT	18. SECURITY CLASSIFICATION OF THIS PAGE	19. SECURITY CLASSIFICATION OF ABSTRACT	20. LIMITATION OF ABSTRACT
Unclassified	Unclassified	Unclassified	UL

Abstract

Title of Dissertation: Reactive Compatibilization in Immsicible Polymer Blends.

Nora Beck Tan, Doctor of Philosophy, 1994

Dissertation directed by: Dr. Robert M. Briber, Assistant Professor
Department of Materials & Nuclear Engineering

There has been considerable interest in recent years in the development of novel polymeric materials through blending rather than through development of new chemical structures. Blending may be chosen for several reasons, for example, tailoring properties to meet a specific need or simplifying recycling efforts by reducing separation procedures. Development of useful blends is challenged by the inherent immiscibility of most polymers with one another, which results in coarsely phase separated polymer mixtures in which the interphase interfaces are compositionally sharp and mechanically weak. Recent research efforts have concentrated on microstructural control through reactive compatibilization, a procedure in which functional groups are incorporated onto the polymer chains of the blend components and react during the processing to form copolymers that stabilize the dispersion. While some effort has been directed at understanding the relationship between reactivity and morphology, study of the effects of in-situ copolymer formation on the adhesion of interphase interfaces has been neglected. It is the purpose of this investigation to concentrate on both aspects of reactive compatibilization, morphology refinement and interphase adhesion. Two

reactive blend systems have been evaluated. In the polystyrene/nylon system, functionalization of blend components to levels of only ~1% has produced a 60% reduction in the size of the dispersed phase and a 100% improvement in interphase adhesion. The in-situ formation of copolymers has been confirmed and for the first time quantified through a combination of spectroscopy and microscopy. The results from the second system, sulfonated polystyrene/poly(2-vinyl pyridine), are even more impressive. Ionic interactions between sulfonate and pyridine groups generate interchain crosslinks in solution blends of these polymers, suppressing phase separation to a size scale of <0.01 μm. The interfacial adhesion, quantified using a measure of interfacial toughness, was improved dramatically by reactivity, from ~2 J/m^2 at the unreactive interface to > 150 J/m^2 at the optimum sulfonation. This striking enhancement of interphase adhesion has not been previously documented for reactively reinforced interfaces. This investigation has conclusively demonstrated the efficiency of reactive compatibilization at controlling the microstructure and reinforcing the interfaces in immiscible polymer blends.

REACTIVE COMPATIBILIZATION IN IMMISCIBLE POLYMER BLENDS

by

Nora Colleen Beck Tan

Dissertation submitted to the Faculty of the Graduate School
of The University of Maryland in partial fulfillment
of the requirements for the degree of
Doctor of Philosophy
1994

Advisory Committee:

Assistant Professor R. M. Briber, Advisor
Associate Professor D. I. Bigio
Assistant Professor I. Lloyd
Dr. D. G. Peiffer
Professor T. G. Smith
Professor M. Wuttig

Dedication

to my husband,

my love,

my life

Acknowledgment

I have been fortunate to have had the guidance of many people throughout my graduate studies, faculty, fellow students, friends and especially my husband and my family, and I am grateful to all of them for their advice and support over the past five years.

I am most indebted to my thesis advisor, Dr. Robert Briber, who is a kind and patient teacher and has opened the door for me to the field of polymer physics. I have learned from Professor Briber's example to always be open to new ideas and new alliances, and to make the most of all available resources--lessons which have helped me to become a better scientist, and which I believe will serve me well regardless of where the future may lead.

I would like to express my gratitude to the members of my thesis committee, not only for their efforts in reviewing this dissertation, but also because each of them has contributed to this work in some way, by offering advice from a unique perspective or through the sharing of their experience and technical expertise. I would also like to acknowledge Dr. D. G. Peiffer for providing materials, Dr. J. D. Barnes and Dr. B. J. Bauer for assistance with experiments, Prof. B. Pourdeyhimi, Prof. T. G. Smith and Dr. W. Chappas for sharing laboratory equipment, and Dr. Li-Ying Yang, Dr. Liqin Wang, and Mr. Shih-Kuan Tai for help with data acquisition and analysis.

Financial support for this work was provided by the National Defense Science and Engineering Graduate Fellowship Program.

Table of Contents

List of Tables

List of Figures

Chapter 1:
Introduction

Interest in the development of polymer blends stems from the economic and environmental advantages in producing improved polymeric materials through the blending of existing polymers, rather than through development of new synthetic polymers. Blending may be used to combine the attractive properties of two polymers and/or to improve the deficient properties of a given polymer. Imparting solvent resistance to an amorphous material through addition of a crystalline phase and improving the impact resistance of brittle materials through incorporation of a dispersion of rubber particles are examples of improvements which may be made through blending of polymers.

While some pairs of polymers exhibit complete miscibility over all ranges of temperature and blend composition, the majority of polymer pairs do not. Most polymer pairs are thermodynamically incompatible due to the small mixing entropy in mixtures of long chain molecules. Typical useful blends are usually mixtures of two (or more) immiscible or partially miscible polymers, and exhibit a microscopically inhomogeneous structure. The properties of immiscible blends are strongly dependent on the size and distribution of phases and the strength of the interphase interface(s). The development of many useful blends depends on the control of two important aspects of their structure. First, a stable dispersion of one polymer in the other must be realized, and second, the interface between the two polymeric components of the blend must be strong enough to support load transfer. The typical approach to managing this problem is to add block copolymer

'compatibilizers' to the mixture. This technique involves adding a block copolymer of the type A-B to a mixture of polymers A and B. The copolymers segregate to the A/B interfaces and act as an emulsifier thereby lowering the A/B interfacial tension, improving the resistance to particle coalescence, and stabilizing the dispersion. If the blocks of the A-B copolymers are sufficiently long then they can extend into the homopolymer phases and entangle causing mechanical linking which leads to a strong A/B interface. The drawbacks to traditional compatibilization are: 1) separate fabrication of A-B copolymers is required, which is prohibitively expensive in most cases, 2) it is difficult to properly disperse the block copolymers during processing so that they are positioned at the interfaces, and 3) the amount of compatibilizer which may be added is limited to low concentrations by the formation of copolymer micelles.

A novel approach to the modification of interfaces in incompatible blends which has been recently receiving much attention is reactive compatibilization, in which compatibilizers are formed in-situ at the interfaces. Homopolymer blend components which have reactive groups incorporated along the chains are utilized. Functional pendant or end groups are inherent to many types of polymers and may be added to others though relatively cost efficient processes such as small-molecule grafting, conversion of existing moieties or copolymerization. The functional groups come in contact during mixing of the two polymers and react, forming bonds between the homopolymers at the interfaces. Recent studies have concentrated on the control of blend morphology which may be achieved through this type of reactive compatibilization scheme. It has been demonstrated that the dispersion of the minor polymer blend component decreases in average size with increasing concentration of functional groups, and that a homogenous

material may be achieved at sufficiently high functional group concentrations. There has been no work published to date on the effects of in-situ compatibilizer formation on the strength of the interfaces between blend components. Interfacial properties are important for a variety of applications involving several materials in addition to blending, especially those in which polymer laminates are formed, such as in composites or electronic packaging.

The purpose of this research is to investigate the effects of reactive compatibilization in immiscible polymer blends, focusing on the interfacial property improvements and morphology issues. Two very different blend systems are studied. In the first, in-situ covalent bonding is employed to generate triblock compatibilizers in polystyrene/nylon blends via the reaction of pendant oxazoline groups on polystyrene chains and reactive nylon end groups. Though very low functional group concentrations are involved, significant refinement of the microstructure results. Interfaces are also strengthened substantially. In the second blend system, sulfonated polystyrene/poly(2-vinyl pyridine), graft copolymers are generated via ionic crosslinking between the basic nitrogen of the pyridine ring and sulfonic acid groups grafted to the polystyrene chains. The ionic interaction is found to be a highly effective compatibilizing mechanism, resulting in refinement of blend morphology to the extent that phase separation is suppressed even on size scales of ~0.01 μm. Interfacial property improvements are equally impressive. At sufficiently high acid concentration, interfacial fracture toughness may be improved by over two orders of magnitude. In addition, comparison with investigations of similar properties in block copolymer compatibilized systems indicate that reactive compatibilization may be considerably more efficient than the traditional compatibilization routes.

In the chapter that follows, the technical issues which are most relevant

to the study of morphology and interfacial properties of blends will be summarized and a survey of related literature presented. Experimental methods and materials are discussed in Chapter 3. The major findings of this research program are highlighted in Chapters 4 and 5, which address the behavior of reactive polystyrene/nylon and sulfonated polystyrene/poly(2-vinyl pyridine) blends, respectively. Conclusions are presented in Chapter 6, and finally, some suggestions for future study are given in Chapter 7 based on issues whose importance has surfaced as a result of this investigation.

Chapter 2:
Technical Background

The purpose of this chapter is twofold; 1) to introduce the concepts and definitions necessary for understanding of the chapters that follow, and 2) to briefly review the literature related to the problems addressed in the research program. In the first section the concept of miscibility in polymer systems is presented and is defined in terms of its thermodynamic origin. The fundamentals of compatibilization are also discussed, as well as their extension to reactive compatibilization which is the central focus of this study. In Section 2, the literature pertaining to compatibilization is summarized, with the discussion divided between morphology studies and model interfacial studies. Finally, the objectives and approach of the research program are clarified through the terms presented and their contribution to the current body of knowledge is discussed.

2.1 Definition of Concepts and Terms

2.1.1 Miscibility

At the center of any discussion of polymer blends is the idea of miscibility. Conceptually, miscibility in a polymer blend is the analog of solubility in a mixture of small molecules. Miscible polymer blends form a single, homogeneous phase upon mixing and have macroscopic properties typical of a single phase material [1,2,3]. Defining a blend of A and B homopolymers as miscible implies molecular mixing at the segmental level. In practice, complete miscibility is rare, and occurs only when the interaction between A and B monomer segments is attractive or only very weakly

repulsive. There are some situations where a given polymer pair forms homogeneous mixtures over a restricted range of composition and temperature (partial miscibility). In most cases, however, mixtures of polymers are immiscible, forming a two phase structure in which the interfaces are compositionally sharp and mechanically weak. Much of the study of polymer blends is concerned with understanding and controlling miscibility and phase separation.

The inherent immiscibility of most polymer pairs is thermodynamic in origin. The free energy of mixing can be represented according to the basic thermodynamic equation:

$$\Delta G_{mix} = \Delta H_{mix} - T\Delta S_{mix} \qquad (2\text{-}1)$$

where ΔG_{mix} represents the Gibbs free energy of mixing, ΔH_{mix} the enthalpy of mixing and ΔS_{mix} the entropy of mixing. The conditions of miscibility are:

$$\Delta G_{mix} < 0$$
$$\text{and} \qquad (2\text{-}2)$$
$$\left(\frac{\partial^2 \Delta G_{mix}}{\partial \varphi_i^2}\right)_{T,P} > 0$$

where ϕ_i is the volume fraction of component i in the mixture. The expression for ΔG_{mix} in mixtures of macromolecules was first derived by Flory and Huggins, who used a lattice model to derive the energy expression in terms of the volume fractions of the components, ϕ_i, and their respective degrees of polymerization, N_i [4]:

$$\frac{\Delta G_{mix}}{kT} = \chi_{AB}\phi_A\phi_B + \frac{\phi_A}{N_A}\ln\phi_A + \frac{\phi_B}{N_B}\ln\phi_B \qquad (2\text{-}3)$$

where χ_{AB} is the interaction parameter or the Flory interaction parameter and is related to intermolecular interactions. The first terms in Eq. (2-3) is enthalpic, and may take either positive or negative values. The last two terms represent the entropy of mixing, derived by assuming the entropy to be combinatorial in origin. The entropic contribution is always negative and therefore favors mixing. The entropic terms, however, being proportional to $(N_i)^{-1}$, are always small for mixtures of long chain molecules where N is typically on the order of 10^3-10^5, thus the immiscibility which is commonly observed is mainly a result of the small mixing entropy. Miscibility, therefore, is largely controlled by the interaction parameter, and only achieved when χ_{AB} is very small or negative. The interaction parameter is known to be a function of temperature according to the relation:

$$\chi_{ij} = C_1 \pm \frac{C_2}{T} \qquad (2\text{-}4)$$

where C_i are positive constants [1,3]. The temperature and composition dependence of the interaction parameter are responsible for partial miscibility in some systems.

While the thermodynamic origin of miscibility is clear, an acceptable experimental definition for miscibility is more elusive. First approximation tests for miscibility are often simple, such as transparency versus turbidity in cast films of blends. The existence of two separate glass transition temperatures is a commonly used and unambiguous verification of phase separation and immiscibility in a polymer mixture. The reverse is not

necessarily true, however, as this measurement does not probe the structure on a very fine scale. Experimental verification of miscibility often requires probing the structure on progressively finer scales, such as those accessible by electron microscopy, small angle scattering, and spectroscopic methods.

2.1.2 Compatibilization

Compatibility has often been used as a synonym for miscibility. For the present purposes the term compatibility will be reserved for immiscible blends which have been stabilized with respect to morphological changes by some alteration of the blend components and/or the addition of interfacial agents. Another useful definition was given by Gaylord when he defined operational compatibility as "the absence of separation or stratification of the components of the polymeric alloy during the expected useful lifetime of the product" [5]. The process by which compatibility is brought about will be called compatibilization.

Traditionally, compatibilization has been achieved through the addition of a block copolymer acting as an interfacial agent. For example, an A-B diblock copolymer may be added to a blend of homopolymers A and B (Figure 2.1). Copolymers position themselves at the interfaces and serve to reduce the interfacial tension, creating a stable emulsion, and under certain circumstances may also increase the interfacial strength. There are many variations on this theme, such as using triblocks instead of diblocks, or A-C copolymers where C is miscible with B, but the mechanism of compatibilization remains the same.

2.1.2.1 Stabilization of the Microstructure

The issue of morphology refinement due to compatibilization is

generally quantified by measures of phase size in the final microstructure. Polymers are commonly blended in ratios of about 10:90-30:70 by weight, which leads to a microstructure in which the minor component is dispersed in a matrix of the major component. The final size of dispersed second phase regions is controlled by many factors. Those most commonly cited include interfacial tension, melt viscosity and the viscosity ratio of the two components, melt elasticity, processing history, thermal treatment and blend composition [6-10]. Compatibilization has been associated with the dependence of second phase dimension on interfacial tension.

There are a number of theories for predicting size of dispersed phases in fluid mixtures. The origins of this field, and the basis for most theoretical analyses, are traced back to the Taylor theory of droplet breakup in Newtonian fluids [11]. Taylor's classic work predicts:

$$d = \frac{\gamma_{AB}}{G\eta_m}\left(\frac{16\lambda + 16}{19\lambda + 16}\right) \qquad (2\text{-}5)$$

where d is the droplet diameter, γ_{AB} is the interfacial tension between phases A and B, G is the shear rate of deformation, η_m is the matrix viscosity, and λ is the ratio of the dispersed phase viscosity to the matrix phase viscosity, η_d/η_m. Modifications to this theory do not, in general, alter the direct dependence of the droplet diameter on the interfacial tension [6,9].

The interfacial tension in an immiscible polymer blend is determined by the monomer-monomer segment interactions and is therefore related to the Flory interaction parameter. The dependence has been developed by Helfand and Tagami [12] and Helfand and Sapse [13], in which a random walk statistics are assumed for the polymer chain, and a modified diffusion

equation is employed to describe a mobile monomer unit as being under the influence of a mean field created by surrounding chains. The result is the prediction that interfacial tension is directly related to the interaction parameter according to the relation:

$$\gamma_{AB} = \left(\chi_{AB}/6\right)^{1/2} \rho bkT \qquad (2\text{-}6)$$

where ρ is the monomer number density, b is a statistical segment length, k is the Boltzman constant and T is absolute temperature. Though there have been some modifications to the theory, the physics behind this result are generally believed to be correct and the equation gives reasonable agreement with experiment [14]. Compatibilization of an A/B interface involves a reduction in interfacial tension caused by the preferential segregation A-B copolymers to this region. The segregation is driven by enthalpic effects; copolymers arrange themselves such that the A segments extend into the A phase and the B segments extend into the B phase, thus minimizing the total number of A/B contacts in the system. The resulting geometry at the interface is that of a thin film where the A-B junctions are located and there is some mixing of A and B segments, from which A and B 'brushes' extend (Figure 2.1). This effect has been quantified by Liebler [15] in a seminal paper. The reduction of interfacial tension is found to vary as a function of the number of chains per unit interfacial area and the degree of polymerization of both homopolymer chains and copolymer chains. Liebler's analysis predicts that the interfacial tension decreases as the number of chains across the interface increases, and for a given interfacial chain density, copolymer molecules which are long relative to the homopolymers are more efficient at reducing

the interfacial energy than smaller molecules. Liebler's study also shows that the amount of copolymer which is available for interfacial absorption is ultimately limited by the formation of copolymer micelles in the bulk. The degree of compatibilization achieved is therefore limited by the critical micelle concentration which occurs at a concentration determined by the Flory interaction parameter and the copolymer composition and molecular weight. Short copolymers may be present in higher concentration and may be easier to disperse through conventional processing, but they are less efficient interfacial agents and, as will be discussed in the next section, are less efficient as strengthening agents.

There is a second microstructural stabilization effect of compatibilization which has received less attention but is certainly noteworthy. It has been experimentally observed that compatibilization is more effective in producing a refined morphology in concentrated systems than in dilute systems, i.e. when the fraction of dispersed phase in the mixture is high [10,16,17]. A mechanism to account for this behavior will be proposed in Chapter 4.

2.1.2.2 Interphase Adhesion

One of the major reasons for compatibilizing blends is to improve the mechanical properties. Compatibilized blends may demonstrate superior mechanical properties relative to their uncompatibilized counterparts, with particularly strong improvement of elongation and impact properties in rubber toughened blends [18,19]. These improvements may be the result of morphology refinement and/or may be related to the enhanced strength of compatibilized interphase interfaces [20,21]. It is important to note that

morphology improvements do not always result in mechanical property improvements. For example, impact strength is often optimized in a given system at a particular particle size, therefore any compatibilization scheme which resulted in refinement of particle size below this optimum would decrease the impact strength.

The effects of compatibilization on interfacial adhesive properties have recently been clarified through model studies of interfacial toughness. The strengthening properties of copolymers at interfaces arise from their contribution to the energy of failure. The failure mechanisms are dependent on the molecular weight of the blocks in the copolymer relative to the entanglement molecular weight of the component polymers, the monomer/monomer friction coefficients, and the areal density of copolymer chains at the interface [22-28]. For low molecular weight blocks, interfacial copolymer chains pull out of the homopolymer during failure, contributing a relatively small work of pull out to the failure and slightly increased toughness. For copolymer chains which are long with respect to the entanglement molecular weight of the homopolymers, the copolymers are efficiently entangled with the bulk material, and a bond must be broken during interfacial failure. The energy required to break these bonds contributes to the failure energy and results in modest increases in interfacial toughness. Substantial contributions to interfacial adhesion are made with the combination of long copolymer blocks and high interfacial areal density of copolymers. When the interfaces between glassy materials are compatibilized under these conditions, the stress contribution on the interface from the high density of breaking bonds may exceed the bulk crazing stress in one of the homopolymers, resulting in the formation of stable crazes, a process which absorbs a large amount of energy during the failure process and may result in

improvements in interfacial toughness of up to two orders of magnitude. Toughening of compatibilized interfaces is a central focus of this work and will be discussed more fully in Section 2.2.2.

2.1.3 Reactive Compatibilization

Reactive compatibilization refers to a process whereby blends are compatibilized via the *in-situ* generation of copolymers in solution or in the melt. Copolymers are formed when complementary functional groups on each of the blend components meet and interact during the blending process. Interactions may take the form of covalent, ionic or hydrogen bonds. Functional groups occur in many varieties, for example, as part of the monomer structure, such as the carboxylic acid of acrylics; as end groups, such as amine end groups in nylons; or they may be added in small concentration to the homopolymer chains by random copolymerization, conversion of existing moieties, or grafting. The architecture of the copolymer formed may be varied by changing the position of the functional groups, i.e. end-group/end-group reactions create block copolymers, end-group/main chain reactions result in single graft architecture, and main-chain/main-chain interactions lead to star or crosslinked configurations. The wide availability of functionality leads to great versatility of the reactive processing technique as evidenced by its use in blends of many types of commercial polymers, including polyamide/polyolefin blends, rubber/glassy polymer blends, and polyester mixtures. Potential reactions, functionalities and blend systems previously studied are reviewed in references 29-32.

The mechanisms of morphology stabilization and interfacial toughening in reactive systems should be the same as those discussed above for blends which have been compatibilized by the more traditional method of

block copolymer addition. The same theoretical and mechanistic arguments apply, though some redefinition of the junction density may be necessary for copolymer architectures which are more complex than diblocks.

Reactive compatibilization has many advantages over traditional compatibilization, in terms of efficiency, versatility, and cost. First, reactive compatibilization may be more efficient than traditional compatibilization due to the *in-situ* nature of the process. Copolymers are formed at the interfaces during the blending process, therefore there are no difficulties associated with dispersing pre-formed copolymers. This issue may be especially important to compatibilization using long copolymers or copolymers of complicated architecture for which diffusion may be difficult. Traditional compatibilization is often limited by the availability of suitable block copolymers, while the reactive process may be applied to any pair of polymers in which functional groups are present and/or may be incorporated onto the blend components. As stated above, functional groups may be incorporated by random copolymerization or grafting, processes which are much more cost-effective than synthesis of specialty block copolymers. Thus, within the limitations imposed by the necessity of functionalizing blend components, reactive processing is clearly a superior alternative to traditional compatibilization.

2.2 Literature Survey

The focus of this section will be divided between two areas, which exhibit only a small amount of overlap. The first part of this section is concerned with reviewing some recent literature in the area of reactive compatibilization which is highly biased towards studies of morphology. General research findings will be summarized along with some detailed

discussion of specific studies which exhibit similarity to the systems studied in this work. In the second section, the issue of improvements in interfacial adhesion as a result of compatibilizer addition will be addressed. Most of the work in this area has utilized model studies to simulate the effects of traditional compatibilization on the interfacial adhesion in immiscible blends. A few studies will also be summarized in which an attempt has been made to simultaneously address the issues of morphology refinement and interfacial properties in melt blends.

2.2.1 Morphology Control via Reactive Compatibilization

Reactive blending has been a subject of much interest over the last 10 years, and the published literature in the area is too vast to summarize. However, previous work has identified several trends concerning parameters which are important to reactive blending. It has been clearly established, in a variety of blend systems, that the microstructure of reactive blends is refined relative to their unreactive counterparts. (See references 16,17 and 33-39 for examples.) This implies reduction of interfacial tension and/or stabilization to coalescence in reactive blends relative to their unreactive counterparts, suggesting the successful reaction/interaction of functional groups. In many cases it has been possible to confirm the formation of copolymers directly, through spectroscopy [34,39-44] or by changes in melt viscosity due to copolymer formation, which may manifest itself during the blending process as a torque increase [35,37,46,47]. Studies focusing on concentration effects have shown that the efficiency of compatibilization is dependent on the concentration of reactive groups; [40,41,37,38] blends become more intimately mixed as the concentration of reactive groups increases. In one notable example, mixing reached a molecular level in PS/poly(methyl methacrylate)

(PMMA) blends when sufficient levels of complementary ionic functionality were introduced via copolymerization into PS and PMMA components[43]. A recent investigation by Song and Baker [42] has addressed the issue of the effect of altering the nature of the reactive group for a given polymer pair while holding other parameters constant. Compatibilization was investigated in PS/PE blends where the PS was functionalized with 6% maleic anhydride, and the PE had a grafted basic functionality of either a tertiary amine or a secondary amine. Both functionalized blends showed refined microstructure and modest mechanical property improvements relative to the unfunctionalized counterpart; however, the blend containing the secondary amine clearly produced more significant morphology refinement than the blend compatibilized using the tertiary amine. Thus, important parameters which must be considered in designing a reaction scheme for blend functionalization include the nature and concentration of functional groups. While the utility of reactive compatibilization methods has been clearly demonstrated, their optimization is still under investigation.

2.2.1.1 Studies in the Compatibilization of Polystyrene/Nylon Blends

Having addressed concerns which are general to reactive blending above, attention will now be focused on studies which are as closely related as possible to the present study. The subject of Chapter 4 is the reactive compatibilization of amorphous nylon/polystyrene (aPA/PS) melt blends, in which the PS has been functionalized by copolymerization with vinyl oxazoline which is co-reactive with nylon end groups. There have been three studies reported to date on the behavior of reactive aPA/PS blends. The first and second are concerned with morphology development in reactive versus unreactive aPA/PS blends [47,48]. In the work of Sundararaj, et. al. the

amorphous nylon component has amine end groups which may react with maleic anhydride (MAn), copolymerized with the styrene. Blending produced a microstructure with dispersed droplets of average size 1.85 μm in the unreactive 80% PS/20% aPA blends, as compared to 0.22 μm in the reactive 80% PS-17MAn/20% aPA blend, a reduction of 8-9 times. Additional measurements indicated a significant reduction in interfacial tension in the reactive blend (~4.5 mN/m) relative to its unreactive counterpart (18 mN/m). Sullivan and Weiss were also able to show significant compatibilization in aPA/PS blends [49]. In this study, ionic interactions between the amide groups of the aPA and sulfonic acid groups copolymerized with polystyrene resulted in particle size reductions of more than two orders of magnitude. In addition, the authors claimed to have crossed the miscibility limit in this system by creating a sufficiently high ratio of amide to acid groups by varying blend composition. The third study of compatibilization in aPA/PS blends focused on the effects of reactivity on interfacial width [49]. Using ellipsometry, the authors showed considerable broadening in the aPA/PS-MAn interface as a function of MAn content, from approximately 13 nm at 8% MAn functionality, to approximately 30 nm at 14% functionality. The thickness of the unreactive interface was not measured, but it is estimated to be less than 5 nm. Since the interfacial width is known to be inversely proportional to the interfacial tension,[12-14] the observed broadening clearly implies successful reduction in the aPA/PS interfacial tension due to functional group interaction, and the direct dependence of this effect on functional group concentration. Thus, results of these studies have demonstrated the feasibility of compatibilizing aPA/PS blends, though there remains room for more careful study of the effects of *in-situ* copolymer formation in this system.

A few related studies have shown effective compatibilization in blends which are similar to aPA/PS, such as PS/Nylon-6,6 [50] and acrylonitrile-co-styrene(SAN)/Nylon-6 [35,40]. In the former case, morphology refinement due to the interaction between the polyamide and MAn copolymerized with PS was demonstrated. In the latter case, morphology refinements and modest improvements in impact strength resulted from copolymerization of PS with MAn, and improved with increasing MAn concentration. This study must be viewed with some caution since the effect of copolymer formation cannot be unambiguously extracted from these results due to the changes in S/AN ratio in the SAN phase due to the addition of PS-MAn. A study by Triacca, et. al. [35] is significant because it represents the only attempt noted in the open literature to use the reaction between oxazoline and nylon end groups for *in-situ* copolymer formation. Unfortunately, the use of this reaction was not a central issue of that study, and a valid comparison between oxazoline functionalized materials and unreactive materials cannot be made from the data available.

The oxazoline functionality which has been used successfully in reactive blending, is reported to be highly reactive, capable of forming covalent bonds with a variety of moieties, such as amines, epoxy, anhydride, hydroxyl and carboxylic acid groups [30]. The reactions of interest in polystyrene-*co*-vinyl oxazoline (PS-ox)/aPA blends are between the oxazoline ring and either the amine or carboxylic acid end groups common to polyamides produced by condensation polymerization. Reactive compatibilization via oxazoline/ carboxylic acid grafting has been studied in a variety of systems including PS/PE, [36,45-46] acrylonitrile-butadiene(NB)/PS,[37] and NB/polypropylene (PP) [51]. These studies have conclusively demonstrated that the co-reactive pair of oxazoline and

carboxylic acid is effective in generating compatibilizing copolymers, even at very low oxazoline contents (<1%).

2.2.1.2 Compatibilization via Ionic Bonding

The development of morphology and control of interfacial toughness in ionically compatibilized polystyrene-co-styrene sulfonic acid/poly(2-vinyl pyridine) (sPS/P2VP) blends is the subject of Chapter 5. In this section some issues specific to ionomer blends will be noted, and some examples from the literature in which compatibilization route closely resembles the approach employed in the present study will be discussed.

Ionomers, as a class of polymers, tend to be difficult to melt process as functionality increases due to interchain ionic interactions [52]. For this reason, polymers with ionic functionality are often solution blended. Solution blending involves dissolving blend components separately in a common solvent, followed by mixing of the solutions. Ionic interactions tend to occur easily in solution without the need for thermal activation. The net result is blending on a much finer scale than may be achieved during conventional blending operations requiring melting of component polymers and dispersive mixing in the melt. This fine scale of mixing therefore must be probed using high spatial resolution experimental techniques, otherwise the blends may be falsely assumed to be miscible [39]. It is possible to achieve miscibility through ionic interactions; a condition which has been achieved in blends of various nylons with neutralized sulfonated polystyrene of sufficiently high functionality, and occurs as the result of several types of ionic interaction, including hydrogen bonding, complexation and ion-dipole interactions [48,53-56].

Much of the work on ionically interacting blends has focused on blends

in which an acid has been neutralized through interaction with a metal cation, and the interchain interaction occurs through this complex. Metal-sulfonate salts are a common functionality and have been used successfully in conjunction with basic functionality to compatibilize various blends including PS/nylon, [48,55] ethylene-propylene-diene elastomer (EPDM)/PS, [57] polybutadiene(PB)/PS, [58] and poly(ethyl acrylate) (PEA)/PS [59]. Effective compatibilization in these blends has been found to be dependent on the type of metal cation used.

In the context of this investigation, it is the acid/base reaction between un-neutralized ionomers which is of primary interest, in particular the generation of interchain crosslinks via interaction between sulfonic acid and pyridine functionalities in PS/P2VP blends. There is evidence from previous investigations that this co-reactive pair is highly successful at compatibilization. For example, direct evidence of morphology refinement was documented in PS/PEA blends in which the PS and PEA components had been copolymerized with low concentrations ($\leq$ 10%) of styrene sulfonic acid and 4-vinyl pyridine, respectively [39]. A spectroscopic study of this system confirmed the formation of sulfonate anions and pyridinium cations. The interaction between these ions accounts for the enhanced mixing [44]. An interesting study provided evidence for copolymer formation through the action of sulfonic acid and amine endgroups on PS and polyisoprene (PI) blend components, respectively, by confirming the occurrence of phase-separation phenomena characteristic of diblock copolymers in this system [60]. Indirect evidence for the formation of ionically crosslinked copolymers in sulfonic acid/4-vinyl pyridine functionalized systems is provided by the documentation of gel formation during solution blending, a phenomena which was observed in the PS/PEA blends mentioned above as well as in

PS/PMMA [43] and PS/PI [61] blends. The behavior of the 4-vinyl pyridine functionality is expected to be similar to, and potentially more efficient than, the 2-vinyl pyridine functionality employed in this study [62,63]. The investigation summarized in this treatise represents the only current attempt to use one fully functional ionomer (P2VP) with a co-reactive ionomer of varying functional group concentration. The previously work summarized above provides ample evidence on which to base the supposition that the reaction between sulfonic acid and 2-vinyl pyridine will effectively compatibilize sPS/P2VP blends.

2.2.2 Improvements in Interfacial Adhesion due to Compatibilization

There has been some difficulty in isolating the nature of compatibilization effects on interfacial properties due to the fact that the mechanical properties of blends tend to be dependent on the size and distribution of dispersed phases as well as the interfacial adhesion between them. It is therefore necessary to remove the morphology variable in order to adequately assess the interfacial effects. Two approaches have been taken to this problem. The first, addressed in section 2.2.2.1, uses processing variations to achieve reactive and unreactive blends with similar particle size ranges. In the second approach, which has been more extensively employed, the properties of interphase interfaces in blends are modeled by the properties of synthetic interfaces in laminates constructed from component polymers (Section 2.2.2.2). Each of these approaches has shown that interfacial adhesion is a significant factor in effective compatibilization.

2.2.2.1 Interphase Adhesion in Polymer Blends

The first suggestion of interfacial control of blend mechanical

properties was made by Angola, et. al. [40] They used PS-MAn to reactively compatibilize nylon-6/SAN blends, and found that while the size of the dispersed phase became constant (after an initial decrease) at sufficiently high MAn concentration, the impact properties of the blend continued to improve in this range. Since the increasing impact property could not be explained by particle size effects, the authors suggested that interfacial adhesive properties were controlling this particular phenomena. This effect has been the subject of several careful studies by W. E. Baker and co-workers, [21,51,64] who have developed a method to control morphology by processing, independent of reactivity, and have therefore been able to compare the properties of unreactive and reactive blends in the same range of dispersed phase size. Investigations have been made of PS/NBR blends and PP/NBR blends, both of which have been reactively compatibilized by grafting between oxazoline (PP, PS) and carboxylic acid (NBR). In each case, the impact properties of reactive blends were clearly superior to those of the corresponding unreactive blends when compared at constant rubber particle size. This is incontrovertible evidence for the important role of interfacial adhesion in successful reactive compatibilization.

2.2.2.2 Model Studies of Adhesion in Compatibilized Blend Interfaces

A series of recent investigations have resulted in the gain of tremendous insight into the mechanisms controlling the adhesion between immiscible polymers through interfacial modification via copolymer addition [23,25,65-71]. These studies have consistently shown that large improvements in interfacial adhesion result directly from copolymer addition. In this review the focus will be on the interfaces between immiscible, glassy polymers. The experimental work on these systems has largely been based on testing of

interfacial fracture toughness using an asymmetric double cantilever beam (ADCB) test [72]. The procedure consists of preparing laminates of immiscible polymers A and B, and then physically separating the layers in a slow and controlled manner. The toughness may be calculated from known values of material constants and from measurement of the crack growth. (See Section 3.3.2 for details.) The immiscible A/B interface is modified by coating one of the homopolymer layers with a film of A-B copolymer prior to joining the A and B layers together. The copolymer organizes itself during the joining process such that the A blocks extend into polymer A and the B blocks extend into polymer B, thus simulating the physical situation at a compatibilized interface. Experimental investigations into the interfacial properties of PS/P2VP, poly(phenylene oxide) (PPO)/PMMA and PS/PMMA systems have all demonstrated an increase of two orders-of-magnitude in interfacial fracture toughness due to copolymer addition [25,66,67]. This large toughness increase was found to be the result of a change in failure mechanism.

2.2.2.2.1 Theory of Interfacial Toughening

The pioneering work of Brown, et. al. [72-75] and the careful study by Creton, et. al. [25] were instrumental in defining many of the parameters which control the adhesion of compatibilized interfaces. The two most important parameters controlling interfacial adhesion were found to be the density of copolymer junctions at the interface, which is a measure of concentration, and the molecular weight of the reinforcing blocks. Several failure regimes have been identified. Modest improvements in toughness are achieved when block copolymers are short compared to the entanglement molecular weight of the homopolymers. In this regime, the pull-out regime, the shorter of the copolymer blocks is pulled out from its parent

homopolymer layer and contributes this pull-out work to the energy of failure. The controlling failure mechanism in this regime resembles the behavior of modified interfaces between rubbery materials, which is also a subject of current interest [26-28, 70, 71, 75]. Similarly modest toughness improvements result in the scission regime, which occurs when the copolymer blocks are long in comparison to the entanglement molecular weight, but present in low concentration at the interface. Failure occurs by scission of the copolymer chains at or very near to the bond between the A and B blocks. The most impressive toughness increases are achieved in the crazing regime which is invoked with the combination of high areal chain density of copolymers (junction concentration) at the interface and reinforcing blocks with length greater than or equal to the entanglement length.

The conditions which specify the controlling failure regime have been predicted by Xu, et. al. and are summarized in the "Failure Mechanism Map" [23-25, 76] which is reproduced in Figure 2.2. This approach predicts which failure mechanism will dominate based on the stress generated on the interface and the areal density of copolymer chains, Σ. The crazing stress is a material constant, independent of Σ, and represents an upper limit for stress. The areal chain density has a limit at $\Sigma=\Sigma_{sat}$, which is a concentration above which any further addition of compatibilizing copolymers results in the formation of other phases, such as copolymer micelles or lamellae, which do not contribute to interfacial strengthening.

The stress for chain scission and the stress for chain pullout each increase from zero linearly with Σ, so only one of these mechanisms may operate at a time. The stress generated on the interface by the chain scission is given by:

$$\sigma_{scission} = f_b \Sigma \qquad (2\text{-}7)$$

where f_b is the force to break the A-B copolymer bond. If the pull-out mechanism is operating, the stress on the interface will be generated by the frictional forces between the copolymer block which is being pulled out and the surrounding bulk homopolymer chains. This stress is given by:

$$\sigma_{pull-out} = f_{fric} N \Sigma \qquad (2\text{-}8)$$

where f_{fric} is a monomer friction coefficient. It is the dependence of $\sigma_{pull-out}$ on N, the degree of polymerization of the block which is being pulled out, that determines which effective force per junction is lesser (f_b or $f_{fric}N$) and thus which mechanism operates. When N is large (relative to the entanglement molecular weight, N_e) the effective force per junction for pull-out is larger than the effective force for scission and chain scission dominates. The interface will fail cleanly by the breaking of copolymer junctions until Σ becomes large enough ($\Sigma=\Sigma_c$) so that the stress on the interface exceeds the crazing stress and the failure mechanism changes to crazing. When N is small, $N<<N_e$, the force per junction for pull-out is less than the force per junction for scission, and the interface will fail by chain pull-out. For these very short blocks Σ reaches Σ_{sat} before sufficient stress is generated to induce crazing, ($f_{fric}N\Sigma_{sat} < \sigma_{craze}$) and the crazing mechanism will not be activated. In the intermediate range, when $N \approx N_e$, it is possible for failure to proceed by chain pull-out at low Σ, followed by a transition to crazing once $\sigma_{pull-out}$ becomes greater than σ_{craze} at an areal chain density designated by $\Sigma=\Sigma_c^*$. This behavior is of course limited by the restriction $f_b > f_{fric}N$, so that pull-out is the favored failure mechanism. The failure regimes and their limitations are

summarized schematically in Figure 2.3. The different failure regimes may be identified experimentally through the scaling behavior of the interfacial fracture toughness with the degree of polymerization of the copolymer blocks, N, and with the areal density of copolymer chains, Σ. The measure of interfacial fracture toughness which has been utilized in most of the theoretical and experimental work is G_c, the critical energy release rate. For slow crack growth in the pull-out regime, Xu, et. al. have predicted that G_c will scale directly with the areal chain density of copolymer junctions at the interface, and also with the square of the degree of polymerization of the block which is pulled out:[25]

$$\text{pull-out:} \qquad G_c \propto N^2\Sigma \tag{2-9}$$

If crazing is the operative mechanism, G_c should exhibit a different scaling behavior. Failure by craze breakdown has recently been analyzed by Brown [22,77] using a new model in which craze breakdown is facilitated by stress transfer between load-bearing craze fibrils via cross-tie fibrils. Brown's analysis predicts the following scaling relation:

$$\text{crazing:} \qquad G_c \propto \Lambda f_s^2 \Sigma^2 \tag{2-10}$$

where f_s is defined as the force to break a polymer chain, and is related to the bond strength, f_b, and Λ is a function of the properties of the craze:

$$\Lambda = \frac{2\pi D}{\sigma_{craze}} \left(\frac{E_2}{E_1}\right)^{1/2} \left(1 - \frac{1}{\lambda}\right) \tag{2-11}$$

where E_1 and E_2 are the elastic tensile moduli of the craze material normal and parallel to the fibril direction, D is the fibril diameter, and λ is the craze extension ratio.

2.2.2.2.2 Experimental Studies of Interfacial Toughening

The different scaling behaviors outlined by Eqs. (2-9) and (2-10) lend themselves readily to experimental verification. In addition, chemical analysis of fracture surfaces can provide evidence to distinguish between failure by chain pull-out and chain scission, while microscopy may be used to verify failure by crazing. This combination of toughness measurements plus surface analysis has been used to investigate each region of the Failure Mechanism Map, and to verify relation (2-10) for craze breakdown. In the earliest work reported by Brown and Cho et. al., the strengthening of PS/PMMA through the addition of PS/PMMA diblock copolymers was investigated [72-74]. These early studies verified the dependence of interfacial adhesion on the interfacial copolymer concentration as well as making the association between a large increase in interfacial toughness and failure by crazing.

An extensive study by Creton, et. al. [25] focused on interfacial toughening of the PS/P2VP system by PS-co-P2VP block copolymers. The failure mechanism and adhesion improvement were studied over a range of block copolymer molecular weights (N) and interfacial copolymer concentrations (Σ). A combination of pyridine staining and deuteration of the PS blocks was employed to allow for detection of the position of the diblocks after fracture. At low N_{PVP}, G_c increased linearly with Σ, and x-ray methods detected the presence of nearly all of the P2VP on the PS side of the fracture

surface, confirming failure by chain pull-out. In this regime, toughness of compatibilized interfaces reached a maximum of about 6 J/m^2 with fully saturated interfaces,($\Sigma \sim 0.10\text{-}0.15$) as opposed to < 2 J/m^2 for the uncompatibilized interface. When interfaces were reinforced with low concentrations ($\Sigma \leq 0.03$) of block copolymers having $N_{PVP} > N_{e,PVP}$ and $N_{PS} > N_{e,PS}$, both the PS and the P2VP were found on the side of the fracture surface corresponding to their respective homopolymer counterparts, indicating that failure occurred by chain scission in the immediate vicinity of the PS-P2VP copolymer junction. Toughness increases were of the same order of magnitude as those for pull-out in the long copolymer, low concentration, regime. For these same copolymers, the transition from scission to crazing was confirmed by fractography and by interfacial fracture studies as the interfacial concentration of block copolymer increases. The toughness increases were extremely large in the crazing regime, for example, with $N_{PVP} \sim 3.5N_{e,PVP}$, $N_{PS} \sim 4.6N_{e,PS}$ and $\Sigma \sim 0.10$, G_c reached 120 J/m^2, an increase of over 60 times relative to the immiscible interface. In this high concentration, high N_i regime, G_c was found to scale with Σ^2, as predicted.

In addition to the high and low N extremes, there have been studies on the PS/P2VP system which have focused on the intermediate N regime. The transition from pull-out to crazing is expected to occur in this range of N [23,76]. In the first of these investigations,[76] the transition from pull-out to crazing was verified experimentally, through a combination of interfacial fracture testing, spectroscopy and microscopy. The transition is clearly evident from the G_c versus Σ plots, where a discontinuous jump from ~6 J/m^2 to ~15 J/m^2 was observed. Careful measurements of the saturation concentration, coupled with parameters from previous studies allowed for

estimation of the monomer friction coefficient, f_{fric}~ $6.3x10^{-12}$N/monomer. The bound for the minimum P2VP block molecular weight necessary to achieve the crazing stress before reaching Σ_{sat} was also estimated at N_{PVP}~80. In the second study, [23] the upper limit on N_{PVP} for failure by pull-out was experimentally demonstrated to be approximately equal to $N_{e,PVP}$. The previous study had predicted a higher upper bound, but had neglected to account for the increase in f_{fric} resulting from increasing N above N_e.

The experimental work has identified supplementary information about the interfacial failure process in the crazing regime in addition to verifying the predicted failure behavior. In particular, the importance of diblock molecular weight under N >> N_e conditions and of structural organization of interfacial copolymers have been elucidated. The maximum achievable toughness in the crazing regime was found to be a function of diblock molecular weight. In the PS/P2VP system, the maximum toughness reached at saturation (G_c^{max}) increases as the block molecular weight increases. This is a very strong effect in the PS/P2VP system, with G_c^{max}~18 J/m^2 for N/N_e^{min}~1, and G_c^{max}~120 J/m^2 for N/N_e^{min}~3.4 [25]. This relation was explored by Char, et. al. over a broader range of molecular weights, up to N/N_e^{min}~7.5, and found that the saturation toughness increases with molecular weight up to a point, reaches a maximum, and then decreases. This decrease is significant in magnitude, for example in the PS/PPO system, G_c^{max}~400 J/m^2 at the optimum molecular weight, but drops to about 50 J/m^2 at the highest diblock molecular weight studied [67].

A second optimization effect has also been identified in the crazing regime. Experimental studies by Brown's group [65-67] and by Creton, et. al. [23] have demonstrated the importance of considering copolymer structure.

For interfaces reinforced with very long block copolymers, the interfacial toughness has been shown to reach a plateau or even decrease slightly once the interface becomes saturated with copolymer ($\Sigma=\Sigma_{sat}$). This result implies that once saturation is achieved, the proportionality between the toughness and the square of the areal chain density is lost. It was suggested that this limit physically represents the interfacial concentration above which no further entanglements may be formed with bulk homopolymer chains. Therefore, as the areal density of chains increases, a point is reached where any new chains being added are more likely to be entangled with another chain in the brush than with a chain in the bulk, a situation which will not result in any additional strengthening. Creton, et. al. showed that by correcting the areal density to represent only the density of chains with at least one effective entanglement, the scaling relationship between G_c and Σ could be preserved. An additional effect of over saturation at the interface has been defined by Brown's group. Through this work [65-67] it has become apparent that for certain compatibilized, immiscible interfaces, G_c will increase with Σ, reach a maximum and then decrease significantly (~75%) upon further increases in interfacial copolymer concentration. This effect has been attributed to the formation of organized copolymer structures at the interface based on the results of chemical analysis of fracture surfaces, and the toughness loss associated with the transition from failure by crazing at the reinforced interface to failure by crazing in a copolymer lamellae. Entanglement in copolymer lamellae is less efficient than entanglement of a single layer brush with the bulk, therefore the switch to lamellae failure from bulk failure results in decreased toughening [65]. Thus, the effects mentioned above highlight the need to account for the physical properties of the brush

when studying interfacial toughening via compatibilizer addition.

The combined results of experiment and theory of interfacial strengthening indicate that several parameters must be considered if control of the interfacial properties in immiscible blends is to be achieved through compatibilization. The 'constant morphology' studies of Baker, et. al. [21,51,64] have illustrated the importance of interfacial adhesion on the macroscopic properties of immiscible blends. Recent research activity in the area of idealized compatibilized interfaces has clarified the parameters controlling their adhesive properties. Adhesion is strongly dependent on the amount of copolymer present at an interface and on the degree of polymerization of the compatibilizing copolymers. Experimental studies have shown that it is possible to achieve large increases in interfacial toughness when high concentrations of long copolymers are used. The boundaries defining the regime in which this highly efficient toughening occurs have been predicted theoretically and verified experimentally. Hence, the current literature in the area of interfacial adhesion between compatibilized, immiscible interfaces has shown the adhesive property to be relevant to successful compatibilization, and readily controlled through the use of properly designed compatibilizers at sufficient concentration.

2.3 Summary

In this chapter, a variety of information has been presented with the aim of clarifying the nature of the research which is the subject of this dissertation, as well as its relevance and synergy with topics of current interest in the area of immiscible blends. Pertinent concepts and definitions were

discussed in the first section, as well as an overview of the accepted mechanisms behind and theory of compatibilization. Perhaps the most useful information was provided in Section 2.2, where the literature concerning the important issues in reactive compatibilization and interfacial modification in immiscible blend systems was discussed. In Section 2.2, it was noted that successful morphology refinement in reactive systems is most dependent on the concentration of reactive groups, which translates in to the concentration of copolymers generated by *in-situ* reaction. This same dependence on copolymer concentration was shown to be highly relevant to promoting adhesion between immiscible interfaces, which is also dependent on the characteristics of the compatibilizing copolymers. These claims have been substantiated by extensive experimental work, the highlights of which were reviewed at length. Having provided this detailed background information, it is now possible to more fully discuss the nature of the research program and its relation to the current body of knowledge in the area of reactive compatibilization.

It is clear from Section 2.2 that reactive compatibilization produces refined microstructures relative to similar unreactive systems, and also that the compatibilization results in improved interphase adhesion. This adhesive effect has been studied in model interfacial systems, and has been unambiguously related to the concentration of copolymers added to the interface. There is a gap in the present understanding of this situation, however, because no one has related the concentration of copolymers formed in the blends to the concentration of copolymers which is necessary to generate significant interfacial toughening. Thus is has not been possible to compare the two bodies of information. It is this issue which is addressed in the study of aPA/PS blends discussed in Chapter 4. This study takes two

directions. First, morphology refinement is verified through traditional blending routes, and the areal chain density of copolymers in the melt blend is estimated through a combination of quantitative spectroscopic techniques and microscopy. This approach provides the first direct attempt to quantify the expected adhesion increase in reactive melt blends due to copolymer formation. Secondly, this study of adhesion in the aPA/PS system is supplemented with some model interfacial toughness studies, which clarify the realistic range of toughening for reactive blends with typical functionality levels. Chapter 5 is also concerned with the model interfacial toughening studies in an immiscible blend, in this case the ionically functionalized sPS/P2VP system. It should be noted that the investigation of toughening resulting from *in-situ* copolymer formation is unprecedented, and the current research program represents the first extensive study of reactive compatibilization at immiscible interfaces. The studies on the sPS/P2VP system provide an excellent basis for comparison between toughening resulting from reactive versus traditional compatibilization, due to the previous study of diblock copolymer compatibilized PS/P2VP interfaces. In addition, morphological characterization of the sPS/P2VP system is also undertaken to retain consistency in this attempt to 'bridge the gap' between the issues of morphology and adhesion in reactive blend systems.

Chapter 3:
Materials and Experimental Methods

The purpose of this chapter is to present pertinent information on the materials used and experimental methods employed in this study. The first section is concerned with materials, and contains information about the chemistry, source, and physical properties of all polymers used in this investigation. The expected compatibilizing reactions and composition of all blends studied will also be detailed. Blending techniques are summarized at the end of Section 3.1, while the methods employed in the bulk characterization of these blends are outlined in the following section. The evaluation of interfacial fracture toughness, which includes specific details of the experimental procedure and equipment are addressed in the last section.

3.1 Materials

3.1.1 Polymers

Six types of homopolymers were used in this study; polystyrene (PS), oxazoline modified polystyrene (PS-ox), deuterated polystyrene (dPS), sulfonated polystyrene (sPS), amorphous nylon (aPA), and poly(2-vinyl pyridine) (P2VP). The monomer structure of each of these materials are illustrated in Figure 3.1 (dPS has the same structure as PS, except all hydrogen atoms are replaced by deuterium).

Two commercial polystyrenes were used for control studies of immiscible blends, one purchased from Aldrich Chemical Company of Milwaukee, Wisconsin, catalog # 18,242-7 and the second obtained from Dow Plastics of Midland Michigan, trade name Styron 666. The oxazoline modified

polystyrene, marketed under the trade name RPS or reactive polystyrene is believed to have been manufactured by Dow Plastics and was purchased through Scientific Polymer Products of Ontario, New York. This polymer is actually the product of copolymerization of styrene with a small amount (~1%) of vinyl oxazoline. Deuterated polystyrenes were purchased from Polymer Laboratories, of Shropshire, UK. Sulfonated polystyrenes were prepared by Dr. Dennis Peiffer of Exxon Research & Engineering Company using the method of Makowski [78]. This procedure involves grafting of sulfonic acid groups onto polystyrene polymer chains. Grafting is performed in solution by direct reaction with a sulfonating agent, such as acetyl sulfate or sulfur trioxide complexes with dioxane, tetrahydrofuran, and trialkyl phosphates. The structure which results resembles a random copolymer of styrene and styrene sulfonic acid. Sulfonated polystyrenes were prepared in a range of concentration spanning 1.67-15.0 mole percent styrene sulfonic acid through sulfonation of Dow Styron 666.

The amorphous polyamide used in this study was supplied by EMS-American Grilon Inc., of Sumter, South Carolina. Its structure is represented as a random copolymer of isophthalic acid (i), 12-aminododecanoic acid (ii), and bis(4-amino-3-methylcyclohexyl) methane (iii), which are present in the molar ratio 1.0:1.057:1.0. The proportions of the various linkages are: ii/ii=12%, i/ii=23%, i/iii=43% and ii/iii=23% [79]. This material is believed to be made by a condensation process and is expected to have inherent functionality at both primary amine and carboxylic acid end groups.

The last material to be used in this study is poly(2-vinyl pyridine). Two commercial grades were used without any further purification. One was obtained from Polysciences, Inc. of Warrington, PA, catalog #19238 and is

designated P2VP-PSCI. The second, trade name Reiline 2200, was obtained from Reilly Industries of Indianapolis, IN and is designated P2VP-R. The functionality of this polymer is inherent at the nitrogen in the pyridine ring. This is the only fully functional polymer, having one reactive group per monomer.

Some properties of each polymer are summarized in Table 3-I. Reactivity of PS-ox and sPS were obtained by chemical analysis. Molecular weight was determined by gel permeation chromatography(GPC) for all polymers. The molecular weight of both P2VP materials was reported by the supplier to be ~200,000 g/mole. The molecular weights of both P2VP's were measured by GPC using polystyrene standards, in which case the measured molecular weights and polydispersity are M_w=78,000 g/mole and M_w/M_n=2.66 for P2VP-PSCI, and M_w=63,000 g/mole and M_w/M_n=2.21 for P2VP-R. These values are useful for comparison and verify that the molecular weight of P2VP-PSCI is higher, but do not necessarily reflect the actual molecular weights due to calculation based on PS standards in the GPC procedure. The manufacturer reported value of ~200,000 g/mole will be used except in cases where it is necessary to compare the molecular weights of the two polymers. The P2VP-R was used only in the interfacial fracture studies discussed in Section 5.2.

The physical properties of reactive polymers are sometimes influenced by addition of the reactive groups. It is therefore necessary to check reactive materials for changes in relevant properties. An example of this is noted in Table 3-I. The glass transition temperature (T_g) of sulfonated polystyrenes increases with the amount of acid addition to the material. The addition of reactivity does not alter all properties; note also from Table 3-I that the molecular weight of sulfonated polystyrenes is believed to be unaltered by the

sulfonation process [80].

3.1.2 Blends

3.1.2.1 PS/Amorphous Nylon Blends

PS/aPA and PS-ox/aPA blends were prepared in composition ratios of 1:99 and 20:80 by weight. The reactions responsible for compatibilization in the PS-ox/aPA system are illustrated schematically in Figure 3.2. Each of the nylon end groups is potentially reactive with vinyl oxazoline groups. The copolymer formed from either reaction has the architecture of a single nylon chain grafted at its end to a polystyrene chain. Oxazoline groups are believed to be approximately randomly distributed along the polystyrene, thus the point of grafting may occur at any position along the polystyrene chain.

Blends were prepared by melt mixing in a Banbury mixer. This is a two-headed batch mixing device with counter-rotating, non-intermeshing roller blades, and was driven by a Brabender Plasti-corder. The mixer was operated at 70% fill level, which is in the range known to optimize break-up and mixing uniformity [81]. The aPA used is known to have some sensitivity to moisture, so aPA pellets were dried in vacuum at 80°C for a minimum of 16 hours immediately prior to processing.

Torque pre-tests were performed on the aPA and various polystyrenes prior to blending. As discussed previously in Section 2.1.2.1, the dispersed phase size in a two phase blend is dependent on interfacial tension, shear rate, matrix viscosity and viscosity ratio. Because the aim of this study was to isolate interfacial tension effects, all blending operations were performed holding other parameters constant. It was therefore necessary to choose an unreactive polystyrene for control which had the same rheological properties as the reactive material, PS-ox. The rheological properties were represented

by the torque during processing in the Banbury mixer, measured under identical conditions to those employed for blending [82]. Torque values and torque ratios for all materials tested are listed in Table 3-II, along with weight average molecular weights and values of melt index reported by suppliers [83]. On the basis of this torque data, unreactive control blends of PS/aPA were made using Styron 666, which has similar viscosity to PS-ox.

All blends were prepared using the following procedure:

1) Blend components were individually weighed and subsequently dry mixed by hand.

2) Mixing equipment was preheated to 180°C.

3) Material was added with the mixer running at <20 rpm.

4) Rotor speed was increased to 50 rpm.

5) Mixing continues at 50 rpm for 10 minutes.

6) Rotors are turned off. Material is removed from the center section of the mixer and immediately quenched in cold water.

Torque and temperature were monitored during the blending process. There were no discernible torque increases in the reactive blends during the course of the mixing. Temperature reached a maximum of 205-210°C due to viscous heat generation during processing.

3.1.2.2 Sulfonated Polystyrene/Poly(2-vinyl pyridine) Blends

Both reactive and unreactive blends of PS/P2VP were prepared in a range of concentrations. In the sPS/P2VP system, there is an ionic interaction between sulfonic acid groups and the pyridine nitrogen (Figure 3.3). The combination of random placement of sulfonate monomers and full functionality of the P2VP chains results in an architecture often described as interchain grafting or interchain crosslinking.

Two types of blends were prepared from sPS and P2VP. First, melt blends were prepared of PS-1.67SO_3H/P2VP in a 20:80 weight ratio, and of PS-5.56SO_3H/P2VP in a 50:50 weight ratio. Melt blends in this system were prepared solely for qualitative, visual analysis because the rheological properties are unknown and the quantity of material available was too limited for their determination by the torque method. Viscosity of sulfonated materials is expected to exceed that of unreactive polystyrene, and to increase as a function of acid content [84]. Melt blends were prepared according to the procedure outlined above, except the blending temperature used in this system was 150 °C, with maximum temperature reaching 175 °C. No torque increases were observed during processing of the reactive blends.

Solution blends of reactive PS-1.67SO_3H/P2VP, PS-3.37SO_3H/P2VP, PS-5.56SO_3H/P2VP and PS-6.91SO_3H/P2VP were prepared. The blending procedure was as follows:

1) Two solutions were prepared; one solution of sPS and one of P2VP. In both cases, the solvent used was a mixture of 80 toluene/20 methanol, by volume. Solution concentration was 1% polymer.

2) The sPS solution was added to the P2VP solution dropwise, over a period of approximately 15 minutes, with constant stirring. In all cases, an insoluble precipitate formed immediately upon the addition of the P2VP solution.

3) Once the entire P2VP solution was added, stirring was continued for an additional 15 minutes.

4) The precipitate was removed from solution and placed in a teflon dish to dry. The drying procedure was 16 hours in air at room temperature, followed by 20 hours under vacuum at 50 °C, and completed with 10 hours under vacuum at 130 °C.

Each blend was initially prepared in 50:50 sPS/P2VP weight ratio. The weight of precipitate recovered increased with acid content. An unreactive control blend was also made by following Steps 1-3, above, followed by precipitation into excess hexanes and subsequent drying by a procedure comparable to Step 4.

3.1.2.3 Sulfonated Polystyrene/Deuterated Polystyrene Blends

Blends of dPS and PS-1.69% SO_3H were prepared in 5:95, 10:90, 50:50, 90:10 and 95:5 weight ratios for the small angle neutron scattering (SANS) experiments. The 50:50 blend was made from the 210,000 molecular weight dPS, while all others were made using the 188,000 molecular weight dPS. Blends were prepared by solution casting from dilute solution of tetrahydrofuran, a common solvent for dPS and PS-1.67% SO_3H. Drying was perfomed under vacuum at 40°C for 4 hours followed by 125°C for 4 hours. After drying, samples were compression molded at 160 ± 15 °C into disks nominally 14 mm in diameter and 0.5 mm thick suitable for the SANS apparatus. Typical times of 20-30 minutes at elevated temperature were used for compression molding of disks, and it is during this step of sample processing that the final physical state of the blend is believed to develop.

3.2 Characterization of Blends

3.2.1 Morphology

3.2.1.1 Microscopy

The morphology of melt blends was examined using optical and scanning electron microscopy. The optical microscopy investigation employed a Olympus BX-60 instrument. Both JEOL 5400 and JEOL 840 instruments were used in the SEM studies. All samples for SEM analysis were

coated with approximately 30 nm of gold-palladium alloy to insure conductivity and protect the surface.

The PS/aPA microstructure was revealed by examining fresh fracture surfaces created by first submerging the material in liquid nitrogen and then inducing brittle fracture with a high impact blow. In addition, some samples were etched in toluene for ~20 minutes to remove the minor PS phase, thus creating images with higher contrast for more accurate determination of particle size. Images were analyzed using Image NIH software. Average particle size and particle size distributions reported represent the contribution from at least 80 particles for each blend.

Microstructural examination of sPS/P2VP melt blends was made on polished sections. Samples were stained with iodine vapor, which reacts with the nitrogen of the pyridine ring, according to reaction (3-1) [85]:

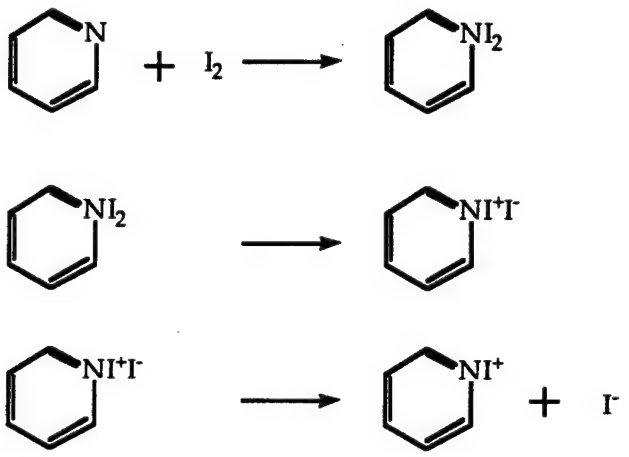

(3-1)

Staining was carried out by enclosing samples in a 90 mm diameter by 50 mm deep glass dish to which ~1g iodine crystals were added. Exposure times ranged from 30-120 minutes. The iodine stain creates contrast between sPS and P2VP which is sufficient to identify the individual phases using backscattered electrons.

3.2.1.2 Small Angle Scattering

Solution blends of sPS and P2VP were examined by small angle x-ray scattering. Samples were prepared as described in Section 3.1.2.2, and in addition were pressed between heated platens at 170 °C and 35 MPa for approximately 5 minutes to densify the samples and smooth the surfaces. Sample thicknesses were in the range of 0.7-0.8 mm. Experiments were performed on the 10 meter small angle x-ray scattering (SAXS) apparatus at Oak Ridge National Laboratory (ORNL) in Oak Ridge, Tennessee [86]. X-rays were produced by a rotating anode generator operating at 40 kV and 100 mA. The instrument has pinhole collimation. Data were corrected for empty beam scattering and dark currents, and adjusted for sample thickness and transmission. Intensity was converted to absolute units through multiplication by a correction factor obtained from a secondary standard. Two dimensional data were reduced to one dimensional intensity versus scattering vector form through circular averaging. Data was gathered over an extended range of scattering vector, Q, from 0.03 - 5.0 nm^{-1}.

SAXS experiments were also performed at the 10-meter SAXS facility at the National Institute of Standards and Technology (NIST) in Gaithersburg, MD [87], on the sPS ionomers in the intermediate range of scattering vector, from 0.2 - 2.5 nm^{-1}. sPS samples were prepared by solution casting from a 20 methanol/80 toluene mixture, followed by a drying procedure similar to the procedure described in Section 3.1.2.2, and pressing at 170 °C, ~35 MPa for 15 minutes. The x-ray source was a rotating copper anode operated at 47 kV and 180 mA with Cu-K_α radiation selected. The instrument uses pinhole collimation of the incident beam. Data were corrected for dark current, empty beam scattering and sample transmission. Two dimensional data were

reduced to one dimensional intensity versus scattering vector form by circular averaging. Absolute intensity correction was made by comparison of scattering by one blend sample measured both at NIST and ORNL, and scaling the NIST data to match the absolute intensity units of the ORNL data.

The compatibility of sPS/dPS blends was studied using small angle neutron scattering using the 30 m instrument of the Cold Neutron Research Facility at NIST [88]. The scattering was recorded at 140°C, which is well above the glass transition temperatures of blend components. The wavelength of incident neutrons used was 5 Å. Data was corrected for empty cell and background scattering, and the intensity subsequently converted to absolute units using a secondary calibration standard.

3.2.2 Evaluation of Reactions

3.2.2.1 Fourier Transform Infra-Red Spectroscopy

Fourier transform infra-red spectroscopy (FTIR) was used to confirm and quantify copolymer formation in PS/aPA blends. Films for FTIR were prepared by pressing a few milligrams of polymer between teflon coated aluminum sheets in a Carver press at 180-200°C and ≤ 60 MPa. A final pressing step at ~ 20 MPa, ~2 minutes between mylar sheets was added to improve film surfaces. Spectra were collected using a Perkin-Elmer 1600 Series FTIR. Data reported are the average of at least 16 scans.

Quantitative analysis of copolymer formation in PS-ox/aPA blends was made by employing a solvent extraction technique. This technique involved:

1) Dissolution of melt blends in warm 2,2-dimethyl formamide, a common solvent for aPA and PS-ox.

2) Mixing of Solution 1 with excess toluene which is a non-solvent for

aPA and a solvent for PS-ox. aPA precipitates (aPA fraction). Supernatant liquid (PS-ox in solution) is removed.

3) The supernatant liquid from Step 2 is poured into excess methanol, which is a PS-ox non-solvent. PS-ox precipitates and is removed (PS-ox fraction). The remaining solution is discarded.

4) Steps 1 and 2 are repeated twice for the aPA fraction. Only the aPA fractions are retained.

5) Steps 1-3 are repeated twice for the PS-ox fraction. Only the PS-ox fraction is retained.

6) Both fractions are dried 16 hours in air, followed by a 12 hours at 50°C in a vacuum oven and finally 5 hours at 160°C under vacuum.

7) The PS-ox and aPA fractions are pressed into individual films and spectra are obtained from these separated fractions of the original melt blend.

Steps 1-6 are also applied to unreactive PS/aPA blends to produce films for the control study. FTIR spectra were also obtained from unreactive PS/aPA blends for calibration purposes (See Chapter 4). These blends, containing less that 10% PS by weight, were solution cast from warm DMF, dried by a procedure similar to Step 6, and pressed into thin films as described above.

3.2.2.2 Thermal Analysis

DSC studies were performed with the aim of measuring glass transition temperatures in all blends and component polymers. A Perkin-Elmer DSC-7 Thermal Analyzer was employed. All experiments were conducted using a heating rate of 20°C/minute with samples under flowing nitrogen. Samples were made by encapsulating a small amount (10 -25 mg) of dry blend or

component polymer in an aluminum pan. Calibration was performed with indium and tin standards. In all cases, the data from the first heating was discarded, and transition temperatures were recorded from the second or third heating. Samples were quenched at 50°C/minute between each run.

3.2.2.3 Dynamic Mechanical Analysis

The sPS/P2VP solution cast blends and sPS and P2VP polymers were studied by dynamic mechanical analysis (DMA), which provides a more sensitive measure of changes in the nature of the transition due to reactivity than DSC. Materials were pressed into thin films, ~50-100 μm thick, and cut into strips 3.5-5 mm in width and 35 mm long. Samples were tested in tension using a Rheometrics Solids Analyzer model RSAII. Strain was applied at a frequency of 1 Hz over a temperature range spanning from 50 - 160 °C. Complex modulus versus temperature data was collected at either 3° or 5°C intervals.

3.3 Evaluation of Interfacial Fracture Toughness

3.3.1 The Asymmetric Double Cantilever Beam Test

The interfacial adhesion between immiscible, reactive polymers was evaluated through measurement of the critical energy release rate (or crack extension force) for interfacial failure using the asymmetric double-cantilever beam (ADCB) test. The test procedure involves inserting a wedge, usually a razor blade, into the interface of a bilayer, which is made by joining two polymer beams under controlled conditions of heat and pressure (Figure 3.4). The insertion of the wedge causes cracking at the interface. The critical energy release rate, G_c, for the interfacial failure under these constant displacement

conditions is a function of the wedge thickness, Δ, the thickness of the beams, h_1 and h_2, the Young's moduli of the materials, E_1 and E_2, all of which are constants, and the measured length of the interface crack, a. The appropriate calculation is made using the equation derived by Kanninen, whose analysis was based on deflection in a cantilever beam which is partially supported on an elastic foundation:[89]

$$G_c = \frac{3\Delta^2 E_1 h_1^3 E_2 h_2^3}{8a^4}\left[\frac{E_1 h_1^3 C_2^2 + E_2 h_2^3 C_1^2}{\left(E_1 h_1^3 C_2^2 + E_2 h_2^3 C_1^2\right)^2}\right] \qquad (3\text{-}2)$$

where

$$C_i = 1 + 0.64\frac{h_i}{a}$$

The measurement of elastic constants is discussed in Section 3.3.3.

The ADCB test was first applied to the study of adhesion between compatibilized, immiscible polymers by H. R. Brown [72,74,89]. Brown had observed a toughness of ~200 J/m^2 across symmetric PS/PMMA interfaces (h_1=h_2), which dropped to ~12 J/m^2 once asymmetry was introduced ($h_1 \neq h_2$). The asymmetry in the test geometry is necessary to compensate for the asymmetry in the elastic properties of the material on either side of the interface.

The nature of cracking at interfaces between dissimilar materials is more complex than fracture in isotropic solids. Unlike the situation at a symmetric interface between identical materials, a crack traveling at an interface between two dissimilar materials is subjected to both Mode I and Mode II opening conditions. Cracks growing in brittle, isotropic, homogeneous materials will tend to orient themselves to maximize the Mode I component, which may result in deflection of the crack path away from the

interface. If the crack is constrained to the interface it is forced to propagate under mixed mode conditions. In addition, the mathematical separation into modes I and II is not possible, though under certain conditions an approximation may be made [91,92].

The difficulty in the solution of this interfacial fracture problem stems from the elastic mismatch across the interface. The result of this mismatch manifests itself as an oscillatory singularity in the solution for the tractions ahead of a crack tip at the bimaterial interface. (The details of the solution are discussed in references 89-92.) The interpretation of this result is that the material on either side of the crack near the crack tip must occupy the same position in space, a non-physical situation. Consequently, the stress and deformation fields of an interface crack can no longer be separated into independent modes, and the apparent ratio of Mode I/Mode II loading is a function of the distance from the crack tip. It has been pointed out by Rice[91] that under certain conditions, the oscillations and the mode mixing occur only very close to the crack tip, in the region where the linear elastic solutions are always invalid. These conditions permit the oscillations and scale effects to be ignored, and as a result, a complex stress intensity factor, K^* may be used to describe the stress pattern at the tip in the bimaterial interface. As the elastic constant differences between the materials become small, K^* may be related to the more common stress intensity factor, $K=K_I + iK_{II}$, with the mode mixity described by the phase angle, $\Psi=\tan^{-1}(K_I/K_{II})$.

The degree of asymmetry across the interface may be quantified by the Dundars parameters, α and β. α is a measure of the mismatch in the plane tensile modulus across the interface, while β is a measure of the mismatch in the in-plane bulk modulus across the interface. These parameters take the

form:

$$\alpha = \frac{\mu_1(\kappa_2 + 1) - \mu_2(\kappa_1 + 1)}{\mu_1(\kappa_2 + 1) + \mu_2(\kappa_1 + 1)} \tag{3-3a}$$

$$\beta = \frac{\mu_1(\kappa_2 - 1) - \mu_2(\kappa_1 - 1)}{\mu_1(\kappa_2 + 1) + \mu_2(\kappa_1 + 1)} \tag{3-3b}$$

where μ is the shear modulus and κ is a function of the Poisson's ratio, ν, following the relation $\kappa_i = 3 - 4\nu_i$ for plane strain. The Dundars parameters may be calculated using previously reported Poisson's ratios for the PS/P2VP system,[25] an estimate of ν=0.333 for aPA, and values of the elastic constants measured in this study (Section 3.3.3). For PS/P2VP, β = 0.0123, and the estimated value for the PS/aPA system is β = 0.0519. In both systems, β is small enough to expect an error of less than 0.5% from the approximation $\beta \approx 0$ [92] which allows for the separation of the complex interfacial stress intensity factor into Mode I and Mode II components, and negates the dependence of the phase angle on distance from the crack tip. Therefore, for the immiscible polymer pairs considered in this study, the stress field at the crack tip should be completely characterized by the critical energy release rate, G, and the phase angle, Ψ.

In this investigation, the aim was to examine the effects of altering the interfacial properties on the interfacial toughness rather than the effects of altering the phase angle on the toughness. The minimum toughness was determined as a function of beam thickness ratio to establish the proper Ψ for evaluating properties of the interface. The toughness was then measured at constant phase angle and its value related to the level of interfacial

compatibilization. The dependence of the phase angle on the test geometry must be considered if the proper testing conditions are to be achieved. Recent simulation work by Xiao, et. al. [95] has examined the effects of test geometry on the phase angle and the critical energy release rate. They showed that the phase angle is insensitive to changes in the crack length, which translate into changes in toughness, provided the ratio of the crack length to the thickness of the stiffer beam is greater than ~4 for polymer pairs having a modulus ratio E_1 ~ (1-2) E_2. Similarly, the simulations showed that the toughness was insensitive to the length of the sample, provided the crack length was less than or equal to the length of the unbroken ligament. All of the fracture toughness measurements made in this study were designed to meet these two criteria.

3.3.2 ADCB Testing Procedures and Apparatus

3.3.2.1 Sample Preparation

Plates of all polymers were prepared by compression molding into frame molds 1-3 mm in thickness at temperatures of ~(T_g + 50 °C) under ~35-70 kPa. Bilayers were formed by joining the plates at constant temperature and slight contact pressure. Plates were dried for a minimum of 16 hours at 80 °C under vacuum prior to joining. In all cases the samples were allowed to cool slowly in the mold over a period of about 1.5 hours without applied pressure after this bonding step. Bilayers were cut into strips ~9.5 mm wide by 50 mm long for interfacial fracture testing.

In the PS/P2VP system, joining temperature was restricted to ≤ 155°C due to degradation of P2VP, thus all PS, sPS/P2VP bilayers were joined at 150 °C for one hour. PS, sPS/P2VP samples were allowed to equilibrate at ambient conditions before testing.

PS, PS-ox/aPA plates were joined at ~180-190 °C for one hour. In the PS-ox/aPA system, some test strips were annealed after joining under flowing nitrogen at 150 °C to evaluate effects from the kinetics of the grafting reaction. All PS, PS-ox/aPA samples were dried at 80 °C under vacuum for at least 12 hours immediately prior to testing.

3.3.2.2 Testing Apparatus

A computer controlled testing and video data acquisition apparatus was constructed for measuring interfacial fracture toughness. A schematic of the system is given in Figure 3.5, and the support block and sample position are shown in detail in Figure 3.6. The sample is free-standing, supported from beneath and behind by an aluminum block. The razor blade is inserted into a precrack at the interface by a screw driven mechanism. The screw is turned by a step motor controlled by a microstepping indexer which allows division of the step into very small increments. All experiments were run at a razor insertion speed of 3×10^{-6} m/s. The indexer is programmable and is controlled by a personal computer running terminal emulation software (Appendix A). The data acquisition system consists of a CCD camera and a personal computer fitted with a Coreco, Inc. frame grabber board. The camera is positioned above the sample, and images of the sample are recorded at fixed intervals during testing. An example of image data collected from an actual failure experiment is shown in Figure 3.7. Image acquisition is controlled by a computer program which calls the record function at fixed time intervals (Appendix B). Crack length is extracted from recorded images using commercial image processing software.

3.3.2.3 Testing and Data Reduction

Interfacial toughness measurements are made in the steady state crack growth regime. Twenty images are recorded during the course of each fracture test at intervals of 210 seconds. The crack length is extracted from each image, and the region of approximate steady state growth is identified. In typical tests, the crack length will either increase or decrease steadily during the initial stages of growth, eventually reaching a relatively constant value which characterizes the steady state regime. Interfacial toughness is calculated using Eq. (3-2) for each crack length recorded in the steady state regime, along with the standard deviation for the sample. Typical tests yield about 12-15 valid measurements. Note that the accuracy in the measurement of G_c is a function of the strength of the interface. For example, the measurement error, +/- one image pixel or 0.12 mm, is equivalent to ~8.5 J/m^2 for short cracks corresponding to G_c ~100-175 J/m^2 (6.2% midrange) while +/- 0.12 mm is equivalent to only ~ 0.08 J/m^2 for long cracks corresponding to G_c ~4-5 J/m^2 (1.8% midrange).

3.3.3 Measurement of Mechanical Properties

Knowledge of polymer elastic constants is required for the toughness calculation, Eq. (3-2). The elastic constants were measured in flexure under three point bending in accordance with the geometry established in ASTM D 790 [96] (Figure 3.8). All samples were prepared under the same conditions as the plates used to make the fracture toughness samples, in order to get the best representation of fracture sample properties. Tests were conducted using a SINTECH 20 instrument running Testworks software at the slowest possible machine crosshead speed, 0.002 inches/minute. This crosshead speed corresponds to a strain rate in the outer fiber of 1.2×10^{-5} m/s for the testing

geometry used, which is a reasonable approximation to the straining rate in the outer fibers during the fracture tests, which span the range of 10^{-5} to 10^{-7} m/s. (Because the straining rate in the outer fiber is a function of the crack length and the beam thickness it is not constant for each fracture sample.)

Flexural strength and tangent modulus of elasticity were calculated for each material. At least three samples of each polymer were tested, and the results averaged. All polymers except aPA failed in a brittle manner. The aPA samples did not break during the course of the test. Mechanical properties of all polymers used in this investigation are listed in Table 3-III. The results of the mechanical property investigation show that the room temperature modulus of PS is not significantly affected by sulfonation. The strength of the sulfonated materials exceeds that of the PS (Dow Styron) starting material, but is otherwise not dependent on sulfonation level. A value of 3.5 GPa was used for all sPS materials in the calculation of the interfacial toughness.

3.3.4 Failure Analysis

The fracture surfaces of bilayer beams were examined after interfacial fracture testing using optical and scanning electron microscopy. (See Section 3.2.1.1 for instrument details.) Surface chemical analysis was also performed in the SEM using wavelength dispersive spectroscopy (WDS). Under the operating conditions employed, WDS is expected to be able to detect elements which are present in concentration of ~0.5% by weight probing a depth of ~1 μm from the sample surface. The P2VP sides of the fracture were probed for sulfur, which is evidence of sPS adherent to the surface. sPS sides of the fracture surface were stained by exposure to iodine vapor which reacts with pyridine and analyzed for traces of iodine, indicative of adherent P2VP.

Chapter 4:
Compatibilization via Covalent Bonding in Reactive Polystyrene/Amorphous Nylon Blends.

The effects of reactivity on the interactions between functionalized polystyrene and amorphous nylon are the subject of this chapter. The first section is concerned with blend morphology. The nature of the refinement of the dispersed phase and the mechanisms which control this phenomena are discussed. Quantitative evaluation of the compatibilizing effect of copolymer formation are summarized in the second section. The final section is concerned with the improvement in interfacial adhesion resulting from in-situ compatibilizer formation in PS-ox/aPA blends, and the conditions which favor efficient interfacial toughening in this system.

4.1 Morphology of PS/aPA and PS-ox/aPA Blends

The addition of reactive functionality to the PS molecules causes significant changes in the morphology of PS/aPA blends. The microstructures of both reactive and unreactive 20:80 PS/aPA blends are shown in SEM micrographs in Figures 4-1 and 4-2. In Figure 4-2 the PS particles have been removed by etching with toluene to clearly show the location of the particles. Quantitative image analysis indicates that the size of the dispersed PS phase in the reactive PS-ox/aPA blend is about 60% smaller than in the unreactive PS/aPA blend. Particle size is represented by an equivalent diameter, which is calculated from the measured area of the particle assuming spherical shape. The particle size distributions and their

characteristics are illustrated in Figure 4.3 and Table 4-I, respectively [97]. Since the blends were processed under identical conditions, and the polystyrenes have very similar melt properties, the observed change in the morphology may be attributed directly to the effects of reactivity. The refinement of the microstructure implies the formation compatibilizing copolymers, which reduce interfacial tension and stabilize the dispersion, as discussed in Chapter 2. These findings illustrate the efficiency of reactive compatibilization; only ~1.2 mole % of reactive oxazoline groups, in the presence of a similar number of reactive aPA endgroups, resulted in significant changes in the structure of the blend.

In addition to having a smaller average particle size, the breadth of the distribution in the reactive blend is much smaller than in the unreactive blend. This suggests that coalescence effects may be more important in determining the final droplet size in the PS/aPA system than in the PS-ox/aPA system. Further evidence for the importance of coalescence may be gained from comparison of estimated particle size in dilute systems with actual particle size measured. The particle size may be estimated from the Taylor theory (Section 2.1.2.1, Eq. 2-5) for the unreactive blend if the viscosity ratio is approximated by the torque ratio (Table 3-II), the matrix viscosity is approximated as ~10 kPa-s [47,104], the shear rate is $G \sim 0.75S \sim 37.7\ s^{-1}$ [82] where S= 50 rpm is the mixing speed (Section 3.1.2.1), and the interfacial tension is taken as 0.018 N/m from measurements on a similar system [47]. The Taylor theory predicts r~0.025 μm, an order of magnitude smaller than measured, which implies that coalescence effects are important for the blends. For this reason, very dilute blends of both types were mixed in a 1:99 ratio with the intention of evaluating particle sizes under conditions which are less sensitive to coalescence. The microstructures of the 1:99 blends are shown in

Figure 4.4. Due to the very small size of the particles, it was not possible to image them clearly enough for quantitative analysis. Estimates made from the micrographs indicate that the dispersed phase size in both PS/aPA and PS-ox/aPA blends are in the range of 0.01 to 0.1 μm. A comparison of particle sizes in the dilute 1:99 blends and the 20:80 blends suggests that the particle size is more strongly dependent on concentration in the unreactive blend than in the reactive blends, which again implies a more significant contribution of coalescence in the uncompatibilized system. Similar behavior has been observed in PS/elastomer blends [11,16] where the average size of the dispersed second phase was found to be insensitive to concentration changes in reactive blends, while increasing with concentration for the unreactive blend counterparts.

A theoretical interpretation of particle size effects on coalescence has been given by Elmendorp and van der Vegt [6,98], who studied the development of blend morphology in simple shear flow. They considered the case where two identical droplets approach in the melt at a distance which is less than the sum of their radii. Collision is inevitable under these conditions, and the droplets are believed to flatten on their interacting surface due to the hydrodynamic force propelling them towards each other (Figure 4.5). A thin film of the matrix phase is trapped between the flattened surfaces and is continuously expelled as the pair of droplets approach each other and the doublet simultaneously rotates until the pair is reoriented such that it may separate. The trapped film of the matrix phase is thinnest at the point just before the reorientation is complete. If the film becomes thin enough it may rupture under the influence of fluctuations induced by van der Waals forces, resulting in coalescence of the droplets.

Elmendorp's study predicts that the coalescence probability increases

as the droplet diameter decreases, the opposite situation to the experimentally observed behavior. Some speculation was made in the treatise about changes in interface mobility due to compatibilization which resulted in a decreased probability of coalescence, though the physical justification for this assumption was unclear. There is a fundamental physical aspect of the coalescence problem unique to compatibilized interfaces which may account for the enhanced stability of the dispersion but which has not been previously considered in this regard. In compatibilized systems, there is a repulsive force between the droplet faces due to the interaction of the copolymers located at the interface. If van der Waals forces are ultimately responsible for coalescence, then they must outweigh these repulsive forces if coalescence is to take place.

The relative values of the attractive and repulsive forces may be balanced to illustrate the regime in which copolymer conformation effects are most important. The hydrodynamic force will be neglected, approximating the static case or the point at which the droplet pair is nearly in position to either separate or coalesce. (Figure 4.5, bottom) The area of importance is assumed to be the film region between the flattened sections of each droplet. The geometry in this region is approximated by parallel plates. The van der Waals attractive forces across two parallel plates separated by a distance d are given by the expression:

$$F_{vdW} = -\frac{A}{6\pi d^3} \qquad \text{per unit area} \qquad (4\text{-}1)$$

where A is the Hamaker constant which can be calculated from known dielectric constants and refractive indices of the polymers [99]. The force due

to confinement of the copolymer chain becomes significant when the chain's random walk configuration is restricted by the approaching surface of the second particle. The configurational forces take different forms in the high and low grafting density regimes, which are defined by the relative size of the molecule and the interfacial spacing between grafting points (Figure 4.6). In the high grafting density regime, $L=1/\sqrt{\Sigma} < R_g$, the expression for the force between the interfaces (parallel surfaces) is given by: [99-101]

$$F_d \approx \Sigma^{1.5}\left[\left(\frac{2L_{brush}}{d}\right)^{9/4} - \left(\frac{d}{2L_{brush}}\right)^{3/4}\right]k_BT \quad \text{per unit area} \qquad (4\text{-}2)$$

where k_B is Boltzman's constant, T is temperature, Σ is the number of copolymers per unit area of interface, L_{brush} is the thickness of the grafted layer, and $R_g = b\sqrt{(N/6)}$ is the radius of gyration of a molecule exhibiting Gaussian statistics having degree of polymerization N and step length b. Equation (4-2a) is valid for high surface coverage of copolymer over the range of $d < 2\,L_{brush}$, where $R_g \le L_{brush} < R_g\sqrt{N}$. In the low grafting density regime, $L=1/\sqrt{\Sigma} > R_g$, the form of the repulsive force is based on the work by Dolan and Edwards: [99,102]

$$F_d \approx \Sigma\left[\frac{\pi^2 R_g^2}{3}\frac{1}{d^3} + \left(\frac{3}{8\pi R_g^2}\right)^{1/2}\frac{1}{d}\right]k_BT \quad \text{per unit area} \qquad (4\text{-}3a)$$

or

$$F_d \approx \Sigma\frac{6d}{R_g^2}\exp\left(\frac{-3d^2}{2R_g^2}\right)k_BT \quad \text{per unit area} \qquad (4\text{-}3b)$$

Equation (4-3a) is valid for $d \leq 3R_g$, while Equation (4-3b) gives the proper relation for $d \geq 3 R_g$.

The total force per unit particle contact area as a function of the separation distance is given by the sum of expression (4-1) and (4-2) or (4-3). For the PS/aPA system the Hamaker constant is estimated from the material properties, $A \sim 1.3 \times 10^{-19}$ J at 200 °C [103,104]. If a typical value for the step length, b = 0.7 nm, is used, and L_{brush} is approximated by its minimum value, R_g, it is possible to predict the total interaction force between compatibilized polymer surfaces.

The force balances in the high and low grafting density regimes are illustrated in Figure 4.7 and 4.8 for various typical values of N and Σ, and T=200°C. The interactive force becomes more repulsive (positive) as the copolymer concentration at the interface is increased, either by increasing molecular weight at constant Σ, or by increasing Σ at constant molecular weight. In the high grafting density regime, the net force is repulsive in the range $d > 1.0$ nm and $d \leq 2R_g$ for all N and Σ In the low density regime, there is a minimum amount of copolymer at the interface necessary to produce a net repulsive force at the interface, and the force acts over a much smaller range. Clearly, under conditions where the interfacial grafting density is high and/or the copolymer chains are long the repulsive copolymer interactive forces are substantial relative to the van der Waals forces, and are sufficient to cause a net repulsion between the particle surfaces.

In the PS/aPA blends, the aPA segment of the copolymer is on the surface of the particles, and has $N \sim 110$ and $\Sigma \sim 0.02$ (Sections 2.1, 4.3 and Appendix C). It is difficult to estimate the step length of a complex molecule such as the aPA monomer (Figure 3.1); however, it is reasonable to assume

that the step length will be at least as large as the step length of Nylon 12, b=1.36 nm [105], which is identical to segment ii of the aPA monomer, and comprises approximately half of the bonds on the polymer backbone. Under these conditions L~8.5 nm > R_g ~5.8 nm. The force versus interparticle distance curve calculated at the melt processing temperature of 200°C using Equations (4-1) and (4-3) is shown in Figure 4.9. For the PS-ox/aPA system, the calculated net force between the particle surfaces is repulsive when the surfaces are separated by less than ~15 nm. The total force is sensitive to the step length, which has been approximated with a lower bound, and will become more repulsive and act over a greater range as the step length increases. While the static surface interaction force balance gives only an approximation to the actual physical situation, the results clearly show that steric effects from brush compression are significant relative to van der Waals attractions, and may effectively deter coalescence in the reactively compatibilized PS-ox/aPA blend.

4.2 Evaluation of the Compatibilizing Reaction

4.2.1 Thermal Analysis

A standard test for immiscibility in a polymer blend is to identify two individual glass transition temperatures (T_g) using differential scanning calorimetry (DSC). It is obvious from the microstructures, Figures 4.1 and 4.2, that the PS/aPA blends are phase separated. However, in some cases compatibilization may lead to partial mixing in the phases, and a corresponding shift of the two T_g's, toward each other. Transitions in the reactive blend were measured and compared with those of the blend components in order to evaluate the possibility of interphase mixing. (Figure

4.10) The blend exhibits two glass transition temperatures, the positions of which do not differ from the glass transition temperatures of the pure components. This result clearly indicates immiscibility; the blend components retain their identity and are fully phase separated with little mixing between the phases.

4.2.2 Infra-Red Spectroscopy

The nature of the compatibilizing reaction was investigated using Fourier Transform Infra-red Spectroscopy (FTIR), with the aim of directly confirming the generation of copolymers, and quantifying the extent of the reaction. It was not possible to investigate the relative proportions of the two potential reaction mechanisms in PS-ox/aPA blends (Figure 3.3) due to overlap of the absorption frequencies of the monomers with those of the reactive groups. However, the reactivity of oxazolines with both amines and carboxylic acids has been previously verified [46, 106,107].

An extraction technique was used to verify and quantify copolymer formation. The sample preparation, which is detailed in Section 3.2.2.1, involves separation of the blend into its PS-ox and aPA components by exploiting the difference in solubility characteristics between these two polymers. The copolymer molecules, being composed of both PS and aPA, have segments which are soluble in both solvents for PS and solvents for aPA, and may preferentially segregate to one extracted component or be present in both, depending on which solubility behavior dominates. The experimental technique involves carefully separating the blend into its PS-ox and aPA components and subsequently investigating each fraction using FTIR for evidence of the characteristic absorption bands of the other component. The unreactive blend is subjected to the identical procedure and similarly

evaluated to insure that the separation process is successful in isolating the components.

The FTIR scans of the reactive and unreactive polystyrene fractions are shown in Figure 4.11. Arrows indicate the occurrence of an absorption at ~ 3310 cm^{-1} which is absent from the pure polystyrene scan (Figure 4.12). This absorption is characteristic of N-H stretching in the secondary amide group present along the aPA backbone (Figure 3.1) [108], which gives rise to one of the strongest absorptions from the pure aPA and occurs in a frequency range where PS absorptions are minimal (Figure 4.13). A faint absorption at ~3310 is present in the unreactive blend, indicating that separation in the unreactive blend was not fully complete. This absorption is much stronger in the reactive system providing direct evidence for the formation of copolymers. The aPA fractions of both blends were scanned and did not exhibit any absorption which could be assigned to PS, which suggests that the solubility of the copolymers was controlled by the PS segment. It should be noted that the strongest absorptions from the PS molecule overlap with the characteristic absorptions of the aPA, which may interfere with the detection of a small amount of residual PS.

Quantitative analysis was performed to estimate the amount of copolymer formed during the processing. The transmittance, T, of a given component in a mixture is related to its concentration, c, according to the Beer Law:

$$T = \log\frac{I_o}{I} = abc \qquad (4\text{-}4)$$

where b is the thickness of the absorbing medium and a is the absorptivity

[109]. This relationship between T and c may be exploited to gain information about the concentration of the mixture if a suitable calibration is available. For the present purposes, a calibration curve has been generated from dilute unreactive aPA/PS blends which were cast from a common solvent [97]. The effects of film thickness were compensated for by evaluating the transmission of the aPA absorption relative to the transmission of a characteristic PS absorption. (The PS absorption used for normalization is indicated in Figure 4.10.) The calibration curve is fit using linear regression and the fitting parameters subsequently used to calculate the concentration of aPA in the extracted PS fractions (Figure 4.14). The results are:

$c_{aPA} = 0.29\%$ in the PS fraction from the 20PS/80aPA blend

$c_{aPA} = 3.34\%$ in the PS-ox fraction from the 20PS-ox/80aPA blend

It will be assumed that the same amount of residual aPA homopolymer is present in the PS-ox extract as in the PS extract, thus the concentration of aPA due to copolymers is:

$$c_{aPA}^{copolymer} = 3.34 - 0.29 = 3.05\%.$$

This concentration may be readily converted into total copolymer concentration in the blend using the polymer molecular weights listed in Table 3-I and the assumption of one aPA/PS bonding site per aPA chain, yielding a total compatibilizer concentration of ~2.9% (Appendix C). Similarly, the aPA concentration may be used to calculate the percentage of reactive molecules which have successfully grafted to form compatibilizing copolymers, from which the number of PS-ox molecules that have formed a copolymer is estimated to be 11.6% (Appendix C). Thus, for the PS-ox/aPA

blend which was the subject of this investigation, the incorporation of ~1.2% of reactive monomers along the PS chain resulted in the formation of approximately 3% of compatibilizer, by weight, due to grafting of ~12% of PS chains.

4.3 Interfacial Adhesion Between PS-ox and aPA.

The effects of reactivity on the adhesion between PS and aPA was evaluated using the asymmetric double cantilever beam test (ADCB test) which isolates the interfacial properties by using a model geometry (Section 3.3.1). The interfacial fracture toughness was measured as a function of the thickness ratio of each component to determine the sensitivity of the measurement to the difference in elastic constants across the interface. The PS-ox/aPA interfacial toughness was found to be relatively insensitive to the beam thickness ratio, and no wandering of the crack path away from the interface was observed. These conditions indicate that failure is occurring along the interface and insure that adhesive rather than cohesive properties are being measured.

The effects of reactivity on the interfacial fracture toughness are illustrated in Figure 4.15. Though there is some scatter in the data, the reactive interface is consistently showing higher toughness. An average of all data points shown in Figure 4.15 yields:

$G_C = 10.2 \pm 3.6\ J/m^2$	PS-ox/aPA Interface
$G_C = 3.8 \pm 1.6\ J/m^2$	PS/aPA Interface

Thus the adhesion at the reactive interface appears to be on average at least twice that of the unreactive interface.

Though the reactive interface does exhibit superior toughness relative to its unreactive counterpart, the magnitude of the effect is small when compared with the results of previous studies in which preformed block copolymers were physically added to the interface [22,23,25,65-67,72-76]. Previous studies have shown that low toughness is observed under conditions where the copolymer blocks are shorter than the entanglement molecular weight, or when the grafting density at the surface is low. The PS segments of the copolymer chains should be considerably longer than the entanglement molecular weight, which is known to be ~ 27,000 [25]. The entanglement molecular weight of the aPA material is not known, but since entanglement typically occurs at ~400 backbone chain atoms or less [110], and the estimated number of backbone chain atoms for aPA is greater than 3000, it is fair to assume that both segments of the copolymer are sufficiently long to provide entanglement. Thus the observed low interfacial toughness most likely reflects a low grafting density at the PS-ox/aPA interface resulting from low levels of reactivity in this system.

Previous studies have shown that for interfaces compatibilized with long copolymers, $N_{copolymer} > N_{entanglements}$, the interfacial adhesion is a strong function of the areal density of copolymer chains, Σ [25,67]. It was possible to make an estimate for Σ in the PS-ox/aPA melt blends using a combination of quantitative spectroscopy and particle size measurements, resulting in $\Sigma \sim 0.02$ chains/nm^2 (Section 4.2, Appendix C), for which the strength of the reactive interface is typically 1.5-4 times that of the unreactive interface [22,25,65,67]. The copolymer areal joint density at the PS-ox/aPA interface of the bimaterial beams used for the fracture test is not necessarily expected to be the same as the joint density across the particle interfaces of the melt blend due to differences in the manner in which each type of sample was

prepared. The melt blends were heated for a much shorter time than most of the bimaterial beam samples and were also subjected to an aggressive mixing process which increases the probability of co-reactive group contact. The interfacial toughness of bimaterial beams is not very sensitive to joining time and temperature (Table 4-II) which indicates that the conditions in both cases were sufficient to induce the compatibilizing reaction. The issue of probability of contact between reactive groups probably leads to more efficient copolymer generation than the contact molding procedure employed to make the bimaterial interfacial fracture samples. Therefore, the estimate from the melt blend, $\Sigma \sim 0.02$ chains/nm^2, is probably larger than the areal chain density at the PS-ox/aPA interface. Under these conditions, with such a low interfacial density of compatibilizer, the observed modest improvements in interfacial adhesion are in agreement with previous findings [25,65,67].

An attempt was made at improving the interfacial grafting density through extension of the reaction time over a period of several days. In this experiment, several strips were cut from the same sample plate, which was joined at 185 °C for one hour, and were heat treated for periods of up to 100 hours under flowing nitrogen before interfacial fracture testing. The heat treatment temperature was set at 150 °C, just below the T_g of aPA, to insure that the samples maintained geometrical integrity if supported by the aPA beam, but far enough above the T_g of PS-ox to allow for some molecular rearrangement. The result is shown in Figure 4.16. G_c increases approximately linearly from ~8 to ~13 J/m^2 as the time held at temperature increases, indicating a that the number of bonds at the interface is increasing directly with the reaction time. This linearity is consistent with interfacial failure by chain scission, the expected failure mechanism for interfaces reinforced with a low density of long copolymers (Section 2.2.2) Apparently,

the low concentration of reactive groups in this system prohibits the generation of a high enough grafting density to initiate the crazing mechanism necessary for large increases in interfacial toughness.

4.4 Summary

In this Chapter the results of the investigation into the reactive compatibilization PS-ox/aPA blends were summarized. The incorporation of only 1% of reactive oxazoline groups to the otherwise unreactive system resulted in the in-situ generation of approximately 3% of compatibilizer, with approximately 10% of all PS molecules being grafted to aPA molecules. This copolymer formation was effective in stabilizing the dispersion of PS particles with respect to both their average size and their size distribution. The stabilization of the size distribution may be related to steric repulsion between compatibilized particle surfaces, which have been demonstrated to exceed van der Waals attractions between PS particles dispersed in an aPA melt. In addition to the morphology study, the effects of copolymer formation on the adhesion between these two immiscible polymers was assessed using a model geometry that isolates the properties of the interface. The toughness of the reactive interface was found to be about twice that of its unreactive counterpart. This modest improvement is the result of the extra energy added to the interfacial failure from the breaking of copolymer junctions, and is of the expected order of magnitude for these interfaces which are reinforced with an estimated copolymer joint density of less than ~0.02 bonds/nm^2. Overall, this investigation illustrates the potential utility of the reactive compatibilization route both for strengthening of interfaces and stabilization of blend microstructure, the two parameters most affecting the utility of immiscible polymer blends.

Chapter 5:
Compatibilization via Ionic Crosslinking in Sulfonated Polystyrene/Poly(2-vinyl pyridine) Blends

The reactive compatibilization of polystyrene and poly(2-vinyl pyridine) through ionic interactions is the subject of this chapter. PS has been functionalized by addition of sulfonic acid groups, which are capable of forming an ionic bond with the nitrogen of the pyridine ring. This interaction has been found to produce substantial compatibilization effects, both in refining the microstructure of melt and solution blends and also by substantially improving the interphase adhesion. Structural evaluation which has been made by microscopy, dynamic mechanical analysis, and small angle x-ray scattering is summarized in the first section. The interfacial mechanical properties are the subject of Section 5.2, and finally, the feasibility of using sPS as a compatibilizing blend additive is discussed in the last section.

5.1. Structural Analysis of Blends

5.1.1 Microscopy

The ionic interaction between pyridine and sulfonic acid alters the microstructure of sPS/P2VP melt blends as can be seen in SEM micrographs of 20PS-1.67SO_3H/80P2VP and 20PS/80P2VP blends shown in Figure 5.1. The reactive blend has PS-1.67SO_3H domains on the order of 0.5 - 1 μm in size, while the PS domains in the unreactive blend range in size from ~0.5 - 6 μm. It is not possible to make a direct correlation between domain size and reactivity in this system due to differences in the melt viscosity of PS and sPS; however, the viscosity increase due to sulfonation is only ~30% for 2% acid

[111], and the predicted particle size is relatively insensitive to viscosity ratio (Eq. 2-5) which implies that the observed morphology refinement is due largely to the effects of reactivity.

Scanning electron microscopy studies in this system were limited by the sensitivity of reactive blends to damage by electron beam radiation (note the radiation induced cracking in Figure 5.1b). For this reason, the bulk of the structural analysis of sPS/P2VP blends was restricted to other experimental methods.

SPS/P2VP solution blends were examined by optical microscopy, and showed no evidence of phase separation at magnifications up to 500x. This result is not surprising given the resolution limit of the optical microscope. The formation of a gel precipitate during preparation of the reactive blends from solution is indicative of interchain crosslinking, which suggests mixing of the components may be occurring on a molecular level.

5.1.2 Dynamic Mechanical Analysis

The compatibility of sPS/P2VP solution blends was examined by dynamic mechanical analysis through evaluation of the glass transition. The utility of a miscibility evaluation by glass transition temperature (T_g) studies in the sPS/P2VP system is limited by the proximity of the transitions of the blend components. However, there have been some recent studies involving ionic interactions between sulfonic acid and pyridines in which intermolecular crosslinking was found to increase the T_g of the blends above the T_g's of either of the blend components [62,63,112]. Crosslinking is also known to produce other changes in the dynamic mechanical behavior. The aim of the dynamic mechanical study was to evaluate changes in the glass transition and

post-glass transition behavior which may indicate interchain crosslinking.

The complex modulus was measured as a function of temperature for sPS/P2VP blends in the 80-140 °C range. The tensile storage modulus (the real part of the elastic modulus) and the loss tangent (tan δ) versus temperature data for the PS/P2VP, PS-3.37SO_3H/P2VP and PS-6.91SO_3H/P2VP solution blends are shown in Figures 5.2-5.4 along with the data from their corresponding blend components. The transition behavior of the unreactive blend does not differ much from that of the corresponding PS and P2VP components. In the reactive systems, there are two aspects of the blend behavior which differ from that of the blend components; 1) the transition in the blends is clearly broader than in the pure components, and 2) the post-transition plateau modulus of the blends is higher than either of the blend components. The magnitude of these effects is a function of blend reactivity, as shown in Figure 5.5. The broadening effect is common to blends (and copolymers) in which the phases are separated on a very fine scale, on the order of tens of nanometers or less [113,114]. Broadening of the glass transition has also been observed for ionically crosslinked materials, and is attributed to a reduction in the primary relaxation rates of the ionomer [111]. Increases in the post-transition plateau modulus are similarly indicative of crosslinking as predicted by Gaussian rubber elasticity theory [110,115,116]. Thus the dynamic mechanical behavior is consistent with the behavior expected from a system with interchain crosslinking through ionic interaction.

Several recent investigations into ionically interacting systems have correlated the degree of crosslinking in blends to shifts in the transition temperatures [62,63,112]. The transition temperature in a crosslinked polymer may be related to the crosslink density by:

$$\frac{T_g(X) - T_g(0)}{T_g(0)} = \frac{KX}{1 - KX} \qquad (5\text{-}1)$$

where $T_g(X)$ is the glass transition temperature of the crosslinked polymer, $T_g(0)$ is the Tg of the linear polymer, K is a universal constant, and X is the mole fraction of crosslinking sites [117, 112]. Equation (5-1) may be used to predict the T_g of a crosslinked system if the concentration of crosslinking points is known, or conversely, the number of crosslinks may be estimated from the measured transition temperatures. A good example of the latter case was provided by Huglin, et. al. [62,63] who observed an increase in the transition temperature of about 50 °C due to ionic interaction in the fully interacting system poly(vinyl pyridine)/ poly(2-acrylamido-2-methylpropanesulfonic acid), and used the T_g shift to estimate the number of crosslinks in this reactive system. The former case was employed by Smith and Eisenberg who found good agreement between measured and predicted transition temperatures in polystyrene-co-4-vinylpyridine /sPS blends [112]. In the present study, the transition temperature shift was similarly predicted from the acid concentrations using an estimate for the unreactive blend T_g's from the Fox equation:

$$\frac{1}{T_{g_{blend}}} = \frac{W_1}{T_{g1}} + \frac{W_2}{T_{g2}} \qquad (5\text{-}2)$$

where W_i and T_{gi} are the weight fraction and T_g of the blend components, respectively [118]. The onset of T_g and T_g estimates from the peak in tan δ have been made from the dynamic mechanical spectra (Figure 5.6), and are

listed in Table 5-I. The predicted $T_g(0)$ from Eq. (5-2) and $T_g(X)$ from Eq. (5-1), both of which were calculated from the tan δ transition temperature with K=1.0 are also listed in Table 5-I. The predictions for $T_g(X)$ are sensitive to the accuracy of the Tg(0) prediction from Eq. (5-2). In all cases, the transition temperature of the reactive blends are falling between the average value predicted by the Fox equation and the calculated value for a crosslinked blend, which implies less than complete conversion of all reactive groups and/or the dissociation of ionic bonds near the glass transition temperature. The onset T_g values (see Figure 5.6 for definition) are included in the table to emphasize the effect of the choice of definition for the transition temperature. Onset transition temperatures for the blends fall within the range of those measured for the blend components, which is a consequence of transition broadening. The difference between the onset T_g and the T_g from the peak in tan δ may be used as a measure of transition breadth, and quantifies the increase of the broadening effect with reactivity.

5.1.3 Small Angle X-Ray Scattering

A small angle x-ray scattering (SAXS) study was undertaken to further investigate the structural characteristics of sPS/P2VP solution blends. The methods employed allow for probing of the structure on the size scale of about 1-200 nm. In addition, analysis of the decay of the scattered intensity at large scattering vector may yield information about the interphase interfaces in two phase blends.

Plots of the scattering function (I(Q)) versus the scattering vector (Q) for all solution blends are shown in Figure 5.7. (Q is the scattering vector defined as $Q=(4\pi/\lambda)\sin\theta$ where λ is the radiation wavelength and θ is the scattering

angle.) The most significant feature of the scattering curves is the presence of a very diffuse scattering peak from some of the reactive blends, the position of which is dependent on the level of reactivity. The characteristics of this scattering feature are further defined in Table 5-II, in which the dimension of the feature responsible for the scattering (d_{PEAK}) is estimated using the relation $d_{PEAK}=2\pi/Q_{PEAK}$.

There is some question as to the origin of the scattering feature. Sulfonated polystyrene belongs to a class of polymers often referred to as ionomers which have ionic groups incorporated along the polymer chain. sPS ionomers are generally studied in the ionic salt form, where the acid group has been neutralized with a mono- or divalent metal cation. The appearance of a diffuse peak in the 1-3 nm^{-1} region is a common feature of scattering from neutralized sPS ionomers, and has been attributed to clustering and aggregation between acid groups with the corresponding counter-ions. The intensity of the scattering maxima in ionomers is dependent on the type of counter-ion used and the acid content in the material [80, 119-123]. In the free acid form of sPS the acidic hydrogen may act as the counter-ion and produce relatively weak aggregation effects, though the acid level at which this first occurs has not been unambiguously identified [119]. The scattering behavior of the sPS components must therefore be evaluated in order to determine which features of the sPS/P2VP blend scattering are attributed to the sPS component, and which are unique to the blends.

The scattering was measured from the sPS ionomers used in this study for comparison with the blend scattering behavior and the result is shown in Figure 5.8. There is no appreciable scattering maximum in sPS with $\leq 5.56\%$ acid functionality. A weak scattering peak is apparent in the characteristic

range for sPS in which the acid content is ≥ 6.91 %. The peak intensity increases and the peak position shifts towards higher scattering vector (smaller size) as the acid content increases.

The combined results of sPS and sPS/P2VP blend scattering for PS-9.50SO_3H and PS-15.0SO_3H materials are shown in Figure 5.9. In both of these cases, the scattering maxima which is present in the sPS component is suppressed in the blend. Similar behavior has been reported by Douglas, et. al., [124] who observed complete suppression of the zinc neutralized sPS (ZsPS) ionomer peak due to blending with either poly(styrene-co-4-vinyl pyridine) or poly(ethyl acrylate-co-4-vinyl pyridine) at reactivity levels of up to 7.25 mole % acid. Lu and Weiss also reported suppression of the ionomer peak in ZsPS due to blending with nylon 6 [54]. This behavior has been related to changes in the dielectric constant of the medium surrounding the sulfonate group due to mixing of the components at the segmental level, which decreases the electrostatic force between the ion pair resulting in decreased aggregation [54,124]. The dielectric constant of P2VP is larger than PS, thus mixing would increase the average dielectric constant of the medium and decrease the attractive forces between sulfonate groups [125]. However, in this system it is more likely that the reaction between sulfonic acid and pyridine leaves less acid groups free to form aggregates in the sPS phase which results in suppression of the ionomer peak.

The scattering behavior of blends in which the acid content is ≤ 6.91% differs from that observed for the higher acid content materials. There is clearly a scattering maxima in the PS-6.91SO_3H/P2VP blend, and its intensity is higher and its position at lower Q than the ionomer scattering peak from PS-6.91SO_3H (Figure 5.10). The shoulder on the high intensity peak at low Q for the PS-3.37SO_3H/P2VP and PS-5.56SO_3H/P2VP blends is apparently the

result of similar scattering and occurs despite the lack of any ionomer peak in the corresponding sPS components (Figures 5.7 and 5.8). It is possible that the pyridine nitrogen is acting as a counter-ion in these lightly sulfonated materials and causing ionic clustering in the blends. The use of amine counter-ions was previously found to be effective in generating changes in the viscoelastic behavior of sPS characteristic of clustering [111]. However, the effectiveness of amine counter-ions was also found to decrease with increasing 'bulkiness' of chemical groups bonded to the amine nitrogen, and sufficiently large groups were found to be less effective at promoting clustering than the hydrogen counter-ion of the free acid. This result implies that the steric effects involved in clustering using a polymeric amine counter-ion would prohibit ionic clustering. In addition, there is no reason why the pyridine counter-ion should be ineffective at sulfonate contents greater than 6.91 %, on the contrary, the aggregation induced scattering should continue to increase with acid content, which is clearly not the case. Therefore, it is likely that the scattering maxima and shoulder observed for the blends with $\leq$ 6.91 % SO_3H is not representative of ionic clustering.

A second possibility for the origin of this low angle peak in the PS-6.91SO_3H/P2VP, PS-3.37SO_3H /P2VP and PS-5.56SO_3H /P2VP blends is that it is representative of segregation of the sPS and P2VP components. If this is the case, the 'phase separation' must be occurring on an extremely fine scale, on the order of ~5-10 nm (Table 5-II). For comparison, the radius of gyration of a single PS chain in this system is ~13 nm, while the radius of gyration for a chain of length equal to the average length between reactive groups is 1.6 nm, 1.2 nm, and 1.1 nm for 3.37, 5.56, and 6.91% styrene sulfonic acid, respectively. Therefore phase separation is potentially occurring on a scale which is smaller than the length of a single chain, but larger than the distance between reactive

acid sites. In this case, the best model for the blend structure is a network with randomly placed interchain crosslinks in which the segments between the links are segregated. The shift of the scattering peak towards lower Q (larger size) with decreasing reactivity is in agreement with this structural picture. This type of structure has been proposed for ionically crosslinked blends [39], but has not previously been identified experimentally. The absence of a maximum in the higher acid content blends may be due to the limited scattering range which was available for the study of these blends and/or to interference by the scattering of clustered acid groups (hydrogen 'counter-ion') in the sPS component.

A Porod analysis of the scattering of sPS/P2VP blends was also undertaken with the aim of assessing the effects of reactivity on interfacial thickness in the blends. Porod's law states that the scattered intensity from a two-phase system with infinitely sharp boundaries should decrease in proportion to the fourth power of the scattering vector as the scattering vector approaches infinity:

$$\lim_{Q\to\infty}[I(Q)] = \frac{K_p}{Q^4} + I_b \qquad (5\text{-}3)$$

where I_b is the background scattering from concentration fluctuations within the phases and K_p is the Porod constant which is related to structural parameters of the system [126,127]. Deviations from Porod behavior occur in real systems due to finite interfacial width which results in the scattering at high angles decreasing more slowly than the Q^{-4} power law prediction of Eq. (5-3). The observed scattered intensity may be considered a sum of the scattering from an ideal two-phase system which has been modified by an

interfacial smearing function and contains a contribution from background scattering [127]. Analysis of the scattering from real systems from which the background scattering (I_b) has been subtracted yields information about the smearing function which is related to the interfacial structure. The data analysis in somewhat subjective, as the form of the interfacial smearing function is dependent on the type of interfacial gradient assumed, and there are several methods of correcting for the background scattering [127,128]. For the present purposes background scattering is assumed constant and equal to the plateau intensity at high angle (Figure 5.7), and a sigmoidal gradient model (Gaussian smoothing function) is adopted for the interface.

The Porod analysis is applied to sPS/P2VP blends with reactivity from 0-6.91%, for which sufficient unobstructed high angle data was available to make a reasonable correction for the background scattering. The high angle intensity should follow a relation of the form [127]:

$$I(Q) = \left(\frac{K_p}{Q^4}\right)\exp\left(-4\pi^2\sigma^2Q^2\right) \qquad (5\text{-}4)$$

where the exponential term is the square of the Gaussian smoothing function employed to approximate a sigmoidal gradient deviation from the step function across ideal boundaries. σ is the half width of the smoothing function and is a measure of the interfacial width. Based on Eq. (5-4) a plot of $I(Q)Q^4$ versus Q^2 allows for determination of σ from the slope at high Q. An example is illustrated in Figure 5.11. Values of the interfacial width calculated from the slope at high Q ($\sigma = \sqrt{-\text{slope} / 4\pi^2}$) are listed as a function of blend reactivity in Table 5-III. The calculated absolute values for the interfacial width are too small to be physically realistic, probably due to extreme

sensitivity to the background correction. However, the analysis was performed in a self-consistent manner and a comparison of the relative magnitudes of the interfacial widths should be meaningful.

There is a maximum in the relation between interfacial thickness and blend reactivity which was somewhat unexpected. Adding a small amount of reactivity broadens the interface to nearly twice the thickness of the unreactive interface. Increasing the acid content enhances the effect up to a point, after which the interface begins to narrow. The behavior may be explained in terms of diffusive effects. The addition of reactivity to the system results in the formation of interchain grafts. The newly formed sPS-co-P2VP copolymers cannot separate from each other completely due to the physical crosslink resulting in a thicker interfacial layer in which dissimilar chains are in contact. As the reactivity increases, the potential for multiple grafts per chain also increases, resulting in the formation of a highly crosslinked interfacial barrier which prevents any interdiffusion of dissimilar polymers yielding a sharper interface. Similar effects have been observed at reactive interfaces in other systems [49]. This trends is also consistent with the interfacial toughening study discussed in the next section.

It is possible to make an estimate of the actual interfacial thickness as a function of reactivity from the ratio of $\sigma_{reactive}/\sigma_{unreactive}$ and properties of the unreactive system. According to the theory by Helfand [12,13, Section 2.1.2.1], the interfacial width, a_I, is related to the interaction parameter, χ, and the polymer step length, b, according to the relation:

$$a_I = \frac{b}{\sqrt{6\chi}} \qquad (5\text{-}5)$$

The value of the PS/P2VP interaction parameter may be calculated from the empirical relation ([129], Section 2.2.1):

$$\chi_{PS/PVP} = -0.033 + \frac{63}{T} \qquad (5\text{-}6)$$

where T is the absolute temperature. Using the a step length of 0.7 nm [105] and $\chi_{PS/P2VP}$=0.18 at 25 °C (the blend preparation temperature), the estimated interfacial width from Eq. (5-5) for the unreactive blend is ~1.6 nm. Letting $\sigma_{unreactive}=a_I$=1.6 nm, one may calculate interfacial thickness for the reactive blends from the $\sigma_{reactive}/\sigma_{unreactive}$ ratio, and estimate the interfacial thickness in the reactive blends to be ~2-3 nm. This range is typical for interfaces between immiscible polymers[12,13], and the reactive interfaces would ordinarily be considered relatively sharp. In light of the scale of phase separation in this system, however, these thickness are relatively large and the boundaries are relatively diffuse.

5.2. Adhesion at Ionically Reinforced sPS/P2VP Interfaces

The interfacial toughness of sPS/P2VP interfaces was evaluated as a function of reactivity using the asymmetric double cantilever beam (ADCB) test, as discussed in Section 3.3. The ADCB test allows for direct investigation of interphase adhesion by isolation of the interface in a model geometry. Interphase adhesion is quantified through measurement of the strain energy release rate for interfacial failure, G_c, which is a measure of the amount of energy per unit crack surface area that is available for crack extension. Throughout the discussion, the term interfacial toughness will be used in reference to the critical energy release rate, G_c.

5.2.1. Bilayer Asymmetry

Preliminary testing was performed to determine the effects of bilayer asymmetry on interfacial toughness, as discussed in Section 3.3. It is necessary to measure G_c in the minimum toughness region to insure that the measurement reflects true interfacial adhesive properties rather than off-interface cohesive failure. Previous studies of the unreactive PS/P2VP system have determined the minimum toughness region to occur in the range of h_{PS}/h_{Total}~0.59-0.65 [25]. Measurement of the toughness of the unreactive interface between the brands of PS and P2VP polymers employed in this study has yielded similar values of G_c in the same thickness ratio range, indicating h_{PS}/h_{Total}~0.6 is near the correct geometry for measurement of interfacial properties. The proper thickness ratio is determined both by the relative moduli and deformation strengths of the two materials. Though the modulus does not appear to be significantly affected by sulfonation (Section 3.3), the strength does show some dependence (Figure 5.12), which suggests the G_c-thickness ratio dependence could be different at different sulfonation levels. For this reason, the toughness of all sPS/P2VP pairs was evaluated as a function of thickness ratio over a limited range in the vicinity of the expected minimum. Typical results (Figure 5.13) have demonstrated that the minimum toughness or proper asymmetry range occurs at h_{PS}/h_{Total}~0.57-0.62 for all polymer pairs. Any attempt at testing the strongest interfaces outside of this thickness ratio range resulted in beam failure rather than interfacial failure.

5.2.2. Toughness of Reactive sPS/P2VP Interfaces.

The addition of reactivity to the PS/P2VP system creates substantial

reinforcement of the interface. For example, the adhesion at the interface between PS-1.67SO_3H and P2VP is on average three times that of the unreactive PS/P2VP interface. More significantly, the interfacial toughness continues to increase as the functionality of the system increases, reaching as high as ~350 J/m^2 for the strongest interface measured, as compared to <2 J/m^2 in the unreactive pair. This behavior is the direct result of interfacial reinforcement due to copolymer formation. This study represents the first successful demonstration of interfacial toughening by reactive methods, and also the first demonstration of improving adhesion at model immiscible interfaces using ionic interactions. In-situ reinforcement of this magnitude at immiscible interfaces is unprecedented.

Studies of the toughening of sPS/P2VP interfaces have shown that G_c is dependent on several properties of the system, specifically reactivity, molecular weight of the components, and the conditions under which the compatibilizing copolymers are formed. The effects of increasing reactivity at the sPS/P2VP interface are illustrated in Figure 5.14 and 5.15. There is clearly an optimum reactivity for reinforcement in this system. Interfacial toughness increases with the acid content at an increasing rate until reaching the optimum, after which the toughness decreases rapidly into a regime where G_c is relatively insensitive to changes in the system reactivity. The reactivity corresponding to optimum toughening is sensitive to the molecular weight of the component polymers. A comparison of Figures 5.14 and 5.15 shows that the maximum G_c occurs at higher reactivity for higher P2VP molecular weight. (Note: The P2VP's were obtained from different suppliers and there may be differences between the materials other than molecular weight due to different processing; see Section 3.1.1.) The position of the maximum does not seem to be affected by the interfacial bonding conditions; however, the

magnitude of G_c at the peak is clearly increased with extended bonding time, as illustrated in Figure 5.16. This effect in turn seems to be a function of system reactivity, becoming more important as the reactivity increases. Each of these effects gives some insight into the mechanisms responsible for reactive reinforcement of the sPS/P2VP interfaces.

5.2.3. Fractography

The fracture surfaces of sPS/P2VP interfaces were investigated by scanning electron microscopy in order to attempt to gain some insight into the failure mechanisms. Fracture surfaces of lightly sulfonated sPS/P2VP interfaces do not show much evidence of damage at magnifications up to ~2000x, the highest magnification at which the surfaces could be clearly resolved (Figure 5.17a). Once the reactivity becomes high enough to generate a toughness of ~50 J/m^2 the interfaces show evidence of large scale plastic deformation (Figure 5.17b). This characteristic persists out to the highest reactivity levels, even when the toughness decreases significantly.

The scanning electron micrographs suggest that the failure is wandering off of the interface and into the pure components on either side. This possibility was further investigated by wavelength dispersive spectroscopy (WDS), to determine the chemical composition on the fracture surfaces from which the fracture path may be evaluated. The procedure is to inspect both halves of the fractured bilayer for evidence of the 'wrong' component on the fracture surface which would indicate that the crack path has wandered from the interface. Sulfur is readily detected using WDS and was used as a signature for sPS detection. The P2VP is composed only of light elements (C,N,H) which could not be detected by the instrument available. For this reason, the sPS beams were stained with iodine which reacts

exclusively with the pyridine nitrogen and may be used to detect the presence of P2VP (see Section 3.2.1.1). Low magnification scanning electron micrographs of the fracture surfaces from either side of a PS-6.91%SO_3H/P2VP interfacial failure are shown in Figure 5.18, in which parts a) and b) are of the same region on either side of the interface and are therefore mirror images of one another. Corresponding areas are marked with numbers for clarity. The fracture surfaces show that the damage is more concentrated on the sPS side, which is to be expected, as the crazing stress of sPS is lower than of P2VP (Table 3-III, [25]). There are also many features which are common to both sides of the interface. It is in these regions that the crack is traveling away from the interface. The x-ray maps, Figures 5.18c and 5.18d, illustrate the crack wandering effect. The bright spots on the iodine map from the sPS image indicate areas where P2VP is adhering to the sPS surface. Similarly, the bright sections on the sulfur map of the P2VP side indicate regions where sPS is adhered to the P2VP surface. Clearly, once the interface becomes strong enough the failure occurs both adhesively and cohesively, as the crack propagates both along the interfacial plane and into the material surrounding it. Interfaces reinforced with excess acid (9.50 and 15.0%) similarly fail by a combination of adhesive and cohesive failure. In these cases however, the near interface crack propagation appears to create much less damage (Figure 5.19) and the relative proportion of interface to off-interface failure is increased. The fractography suggests that once the system reactivity becomes high enough, the interface is no longer the weakest link, causing the fracture path to wander from the interface.

5.2.4. Toughening Mechanisms

In the present investigation reinforcing copolymers are formed in-situ at the interface from long chain polymer precursors. The average degree of polymerization of both component polymers is N~2000 which is large in comparison with the entanglement molecular weights, N_e~ 260 for P2VP and N_e~ 170 for PS [25]. Interchain reaction will result in copolymers having a minimum of one segment per side with $N > N_e$, and therefore copolymers should be effectively entangled with chains in the bulk material on either side of the interface. Under these conditions, the chain pull-out mechanism of interfacial failure is not expected to dominate, and therefore interfacial failure is most likely occurring by the chain scission or crazing mechanisms (See Section 2.2.2.2.1). It should be noted that all polymers utilized in this study were of a commercial grade and are polydisperse. Consequently all polymers contain some fraction of chains with degree of polymerization in the range of N_e which may pull-out from the interface during failure under conditions of low areal density of copolymer chains at the interface, Σ.

The model of Xu, et. al. ([24], Section 2.2.2.2.1, Figure 2.2) predicts that in the chain scission regime with low interfacial joint density the stress on the interface builds in direct proportion to the number of interfacial bonds. In the reactive sPS/P2VP system the number of interfacial bonds should be directly proportional to the concentration of acid groups. G_c increases due to the additional energy required to break the interfacial copolymer bonds during failure. In the chain scission regime, a linear dependence of G_c on the number of interfacial bonds has been experimentally observed [65]:

$$G_c \sim \Sigma \qquad \text{chain scission regime}$$

Once the stress generated on the interface by the bonds exceeds the crazing

stress in either of the polymers the crazing regime is entered. A craze is a region of heavily voided material that forms ahead of the crack tip in which the voids are separated by fibrils capable of sustaining load. The formation of a craze requires plastic work and increases the energy of fracture [130]. Brown has used localized crack-tip mechanics to model the relationship between the craze microstructure and the fracture toughness [22]. He has shown that the crack opening displacement at the ultimate fibril in the craze, which is directly related to G_c, is proportional to the square of the fibril failure stress, σ_f^2. The stress to break a fibril is in turn directly proportional to the number of entangled strands per unit area within the fibril, Σ. Therefore, $G_c \sim \sigma_f^2$ and $\sigma_f \sim \Sigma$ leading to $G_c \sim \Sigma^2$ (See [22] for the complete derivation).

$$G_c \sim \Sigma^2 \qquad \text{crazing regime}$$

This theoretical relationship between G_c and Σ^2 has been experimentally confirmed [22, 25, 65, 67]. The models of interfacial toughening do not account for the decline in toughness at high reactivity. This region of the G_c versus reactivity relationship will be dealt with separately below.

The toughening mechanisms in the reactive sPS/P2VP system may be evaluated using the scaling relationships discussed in the preceding paragraph by making use of the direct correlation between the areal density of copolymers formed at the interface and the functionality of the sPS surface (Appendix D). For reactive interfaces in the regime where failure is occurring by chain scission, G_c has been found to scale with Σ, and is therefore expected to scale directly with the concentration of sulfonic acid in the system: $G_c \sim [C_{SO_3H}]$. In the crazing regime, G_c has been predicted to scale as Σ^2, and is therefore expected to scale with the square of the acid concentration in the

sPS/P2VP system: $G_c \sim [C_{SO_3H}]^2$. Power law fitting of the data illustrated in Figures 5.14 and 5.15 has shown the scaling exponent, n ($G_c \sim [C_{SO_3H}]^n$), to be greater than n~1 even at the lowest reactivity levels. The best fit to the interfacial toughness versus reactivity curve shows that the experimental scaling is (Figure 5.20):

$$G_c \propto [C_{SO_3H}]^{1.9\pm0.3}$$

for the region where G_c is increasing with reactivity. The power law exponent is close to the predicted exponent n=2 and indicates that crazes are forming as a result of interfacial strengthening by copolymer formation, resulting in the observed large increases in interfacial toughness. The measured values of toughness also support the assertion that a major energy dissipation mechanism is activated in this system. Previous investigations in block copolymer reinforced systems have shown that the interfacial toughness does not exceed ~15 J/m^2 when chain scission in the active failure mechanism [25,65].

There are several features of the physical reinforcement scheme for the reactive sPS/P2VP system which are very different from the previous studies in traditionally compatibilized systems and should be considered in terms of their impact on the interfacial toughening. First, the copolymers are joined by an ionic bond, the strength of which should be lesser than a covalent bond, which would imply that a higher interfacial bond density would be necessary to induce crazing at the interface. The results discussed above indicate that crazing has been activated at the lowest reactivity level measured, corresponding to ~0.05 bonds/nm^2. Crazing at interfaces reinforced by long,

covalently bonded, block copolymers is known to be activated beginning at bond concentrations of ~0.02-0.03 nm^2 [25,67]. Thus though the ionic bonds should be weaker, they are still effective at generating interfacial stress. The apparent discrepancy may be explained by noting that the stress needed to break a polymer chain is a function not only of bond dissociation energy but also depends on thermal motion of the chain, which has been shown to reduce the contribution to the apparent strength from the dissociation energy by ~40% in a typical system [131]. A lower bound estimate for the energy to break the ionic bond may be made from an estimate of the copolymer bond density and the crazing stress using the relation (Section 2.2.2.2.1, [24]):

$$f_b = \frac{\sigma^{craze}}{\Sigma^{transition}} \qquad (5\text{-}7)$$

where the crazing stress may be approximated by the flexural stress. For the sPS/P2VP system the flexural stress is ~58 MPa (Table 3-III) and $\Sigma^{transition}$ must be less than the areal bond density at the lowest reactivity level, ~0.05 chains/nm^2 (Appendix D), leading to $f_b > 1.2$ nN for the ionically bonded chain which is in the same range as measurements and predictions for covalently bonded chains [25,131].

A second important difference between reactively reinforced sPS/P2VP interfaces and traditionally reinforced interfaces is in the architecture of the copolymer chains themselves. Previous studies have concentrated on adding nearly monodisperse diblock copolymers to an interface where they extend into the component polymers forming an interfacial brush. The situation is geometrically different at the reactive interfaces. The bonding site between a sPS chain with randomly placed reactive groups and a fully reactive P2VP

chain has an equal probability of occurring at any position along either molecule, leading to copolymers with the architecture of a star with four unequal arms. In addition, it may be possible for multiple bonds to occur along a given chain, forming loops rather than tethered junctions (the probability of loop formation is discussed more fully below). In either case, from each interchain bond there will be two strands (or blocks) per side as compared to only one per side with diblock reinforcement. The number of strands per side per bond which are long enough to provide effective reinforcement ($N > N_e$) will be dependent on the position of the bonding site relative to the end of the chain. For chains with N~2000 where N~260 leads to effective entanglement, approximately 75% of all bonds will have two segments long enough to provide reinforcement by entanglement with chains in the bulk. The higher density of entangled strands may be expected to lead to more effective strengthening in the reactive system. This appears to be the case, as the highest interfacial toughness reported for traditionally compatibilized PS/P2VP interfaces is ~120 J/m^2 [25], while toughness of reactive sPS/P2VP interfaces reached a maximum of nearly three times as high, G_c~350 J/m^2, under conditions where the average length of reinforcing strands should be similar. This effect may be related to the possibility of generating more copolymer at the reactive interface than may be maintained at a traditionally compatibilized interface. The maximum amount of diblock copolymer which may be used to strengthen an interface is limited by the formation of organized copolymer structures, such as lamellae or micelles. The formation of organized structures from the ionically grafted copolymers generated at the sPS/P2VP interface is unlikely, due to the complicated architecture of the molecules which cannot reconfigure or diffuse readily. Thus, despite the fact that copolymers in the reactive system are formed by

ionic bonding, the interfacial reinforcement of PS/P2VP interfaces via the reactive scheme appears to be a more effective route to interfacial strengthening than traditional compatibilization via block copolymers.

The remainder of the discussion will be concerned with the factors influencing the decline of toughness at high reactivity levels. Similar behavior has been observed by previously at PPO/PMMA interfaces reinforced with PS-co-PMMA diblocks [65,67], but the toughness decline in that system was attributed to the formation of copolymer lamellae at the interface, a situation which is unlikely for ionically crosslinked copolymers of complicated architecture. In this system, the drop-off is probably due either to changes in the material properties as a function of acid level or to ineffective entanglement, each of which will be discussed in turn.

Changes in the material properties with sulfonation are illustrated in Figure 5.12 which shows the sharp decline in flexural strength of sPS once the acid level exceeds ~7%, a trend which has also been observed in neutralized sPS ionomers [133]. The measured values of flexural stress reported in Table 3-III for sPS are not significantly different from crazing stress measured previously for PS and P2VP in flexure [25], and give a reasonable approximation to the crazing stress. The models of Hui and Brown [22, 77] predict that G_c should increase with decreasing crazing stress, which is clearly not the case for sPS/P2VP interfaces (Section 2.2.2.2.1, Eqs. (2-10) and (2-11)). However, the models also predict that G_c is a function of craze microstructure, through the fibril diameter and the draw ratio, which may be affected by sulfonation or ionic clustering. Though there is some evidence that craze structure may be altered by ionomer clustering in neutralized sPS ionomers [134], the effects of ionic clustering on properties of ionomer glasses are not known with sufficient accuracy to speculate further on this point. The

clustering tendency itself, which becomes significant at high acid levels (Section 5.1.3) may have some effect on the toughness in that clustering of acid groups may leave a lesser number free to react with the P2VP resulting in lower areal chain density of copolymers formed. In either case, if the properties of the sPS were wholly responsible for the decline in toughness at high acid content, the decline would be expected to occur at the same level regardless of the P2VP molecular weight, which does not appear to be the case (Figures 5.14, 5.15). Therefore it is unlikely that property changes in the sPS materials due to increasing functionality are fully responsible for the observed decline in G_c at high reactivity level.

In order to more fully understand the toughening behavior at high reactivity it is necessary to consider the geometry of the grafted copolymer layer and how it may change as a function of grafting density. The are two ways in which increasing the areal density of grafts may result in a decrease in the toughening behavior. First, as the grafted layer becomes more dense, the probability that grafted chains become entangled with each other rather than with chains in the bulk polymer may increase, in which case they will not contribute to interfacial toughening. Second, the molecular weight between grafts could become less than the molecular weight necessary for entanglement with chains in the bulk polymer due to multiple grafts along a single chain (Figure 5.21). The first case has been addressed by using the self-consistent mean field theory for interfacial block copolymer segregation developed by Schull and Kramer [25,140]. The analysis showed that the number of grafted sites resulting an effective entanglement increased with the number of grafting sites only up to a point, after which increasing the areal copolymer density did not lead to additional effective entanglements. Numerical simulations also showed that the number of effective

entanglements could be expected to increase up to higher grafting density for long copolymer chains than for shorter copolymer chains. This prediction agrees qualitatively with the results observed for the sPS/P2VP system, in which the declining toughness regime was reached at lower sulfonation when a lower molecular weight P2VP was used (Figures 5.14, 5.15). It therefore is likely that entanglement between grafted chains is occurring at the higher reactivity levels and contributing to the change in the relationship between G_c and reactivity at highly functional interfaces.

The importance of the second route to ineffective entanglement, the multiple grafting case, may be evaluated by making an estimate of the number of grafts per chain using a theory describing chain conformations near a surface. Creton, et. al.[25] have demonstrated that the minimum degree of polymerization for effective interfacial strengthening in the PS/P2VP system must be N~500, which sets the limit for effective entanglement at an average of ~4 contacts per chain. The number of contact points, n_c, of a Gaussian chain with a neutral surface is proportional to the square root of the degree of polymerization of the chain [135-139]:

$$n_c = \alpha\sqrt{N} \qquad (5\text{-}8)$$

where the prefactor, α is dependent on the degree of certainty of the number of contacts. One may state that there is a 90% probability that the number of surface contacts for a given chain will be at least $n_c \sim 0.125*(2000)^{0.5} \sim 6$ [139]. Assuming the initial number of reactive contacts is $n_{rc} \sim [C_{SO_3H}]n_c$ leads to n_{rc}~0.10, 0.20, 0.33, 0.41, 0.60, 0.90 at reactivity levels of 1.67, 3.37, 5.56, 6.91, 9.50, and 15.0%, respectively. Therefore at initial contact, Eq. (5-8) predicts that there will be less than one reactive contact site at the surface per chain and no

multiple grafting. The situation may be quite different given sufficient time for copolymer bonding. DiMarzio and McCrackin [139] have shown that polymers tethered at one end (grafted) may have tens to hundreds of additional contacts with a surface if the surface adsorption energy is attractive. It is difficult to estimate the adsorption energy in a system such as sPS/P2VP in which the adsorption of a sulfonic acid group on a pyridine surface is energetically favorable while the energy between PS and P2VP groups is repulsive, though the average should become more attractive with increasing acid concentration. The SAXS results discussed in Section 5.1.3 have shown that the interphase interfaces in sPS/P2VP solution begin to narrow at higher reactivity levels, suggesting that interfacial gelation (multiple grafting) is occurring. Thus it is reasonable to assume multiple grafting effects contribute to the decline in toughness at high reactivity levels. It is difficult to assign the toughness decline to any one factor, but it appears as if ineffective entanglement is at least partially responsible. Changes in material properties, such as degraded mechanical properties and ionic clustering, may also play a role.

5.3. Miscibility Study in the sPS/PS System

Sections 5.1 and 5.2 have clearly established the utility of sPS as a reactive compatibilizer in systems involving a pyridine counter-ion, both in controlling the phase separation and as an interfacial strengthening agent. Previous studies in the literature have also indicated that strong interactions exist between sulfonic acid and other nitrogen containing moieties, such as amide and amine groups [53, 132]. The interactions tend to be very strong, and result in dramatic changes in the blend microstructure. For many

applications the goal is not to refine the microstructure to the smallest possible scale, but to achieve a second phase dispersion of a specific size. In these cases it may be desirable to dilute the sPS component with unreactive PS, in order to 'fine tune' the microstructure. For this scheme to be effective it is necessary that the sPS be miscible with PS. It is not uncommon for copolymerization to cause changes in the miscibility of blends, and a recent example has specifically identified copolymerization with sulfonic acid to cause immiscibility [141]. For this reason, the effect of sulfonation on miscibility in blends of PS and lightly sulfonated PS was experimentally evaluated. PS-1.67SO_3H/dPS mixtures were prepared in a range of concentrations spanning 5 dPS/95 sPS to 95 dPS/5sPS and studied by small angle neutron scattering (SANS) (Sections 3.1.2.3 and 3.2.1.2). A comparison of the experimental scattering behavior with expected behavior from one phase systems and two phase systems was used to determine if sPS/dPS blends are single phase or phase separated. SANS is uniquely suited for a study of miscibility in the system PS/sPS because it discriminates between the components on the basis of isotopic labeling rather than by changes in physical properties which may be small between PS and lightly sulfonated PS.

The physical state of polymer blends may be determined from SANS experiments through analysis of the scattering function which describes the relation between the scattered intensity and the scattering vector. The scattering function is, in general, distinctly different for one phase and two phase systems. In a miscible, binary system not too far from the phase separation point, scattering will arise as the result of fluctuations in local concentration [142]. The relationship between the scattering function and the structure in such a single phase, binary, interacting system (miscible blend) is

given by the Orstein-Zernike equation [143,144]:

$$I(Q) = \frac{I(Q=0)}{\left[1+\xi^2(T,\phi)Q^2\right]} \qquad (5\text{-}9)$$

where $\xi(T,\phi)$ is the correlation length of the concentration fluctuations at temperature T and composition ϕ, and is related to the interaction parameter χ, the blend composition, ϕ, and the degree of polymerization of the components. Equation (5-9) may be written in the form:

$$\frac{1}{I(Q)} = \frac{1}{I(Q=0)} + \frac{\xi^2(T,\phi)}{I(Q=0)}Q^2 \qquad (5\text{-}10)$$

which demonstrates the linear relationship between $1/I(Q)$ and Q^2 for scattering from a singe phase system in the limit of small Q.

The expected relation between scattered intensity and scattering vector is considerably different for a phase separated blend. The scattering from a two phase system will arise due to differences in scattering length density between the two phases and from the length scale over which these fluctuations occur [145]. A simplified form of the scattering intensity for a randomly dispersed, two phase system with sharp interfaces in the small Q limit has been given by Debye and Bueche [146,147]:

$$I(Q) = \frac{\kappa\phi_1\phi_2 a^3}{\left(1+a^2Q^2\right)^2} \qquad (5\text{-}11)$$

where ϕ_i is the volume fraction of component i, κ is a constant related to the scattering contrast of the monomer species, and a is the correlation distance

which is a measure of the size of inhomogeneities. Eq. (5-11) may be represented in the form:

$$\frac{1}{\sqrt{I(Q)}} = \frac{1}{\sqrt{\kappa\phi_1\phi_2 a^3}} + \frac{a^2}{\sqrt{\kappa\phi_1\phi_2 a^3}} Q^2 \qquad (5\text{-}12)$$

which indicates that a plot of $1/\sqrt{I(Q)}$ versus Q^2 should be linear for scattering from a randomly dispersed, phase separated blend.

The experimental scattering intensity versus scattering vector plot for all PS-1.67SO_3H/dPS blends as a function of scattering vector are shown in Figure 5.22. The lower Q limit of the data range was approximately 0.04 nm^{-1} corresponding to a real space dimension of about 157 nm. Figure 5.23 illustrates the experimental scattering from the 5 dPS/95 PS-1.67SO_3H blend in the $1/I(Q)$ versus Q^2 form. This blend is representative of the behavior of the entire group of blends studied. The agreement between the experimentally measured small angle neutron scattering in the dPS/PS-1.67SO_3H system and the expected behavior for scattering from a single phase system is poor. In contrast, the agreement between the theory of scattering from two phase structures and the experimental results is excellent (Figure 5.24). A linear relation exists between $1/\sqrt{I(Q)}$ and Q^2 for all of the blends studied. This result clearly indicates that the system dPS/PS-1.67SO_3H is immiscible over the concentration range investigated.

From Eq. (5-12) one can see that the square root of the slope-to-intercept ratio from the linearized plot should be equal to the correlation length, which as stated above is an indication of the average size of the inhomogeneities responsible for scattering. The curves of Fig. 5.24 were fit with a linear regression to yield values for the slope and intercept which were used to

calculate the correlation length, a, and are listed in Table 5-IV. Due to the small magnitude of the intercept, the calculation of a is particularly sensitive to small errors in the intercept, and it was not possible to calculate meaningful values for all blends. The values that were obtained indicate that the correlation length is on the order of tens of nanometers or larger.

Though this scattering study determines unequivocally the phase separated nature of dPS/PS-1.67SO_3H blends, these results are somewhat surprising. With such a low concentration of sulfonic acid groups, it was not intuitively obvious that the blends should exhibit phase separation at all, particularly near the concentration extremes. This behavior indicates that the interaction parameter between styrene and styrene sulfonic acid is extremely large. It is possible to make a lower bound estimate for this interaction parameter by invoking the classical Flory-Huggins theory of phase separation [4] along with a copolymer blend modification to the interaction parameter. For a blend of homopolymer A and copolymer ($B_yC_{(1-y)}$)the total interaction parameter for the system may be represented by an effective blend interaction parameter [148,149]:

$$\chi_{blend} = y\chi_{A/B} + (1-y)\chi_{A/C} - y(1-y)\chi_{B/C} \qquad (5\text{-}13)$$

which, for this system with y=0.0167, reduces to:

$$\chi_{blend} = 0.0167\chi_{dS/S-s} + 0.9833\chi_{dS/S} - 0.0164\chi_{S-s/S} \qquad (5\text{-}14)$$

where the subscripts dS, S, and S-s represent the deuterated styrene, styrene, and styrene sulfonic acid monomers, respectively [see also 150-152]. In order

and styrene sulfonic acid the assumptions $\chi_{dS/S\text{-}s} \approx \chi_{S/S\text{-}s}$ and $\chi_i \neq \chi_i(\phi)$ will be used. $\chi_{dS/S}$ may be estimated from the results of Bates and Wignall [153] ($\chi_{dS/S} = 0.2T^{-1} - 2.9\times10^{-4}$) and takes the value of 1.94×10^{-4} at 140°C . The criterion that the interaction parameter for this system (χ_{blend}) must be larger than the value defining the single phase stability limit (binodal) is employed; ($\chi_{blend} \geq \chi_{binodal}$). The value of $\chi_{binodal}$ may be calculated for a blend of phases i and ii by setting the Flory-Huggins chemical potential ($\Delta\mu$) of species 1 (2) in phase i equal to the chemical potential of species 1 (2) in phase ii, and solving the resulting system of equations for χ [1]:

$$\frac{\Delta\mu_1^i}{RT} = \ln\phi_1^i + \left[1 - \frac{N_1}{N_2}\right]\phi_2^i + N_1\chi_{12}\phi_2^{i\,2} = \frac{\Delta\mu_1^{ii}}{RT} = \ln\phi_1^{ii} + \left[1 - \frac{N_1}{N_2}\right]\phi_2^{ii} + N_1\chi_{12}\phi_2^{ii\,2}$$

and

$$\frac{\Delta\mu_2^i}{RT} = \ln\phi_2^i + \left[1 - \frac{N_2}{N_1}\right]\phi_1^i + N_2\chi_{12}\phi_1^{i\,2} = \frac{\Delta\mu_2^{ii}}{RT} = \ln\phi_2^{ii} + \left[1 - \frac{N_2}{N_1}\right]\phi_1^{ii} + N_2\chi_{12}\phi_1^{ii\,2}$$

where

$$\phi_1^i + \phi_2^i = 1$$

$$\phi_1^{ii} + \phi_2^{ii} = 1$$

(5-15)

Equations (5-15) are readily solved by computer. For the most extreme case in this study, the 5dPS/95 PS-1.67SO_3H blend:

$$\chi_{binodal} = 1.76\times10^{-3}$$

and (5-16)

$$\chi_{blend} \approx 2.80\times10^{-4}\chi_{S/S-s} + 1.94\times10^{-4}$$

yielding:

$$\chi_{S/S-s} \geq 5.59 \qquad (5\text{-}17)$$

This value for $\chi_{S/S-s}$ is extremely large compared to typical values for polymer systems reported in the literature. $\chi_{S/S-s}$ represents the interaction between an organic and an inorganic monomer and should not necessarily be compared to previously measured interaction parameters in systems where both components are organic. Taking the broad molecular weight distribution of the PS-SO3H copolymer into consideration would result in a slightly decreased estimate for $\chi_{S/S-s}$ [1,143], but in essence the conclusions from this exercise remain the same. While this method may represent only a lower bound estimate, it supports the experimental results which indicate the interaction between styrene and styrene sulfonic acid must be strong and positive, and prohibits miscibility in this system. These results clearly show that it is not possible to use sPS in dilute mixtures with PS to achieve microstructural control in blends. Control of blend microstructure must be accomplished by controlling the functionality of the sPS starting materials.

5.4. Summary

In this Chapter the results of the investigation into reactive compatibilization in the system sPS/P2VP by ionic interaction were discussed. Ionic interaction was found to be highly effective at promoting compatibility. The addition of only a small amount of sulfonic acid, ~1.7%, refined the structure of PS/P2VP melt blends considerably. The effects in solution blends of sPS and P2VP with varying levels of reactivity were dramatic. SPS and

P2VP formed ionic crosslinks in solution, resulting in blends which were mixed on a molecular level. The structure of the solution blends was studied by dynamic mechanical analysis, in which the reactive blends exhibited the broadened transitions and increased plateau modulus characteristic of crosslinked systems. Interchain crosslinking was also found to be highly effective at suppressing phase separation. SAXS studies have indicated that phase separation in reactive sPS/P2VP solution blends was occurring only on an extremely fine scale, on the order of ~5-10 nm. The effects of ionic interaction on adhesive reinforcement at the immiscible interface were equally impressive. Interfacial toughness increased by two orders of magnitude, from ~2 J/m^2 at the unreactive interface to ~350 J/m^2 for the strongest reactive interface measured. Reactive reinforcement of this magnitude at immiscible interfaces is unprecedented. An optimum reactivity level for interfacial toughening has been identified in the range of ~5.5-7% styrene sulfonic acid. A SANS study was also undertaken to asses the feasibility of using sPS in dilute concentration as a blend additive, and it was found that even small amounts of sulfonation are sufficient to cause immiscibility in dPS/sPS blends. The results imply that the functionality of sPS must be controlled in order to tailor the microstructure of its blends. In summary, this investigation has confirmed the utility of ionic crosslinking for suppression of large scale phase separation and detected, for the first time, changes in the structure of ionically crosslinked sPS/P2VP blends due to the effects of increasing system reactivity. In addition, compatibilization through ionic interaction was proven to be an effective and highly efficient mechanism for promoting interfacial adhesion, generating improvements in interfacial adhesion of up to two orders of magnitude.

Chapter 6:
Conclusions

This investigation has examined the feasibility of using reactive compatibilization methods to control the morphology and promote interfacial adhesion in immiscible polymer blends. Reactive compatibilization methods, in which copolymer compatibilizers are formed in-situ at interphase interfaces during processing, are superior to traditional compatibilization methods, in which copolymers are separately manufactured and dispersed in immiscible blends during processing. Traditional compatibilization methods are more costly due to the necessity of manufacturing specialty copolymers, and suffer from the processing difficulties associated with properly dispersing these copolymers to the interphase interfaces. These issues are circumvented by the in-situ nature of the reactive compatibilization scheme. There have been some studies in reactively compatibilized systems in which the morphology and mechanical properties of immiscible blends have been favorably modified by the incorporation of reactivity. There has been no evaluation to date of the effects of reactive copolymer formation on the adhesion at immiscible interfaces, an issue which is central to the development of useful commercial blends, particularly for applications in which mechanical properties are important. The aim of this study was to investigate and correlate both aspects of reactive compatibilization; the refinement of morphology in immiscible blends and the mechanical reinforcement provided by the formation of copolymers at the interphase interfaces.

Reactive compatibilization has been evaluated in two different immiscible polymer systems. In one system, polystyrene/amorphous polyamide, a small amount of reactivity has been introduced by

functionalization of polystyrene with vinyl oxazoline. The oxazoline group forms an interchain covalent bond by reacting with the endgroups of the polyamide chain, resulting in copolymer formation. Reactive compatibilization has also been studied in an ionically interacting system, sulfonated polystyrene/poly(2-vinyl pyridine). Sulfonic acid groups randomly incorporated onto the polystyrene chains are capable of generating interchain ionic crosslinks, and consequently copolymers, by interaction with the pyridine nitrogens along the poly(2-vinyl pyridine) chains. Compatibilization in the sulfonated polystyrene/poly(2-vinyl pyridine) system was investigated as a function of system reactivity, and produces dramatic changes in both morphology and interfacial mechanical properties at high levels of reactivity. Morphology refinement in both blends was studied using a variety of materials characterization techniques including microscopy and small angle scattering. Interfacial adhesion has been evaluated using a new technique, the asymmetric double cantilever beam test, which isolates the interface in a model geometry and allows for direct measurement of interfacial fracture toughness that is used to quantify interfacial adhesion.

Investigation into the reactive polystyrene/amorphous polyamide system has shown that introducing a small amount of reactivity into the system (~1.2 mole % vinyl oxazoline) produces a significant refinement of morphology in melt blends as well as an increase in the interfacial adhesion by a factor of about 2. Comparison of the morphology in reactive versus unreactive polystyrene/amorphous polyamide blends shows that average size of the minor phase is decreased and the distribution of minor phase particle sizes narrowed in the reactive blend. These results imply that coalescence factors may be important in controlling the final morphology. Quantitative evaluation of copolymer formation using Fourier transform

infra-red spectroscopy has allowed for estimation of the amount of copolymer formed, and has indicated that the grafting density is low in this lightly functionalized system. The adhesion at polystyrene/amorphous polyamide interfaces was found to improve modestly due to the generation of a small amount of interfacial copolymer.

The specific conclusions from the polystyrene/polyamide study are:

1) The dispersion in PS/aPA melt blends is efficiently stabilized with respect to both average size and size distribution by incorporation of ~1.2 mole% vinyl oxazoline onto PS chains. The average size of dispersed PS particles is reduced by ~60% due to the effects of reactivity.

2) The interaction between aPA endgroups and oxazoline groups on the PS chains leads to the formation of compatibilizing copolymers during processing. In a 20PS-ox/80aPA blend, the reaction between oxazoline and aPA endgroups resulted in the formation of ~3% of compatibilizer, by weight, from the reaction of ~12% of PS chains. The areal density of copolymer chains at the particle interfaces was estimated at ~0.02 chains/nm^2.

3) The toughness of the PS-ox/aPA interface, ~10 J/m^2, is on average more than twice that of the unreactive PS/aPA interface,~4 J/m^2. Toughness of reactive interfaces may be improved by extended annealing above the glass transition temperature of PS-ox.

Investigation into reactive compatibilization in the sulfonated polystyrene/poly(2-vinyl pyridine) system has shown that the incorporation of reactivity can dramatically influence the morphology and interfacial mechanical properties of this immiscible polymer pair. Interchain ionic crosslinks were found to form readily, both in melt blends and in solution blends, and effectively refined the blend morphology. Small angle scattering studies have shown that ionic interaction can suppress phase separation in solution blends to an extremely fine scale of <0.01 μm. In addition, ionic crosslinking has been used for the first time to generate interfacial mechanical reinforcement, with impressive effects. The fracture toughness at the immiscible polystyrene/poly(2-vinyl pyridine) interface was improved by over two orders of magnitude when sufficient levels of reactivity were introduced. These large increases in interfacial toughness were found to be a consequence of the initiation of interfacial crazing during failure due to the in-situ generation of a high density of interfacial copolymer through interchain ionic crosslinking. An optimum reactivity for interfacial toughening was observed. Increasing the reactivity above this optimum level resulted in a rapid decline in toughness which has been associated with excessive interfacial reaction resulting in a decrease in effective entanglement between the grafted layer and the free polymer chains and leading to inefficient load transfer. In addition, the miscibility in polystyrene/sulfonated polystyrene blends was evaluated with the aim of assessing the utility of sulfonated polystyrenes as a compatibilizing agent for blends containing unreactive polystyrene. Small angle neutron scattering studies of the structure in these blends revealed that the incorporation of only a small amount of sulfonic acid was sufficient to cause immiscibility in the polystyrene/sulfonated polystyrene system, and

therefore sulfonated polystyrene may not be incorporated into polystyrene blends as a miscible compatibilizing additive.

The specific conclusions from the sulfonated polystyrene/poly(2-vinyl pyridine) study are:

1) Ionic interactions between sulfonic acid and pyridine successfully refine the morphology in melt blends. The addition of ~1.7 mole% styrene sulfonic acid to PS chains results in a reduction of the maximum dimension of the dispersed phase from ~6 μm to ~1 μm in 20PS/80P2VP blends.

2) The interaction between pyridine and sulfonic acid results in interchain ionic crosslinking in sPS/P2VP solution blends. Evidence of crosslinking is provided by shifting and broadening of the glass transition as well as increased plateau modulus in the blends as measured by dynamic mechanical analysis.

3) Phase separation is suppressed in sPS/P2VP solution blends due to ionic crosslinking. The small angle scattering function from blends with ~3.4-6.9 mole% styrene sulfonic acid contains a scattering peak at a position corresponding to a feature ~5-10 nm in size. This peak is believed to result from microphase separation in the blends. The ionic clustering peak in PS-9.50SO_3H and PS-15.0SO_3H is suppressed by blending with P2VP.

4) Analysis of deviations from Porod behavior in the limiting region of the small angle x-ray scattering from sPS/P2VP solution blends has

shown that interfaces in the reactive system are ~1.4-1.9 times as thick as in the unreactive blend. The interfacial thickness increases with reactivity up to a point, after which it begins to narrow with increasing acid concentration.

5) The toughness of PS/P2VP interfaces may be increased by up to two orders of magnitude with sufficient system reactivity, increasing from ~2 J/m^2 at the unreactive interface to >300 J/m^2 for the toughest reactive interface measured. This improvement in adhesion is the direct result of in-situ formation of compatibilizing copolymers at the interface by interaction between sulfonic acid and pyridine groups.

6) There is an optimum reactivity level for reinforcement of sPS/P2VP interfaces, which occurs at ~5-7 mole% styrene sulfonic acid. Increasing the level of reactivity beyond this point results in a rapid decline of interfacial toughness from >150 J/m^2 to ~50 J/m^2.

7) The toughness of the sPS/P2VP interfaces is a function of interfacial bonding time and P2VP molecular weight. Increasing the bonding time increases G_c. Increasing the P2VP molecular weight results in a shift of the optimum reactivity level to higher acid contents.

8) The scaling between interfacial toughness and reactivity in the increasing toughness regime follows a power law with n=1.9. This scaling is in reasonable agreement with the prediction n=2 from the models of Hui and Brown [22,77], and indicates that failure is occurring by an interfacial crazing mechanism.

9) Small angle neutron scattering from dPS/PS-1.67%SO_3H blends was examined over a range of concentrations from 5% to 95% sPS. In all cases, the scattering fit the Debye-Bueche prediction for scattering from two phase systems, which indicates that the addition of ~1.7% styrene sulfonic acid is sufficient to cause immiscibility.

Finally, the results of this investigation have shown that reactive compatibilization may be used to create substantial improvement in interfacial adhesion between immiscible polymers in addition to successfully controlling morphology in immiscible blends. This work represents the first quantitative evaluation of interfacial adhesion in reactive systems and the first documentation of large increases in interfacial fracture toughness at immiscible polymer interfaces due to in-situ copolymer formation. The effects of reactivity on the mechanical properties of immiscible interfaces have been correlated with changes in morphology and physical properties of the corresponding immiscible polymer blends.

Chapter 7:
Suggestions for Future Work

In this last chapter a few suggestions are given for extension of the current study, based on some potentially interesting behavior that was observed during the course of this investigation.

The results of this work have demonstrated, unquestionably, that ionic interactions may be used to generate reinforcing copolymers. In addition, all of the work on the sPS/P2VP system suggests that the interaction between styrene sulfonic acid and pyridine is not only strong but occurs readily and apparently without the need for thermal activation. These characteristics make the sulfonic acid/amine nitrogen interaction an excellent choice for model studies.

Preliminary work on sPS/aPA blends has shown the interaction between these materials is particularly strong, and this system may be a good candidate for studies of interfacial adhesion and morphology refinement in melt blends. A study of sPS/aPA interfaces may be enlightening in terms of failure mechanisms because aPA apparently does not deform by crazing, and there is some question as to whether it would be possible to activate crazing in the PS beam across an interface of this type.

From a commercial standpoint, the interaction between sulfonated rubbers/elastomers and amine or pyridine functionalized thermoplastics may be of interest. Adhesive properties of flexible materials on glassy substrates may be measured using a variety of standard tests, and recent theoretical analysis has suggested the dependence of interfacial strength on strain rate in these systems may be worthy of scientific study.

In addition to study of new ionically reinforced systems, there are a couple of areas in which the sPS/P2VP investigation may be directly extended. One is in the area of copolymer architecture effects on compatibilization, about which little is currently known. The maximum G_c values measured in the sPS/P2VP system are the highest ever reported from an immiscible interface which has been tested under proper conditions of asymmetry. As suggested in Chapter 5, this may be related to the unique architecture of ionically crosslinked chains. In the sPS/P2VP system copolymer architecture effects may be studied using telechelic ionomers, in which the acid groups may be positioned at one or both ends of the molecule, allowing for evaluation of the differences between reinforcement by loops, end-tethered chains and randomly crosslinked chains. This study would be particularly interesting if grafting could be studied between pyridine networks and telechelic PS ionomers, a problem whose geometry closely approximates the case of chains grafted to a wall which has been considered in a number of theoretical treatments.

A second potentially interesting extension of the sPS/P2VP studies would be to manipulate the ionic clustering effect in sPS and examine the effect on interfacial toughening. Clustering produces mechanical changes in ionomers which are similar to those observed by crosslinking. In essence, one may consider the onset of clustering to coincide with a jump in ionomer molecular weight. The interfacial adhesive properties are known to be very sensitive to molecular weight, with chain pull-out occurring at low molecular weight and chain scission occurring at high molecular weight. It may be possible, by starting with low molecular weight ionomers, to cause the transition from pull-out to scission, or from pull-out to crazing by inducing clustering. In any event, the effects of neutralization of acid groups may result

in some significant changes in the interfacial interactions between sPS and P2VP and makes a potentially attractive area of study.

As far as the blending work is concerned, the most interesting result to surface during the course of this study is the potential importance of compatibilization in altering coalescence phenomena in melt blends. Specifically, the role of copolymer brush interaction between compatibilized particle surfaces may play an important role in determining the final morphology of compatibilized blend systems. This is an area in which further study is needed to properly separate the reduction in interfacial tension accompanying compatibilization, and the effects of the copolymer brush in deterring coalescence. Reactive systems are particularly well suited for this type of study, because the copolymers formed by reactive compatibilization methods may be relatively long and the in-situ nature of the copolymer formation assures that they are positioned at the interfaces.

Finally, a note about interfacial properties in systems of low reactivity. Studies in the PS-ox/aPA system have demonstrated that the ADCB test for interfacial fracture is not particularly well suited for studies of systems with low levels of reactivity. The results indicated only small increments in toughness, which is most likely due to the low contact probability of reactive groups at the beam surfaces during sample preparation. This is not really representative of the blend situation which the ADCB experiment seeks to emulate. The probability for contact during blending is much higher due to the aggressive nature of the mixing process. For systems such as this, a better approach to study of interfacial toughening may be to generate the copolymers, reactively, in a separate step and subsequently add them to the interface, as has been done in previous studies of interfaces traditionally reinforced with diblocks. A 'calibration curve' may then be generated relating the measured toughness to

the amount of copolymer at the interface. This calibration curve may be used to estimate the toughness of interfaces in reactive melt blends, in which the interfacial density of copolymers is evaluated using a suitable technique such as extraction. The intimate mixing needed for successful interchain reaction may be achieved by solution blending, and the progress of copolymer formation may be followed by monitoring molecular weight. Preliminary studies in the PS-ox/PMMA-co-maleic anhydride system have indicated that this method successfully produces copolymers. This approach, though involved, may be a viable route for studying the low reactivity systems which are of commercial interest. It provides the advantage of requiring only small amounts of reactive material for the toughness experiments, and opens the opportunity for study of the interesting case of simultaneous phase separation and interchain reaction in the solution blends.

APPENDIX A: Program for the Microstepping Inexer

Program code to drive the IMS Microstepping Indexer.

Commands:	Description:
0 H 0	Select resolution mode. Mode 0 is fixed resolution.
2 D 7	Set microstep resolution. The motor has 1.8°/step or 360°/1.8°=200 steps/revolution. Divide 7 sets the resolution at 1/128 of a full step, so the final resolution is 200*128=25,600 steps/revolution.
4 K 0 50	Sets the acceleration/deceleration of the motor. K 0 50 is equivalent to fully acceleration to start-up speed (0), decelerate in 500(max)/50=10 steps.
7 M 85-	Move at a fixed velocity of 85 steps/second.
10 W 65000	Wait for 65,000 milliseconds. 65,000 is the maximum
13 W 65000	waiting time. The motor moves at the fixed velocity
16 W 65000	for the duration of the wait.
19 W 65000	
22 W 65000	
25 W 65000	
28 W 65000	
31 M 0+	Move at 0 velocity. This command stops the motor.

The motor turns a 1/4"-28 screw which drives the crack insertion. A 1/4"-28 screw has 28 threads/inch= 28 rev./in or 1102.4 rev./m. The motor is set for 25,600 rev. per step, 85 steps/second. The crack insertion rate is:

$$\frac{1}{25600}\text{rev/step} * 85\text{step/sec} * \frac{1}{1102.4}\text{m/rev} = 3.01 \times 10^{-6}\ \text{m/s}.$$

APPENDIX B: C++ Code for Image Aquisition

C++ code for automated image storage using a CORECO OCULUS TCX, 2MB Frame Grabber.

```
#include <stdio.h>
#include <stdlib.h>
#include <limits.h>
#include <time.h>
#include <odx.h>
#include <opr.h>
static void progress( int y, int ylen);
/* These typedef are compatible with TIFF V:4.2 */
typedef unsigned int WORD;
typedef unsigned long DWORD;
typedef struct
  {
  WORD  ByteOrder;
  WORD  Version;
  DWORD OffsetOfIFD;
  } HEADER;
typedef struct
  {
  WORD  Type;
  WORD  Size;
  DWORD Length;
  DWORD Value;
  } TAG;
#define BUF_SIZE    UINT_MAX        /* Use a buffer as large as possible */
#define ENABLE_RGBI  /* Define this symbol to get support for RGB Interlaced Frame
Buffer */
#undef  ENABLE_RGBI  /* Not already supported */
#define FILL        0
#define BITSPOS     (sizeof(HEADER) + sizeof(WORD) + 8 * sizeof(TAG))
#define STRIPSPOS   (BITSPOS + 3 * sizeof(WORD))
void    delay(int ns);
void main()
{
static  int Counter = 1;
int     i,nodx, fb, dels, sts,xlen, ylen, dxlen,dylen;
char    Name[256], prefix[4];
time_t timenumber;
/**initialize board**/
nodx=odxbind();
if( nodx < 1)
        {
        printf("Cannot access any ODX Driver\n");
        return;
        }
/*start continuous grab*/
fbgrab(-1);
/* windows */
pwin (0,0,512,384);
dwin (0,0,512,384);
/*program */
printf("\n\nEnter prefix for data files, 4 characters\n");
```

```
scanf("%s",&prefix);
printf("\n\nEnter time delay between frames (seconds, minimum=41 s) \n");
scanf("%d",&dels);
dels=dels - 41;
if ( dels < 0) dels = 0;
        for ( i = 0; i < 20; i++){
                sprintf(Name, "%s%d.tif",prefix,Counter);
                printf("Image being stored is # %d\n",Counter);
                Counter ++;
                pwin( 0, 0, opr_inq( DWIN_XLEN), opr_inq( DWIN_YLEN));
         /*             The following two statements are for use in
                       determining the time to store an image.  For
                       512X384 images the time is 41 sec
                time(&timenumber);
                printf("time is %s",ctime(&timenumber));*/
                init_tick();
                sts = fbsave( Name, progress);
                printf("Status is %d\n", sts);
                free_tick();
                delay(dels);
                }
        xlen=opr_inq(PWIN_XLEN);
        ylen=opr_inq(PWIN_YLEN);
        dxlen=opr_inq(DWIN_XLEN);
        dylen=opr_inq(DWIN_YLEN);
        printf("\nProcessing window: %d,%d",xlen,ylen);
        printf("\nDisplay window: %d,%d",dxlen,dylen);
         /** done go turn off the board **/
        fbgrab(0);
        return;
}
 /* Delay routine from p. 280, Levanthal */
void delay (int nsecs)
{
        int nm, nmend, ns, nsend;
        time_t timenumber;
        struct tm *timestruct;
        /* get current time */
        time(&timenumber);
        timestruct = localtime(&timenumber);
        /* compute target time */
        nm = timestruct->tm_min;
        ns = timestruct->tm_sec;
        nmend = nm + nsecs/60;
        nsend = ns + nsecs%60;
        nmend += nsend/60;
        nsend %= 60;
        nmend %= 60;
        /* wait */
        while ((nmend != nm) | | (nsend != ns)) {
                time(&timenumber);
                timestruct = localtime(&timenumber);
                nm = timestruct->tm_min;
                ns = timestruct->tm_sec;
                }
        return;
}
// this is where the save begins
```

```
int fbsave( char *name, void (*progress)(int, int))
 {
 int xmin, ymin, xlen, ylen;       /* window to save */
 unsigned dy;                  /* Number of line saved in a single transfer */
 char *buf;                    /* Transfer buffer */
 FILE *fp;                     /* File Handle */
 int y;                       /* Line counter for a single page */
 int ycount;                   /* Line counter fot full image */
 int page, nbpage;                /* For RGB multi-pages support */
 int grlsiz;                  /* Number of bytes per pixel */
  /*****************************************************/
   /* Definition of TIFF header for each FBTYPE        */
   /*****************************************************/
  /* Minimal TIFF Header for monochrome image */
 static struct monotiff
   {
   HEADER Header;
   WORD EntryCount;
   TAG SubfileType;
   TAG ImageWidth;
   TAG ImageLength;
   TAG BitsPerSample;
   TAG StripOffsets;
   TAG PhotometricInterpretation;
   } monoheader =
   {
   { 0x4949, 42, sizeof( HEADER)},  /* Header */
   6,                        /* Number of tags */
   { 0xff, 3, 1, 1},            /* SubfileType */
   { 0x100, 3, 1, FILL},          /* ImageWidth */
   { 0x101, 3, 1, FILL},          /* ImageLength */
   { 0x102, 3, 1, FILL},          /* BitsPerSample */
   { 0x106, 3, 1, 1},           /* PhotometricInterpretation */
   { 0x111, 4, 1, sizeof(struct monotiff)},  /* StripOffsets */
   };
  /* Minimal TIFF Header for RGB, multi-planes image */
 static struct rgbPtiff
   {
   HEADER Header;
   WORD EntryCount;
   TAG SubfileType;
   TAG ImageWidth;
   TAG ImageLength;
   TAG BitsPerSample;
   TAG PhotometricInterpretation;
   TAG StripOffsets;
   TAG SamplesPerPixel;
   TAG PlanarConfiguration;
   WORD RedBits;
   WORD GreenBits;
   WORD BlueBits;
   DWORD RedStrip;
   DWORD GreenStrip;
   DWORD BlueStrip;
   } rgbPheader =
   {
   { 0x4949, 42, sizeof( HEADER)},  /* Header */
   8,                        /* Number of tags */
```

```
    { 0xff, 3, 1, 1},          /* SubfileType */
    {0x100, 3, 1, FILL},       /* ImageWidth */
    {0x101, 3, 1, FILL},       /* ImageLength */
    {0x102, 3, 3, BITSPOS},    /* BitsPerSample */
    {0x106, 3, 1, 2},          /* PhotometricInterpretation */
    {0x111, 4, 3, STRIPSPOS},  /* StripOffsets */
    {0x115, 3, 1, 3},          /* SamplesPerPixel */
    {0x11c, 3, 1, 2},          /* PlanarConfiguration */
    FILL,                      /* RedBits */
    FILL,                      /* GreenBits */
    FILL,                      /* BlueBits */
    FILL,                      /* RedStrip */
    FILL,                      /* GreenStrip */
    FILL,                      /* BlueStrip */
    };
#ifdef ENABLE_RGBI
  /* Minimal TIFF Header for RGB, interlaced image */
  static struct rgbItiff
    {
    HEADER Header;
    WORD EntryCount;
    TAG SubfileType;
    TAG ImageWidth;
    TAG ImageLength;
    TAG BitsPerSample;
    TAG PhotometricInterpretation;
    TAG StripOffsets;
    TAG SamplesPerPixel;
    TAG PlanarConfiguration;
    WORD RedBits;
    WORD GreenBits;
    WORD BlueBits;
    } rgbIheader =
    {
    {0x4949, 42, sizeof( HEADER)},  /* Header */
    8,                         /* Number of tags */
    { 0xff, 3, 1, 1},          /* SubfileType */
    {0x100, 3, 1, FILL},       /* ImageWidth */
    {0x101, 3, 1, FILL},       /* ImageLength */
    {0x102, 3, 3, BITSPOS},    /* BitsPerSample */
    {0x106, 3, 1, 2},          /* PhotometricInterpretation */
    {0x111, 4, 3, sizeof( struct rgbIheader)},  /* StripOffsets */
    {0x115, 3, 1, 3},          /* SamplesPerPixel */
    {0x11c, 3, 1, 2},          /* PlanarConfiguration */
    FILL,                      /* RedBits */
    FILL,                      /* GreenBits */
    FILL,                      /* BlueBits */
    };
#else
  if( opr_inq( FBTYPE) == 2)       /* If RGBI not supported */
    return( -2);                   /* Return the File Creation Error message */
#endif
   /*****************************************************/
     /* Get size of window to transfer                   */
   /*****************************************************/
  xmin = opr_inq( PWIN_XMIN);      /* Get size of window to save */
  ymin = opr_inq( PWIN_YMIN);
  xlen = opr_inq( PWIN_XLEN);
```

```
ylen = opr_inq( PWIN_YLEN);
 if( opr_inq( PIXSIZ) > 8)        /* Get number of bytes per pixel */
  grlsiz = 2;
else
  grlsiz = 1;
 /*****************************************************/
 /* Allocate transfer buffer                          */
 /*****************************************************/
dy = BUF_SIZE / xlen / grlsiz;    /* Number of lines saved in a single transfer */
if( dy > ylen) dy = ylen;         /* Small window, only 1 transfer required */
buf = malloc( dy * xlen * grlsiz); /* Allocate transfer buffer */
if( buf == NULL) return( 1);      /* Check if allocation successful */
/*****************************************************/
 /* Open File and Write Header                        */
/*****************************************************/
fp = fopen( name, "wb");          /* Open file for writing, untranslated */
if( fp == NULL) return( 2);       /* Check if successful */
switch( opr_inq( FBTYPE))         /* Write Header according to FBTYPE */
  {
  case 0:  /* Monochrome image */
        nbpage = 1;
        monoheader.BitsPerSample.Value = grlsiz * 8;
        monoheader.ImageWidth.Value = xlen;
        monoheader.ImageLength.Value = ylen;
        fwrite( &monoheader, sizeof(struct monotiff), 1, fp);
        break;
   case 1:  /* RGB, multi-plane */
        {
        long SizeOfPlane;
        SizeOfPlane = xlen * (long) ylen * grlsiz;
        nbpage = 3;
        rgbPheader.ImageWidth.Value = xlen;
        rgbPheader.ImageLength.Value = ylen;
        rgbPheader.RedBits = grlsiz * 8;
        rgbPheader.GreenBits = grlsiz * 8;
        rgbPheader.BlueBits = grlsiz * 8;
        rgbPheader.RedStrip = sizeof(struct rgbPtiff);
        rgbPheader.GreenStrip = sizeof(struct rgbPtiff) + SizeOfPlane;
        rgbPheader.BlueStrip = sizeof(struct rgbPtiff) + 2 * SizeOfPlane;
        fwrite( &rgbPheader, sizeof(struct rgbPtiff), 1, fp);
        break;
        }
#ifdef ENABLE_RGBI
   case 2:  /* RGB, interlaced */
        nbpage = 1;
        rgbIheader.ImageWidth.Value = xlen;
        rgbIheader.ImageLength.Value = ylen;
        rgbIheader.RedBits = opr_inq( PIXSIZ) / 3;
        rgbIheader.GreenBits = opr_inq( PIXSIZ) / 3;
        rgbIheader.BlueBits = opr_inq( PIXSIZ) / 3;
        fwrite( &rgbIheader, sizeof(struct rgbItiff), 1, fp);
        break;
#endif
   }
 /*****************************************************/
 /* Write Image Data to File                          */
 /*****************************************************/
 ycount = 0;
```

```
  for( page = 0; page < nbpage; page++)  /* Process each page of the image */
    {
    opr_set( PFBPAGE, page);          /* Select page */
    for( y = 0; y < ylen; y += dy)     /* Increment line counter by the number of line
transferred */
          {
          int count, nbline;
          if( ylen - y < dy) nbline = ylen - y;  /* Last transfer, remaining lines */
          else nbline = dy;
          pwin( xmin, ymin + y, xlen, nbline);   /* Set window to transfer */
          rdbuf( buf, xlen);                /* Transfer image to temporary buffer */
          count = xlen * nbline;              /* Number of items to transfer */
          if( fwrite( buf, grlsiz, count, fp)    /* Transfer temporary buffer to file */
            != count) break;                 /* Break loop if not enough space */
          ycount += nbline;                  /* Update total number of lines transferred */
          (*progress)( ycount, ylen * nbpage);   /* Inform user from progress of transfer */
          }
    }
  /*******************************************************/
    /* Free Resources                                      */
    /*******************************************************/
  free( buf);                  /* Free allocated memory */
  fclose( fp);                 /* Close file */
  pwin( xmin, ymin, xlen, ylen);     /* Restore PWIN */
   if( y < ylen) return( 3);         /* Check if fwrite error */
  else return( 0);               /* No errors */
  }
 /*********************************************************
 To produce the executable, you must link the following object files:
 fbload.obj odxcall(MODEL).obj tick.obj mouse.obj box.obj
*********************************************************/
static void progress( int y, int ylen)
  {
  int time;
  time = tick();
  printf("Time: %5d ms %3d%% complete\r", time, (int)(y * (long) 100 / ylen));
  }
```

APPENDIX C: Calculation of the Copolymer Concentration

From the calibration curve, Figure 4.13, one may deduce:

$$c_{aPA}^{copolymer}\Big|_{extract} = \frac{m_{aPA}}{m_{aPA} + m_{PS}} = 0.0305$$

from which:

$$\frac{m_{aPA}}{m_{PS}}\Big|_{extract} = 0.0315$$

and:

$$c_{aPA}^{copolymer}\Big|_{blend} = \frac{m_{aPA}}{m_{PS}} * \frac{m_{PS}}{m_{blend}}$$

$$= 0.0315 * 0.2 = 6.29 \times 10^{-3}$$

yielding:

$$\frac{n_{copolymers}}{m_{blend}} = c_{aPA}^{copolymer}\Big|_{blend} \div MW_{aPA}$$

$$= 6.29 \times 10^{-3} / 62500 = 1.01 \times 10^{-7}$$

and finally:

$$c_{blend}^{copolymer} = \frac{n_{copolymers}}{m_{blend}} * (MW_{PS} + MW_{aPA})$$

$$= 1.01 \times 10^{-7} * (230000 + 62500) = 0.0294$$

or 2.9% copolymers in the blend, by weight.

Similarly,

$$\frac{n_{PS}^{copolymer}}{n_{PS}^{blend}} = \frac{n_{PS}^{copolymer}}{m_{blend}} * \frac{m_{blend}}{m_{PS}} * MW_{PS}$$

$$= 1.01 \times 10^{-7} * (1 / 0.2) * 230000 = 0.116$$

or 11.6% of all PS chains which have a graft.

One may also estimate the areal density of copolymer joints across the PS-ox/aPA interface using an estimate to the surface to volume ratio of the blend from the quantitative analysis of the morphology. From the average

particle size, Table 4-I:

$$\frac{S_{particle}}{V_{particle}} = \frac{4\pi r^2}{\frac{4}{3}\pi r^3} = \frac{3}{r} = 16.7\ \mu m^2/\mu m^3$$

and

$$\frac{S_{particle}}{V_{blend}} = \frac{S_{particle}}{V_{particle}} * \frac{V_{particle}}{V_{blend}} = \frac{S_{particle}}{V_{particle}} * \frac{m_{PS}/\rho_{PS}}{m_{blend}/\rho_{blend}}$$

$$= 16.7 * \frac{0.2/1.04}{1.0/(0.2*1.04+0.8*1.06)} = 3.39\ \mu m^2/\mu m^3$$

from above:

$$\frac{\#\,copolymers}{V_{blend}} = \frac{n^{copolymers}}{m_{blend}} * \frac{\#\,copolymers}{mole} * \frac{m_{blend}}{V_{blend}}$$

$$= 1.01x10^{-7} * 6.023x10^{23} * 1.056 = 6.81x10^{16}$$

and:

$$\Sigma = \frac{\#\,bonds}{S_{particle}} = \frac{\#\,copolymers}{V_{blend}} * \frac{V_{blend}}{S_{particle}}$$

$$= (6.81x10^{16} + 3.39) * 10^{-18}$$

$$= 0.020\ bonds/nm^2$$

APPENDIX D: Estimation of Σ

The areal density of reactive sites may be estimated using the material density by assuming the percentage of the sPS surface which is reactive is equal to the percentage of reactive monomers.

For polystyrene:

$$\rho_{PS} = 1.04 g / cm^3 = 1.04 x 10^{-21} g / nm^3$$

and the monomer molecular weight is M_{mon}=104 g/mole, yielding:

$$\rho_{mon} = 1.04 x 10^{-21} \frac{g}{nm^3} * \frac{1 mole}{104 g} * 6.02 x 10^{23} \frac{monomers}{mole} = 6.02 \frac{monmers}{nm^3}$$

from which:

$$V_{mon} = 1 / \rho_{mon} = 0.17 \frac{nm^3}{monomer}$$

and:

$$A_{mon} = \pi \left(\frac{3}{4\pi} V \right)^{2/3} = 0.37 \frac{nm^2}{monomer}$$

or:

$$\rho_{mon}^{A} = 2.7 \frac{monomers}{nm^2}$$

where ρ_{mon}^{A} approximates the surface area per monomer.

Assuming that the areal density of reactive sites is equal to the percentage of reactive surface area, which is approximated by:

$$\Sigma = [C_{SO_3H}]\rho^{A}_{mon}$$

leads to an estimate of Σ at different reactivities for the sPS/P2VP interface:

$[C_{SO3H}]$	Σ (reactive sites/nm^2)
0.0167	0.05
0.0337	0.09
0.0556	0.15
0.0691	0.19
0.095	0.26
0.150	0.41

Note that Σ is directly proportional to $[C_{SO3H}]$.

APPENDIX E: Figures

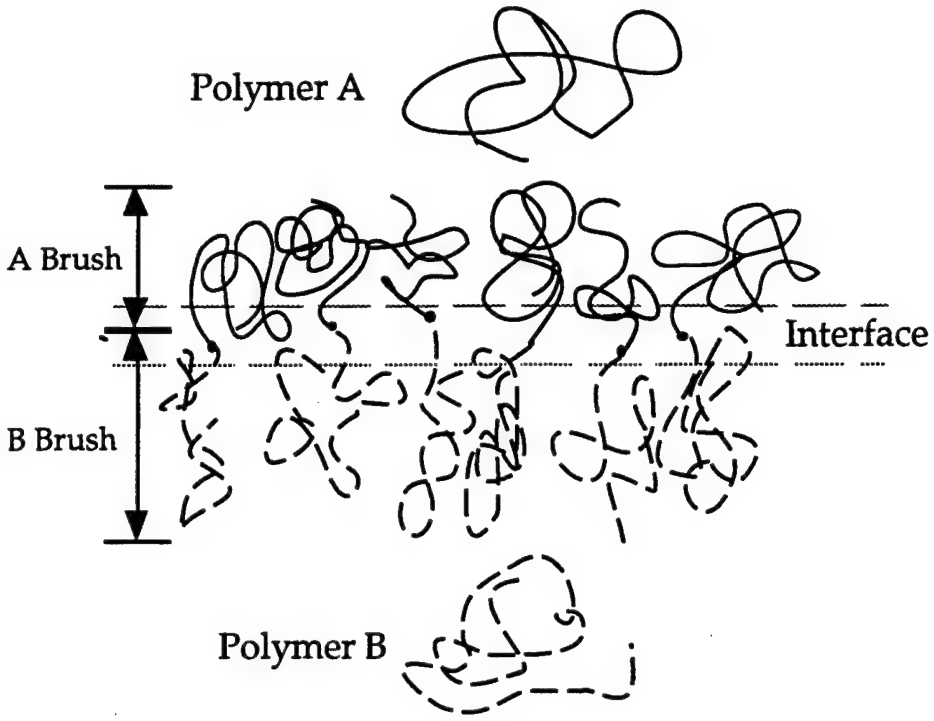

Figure 2.1. Schematic representation of copolymer segregation at an A/B interface.

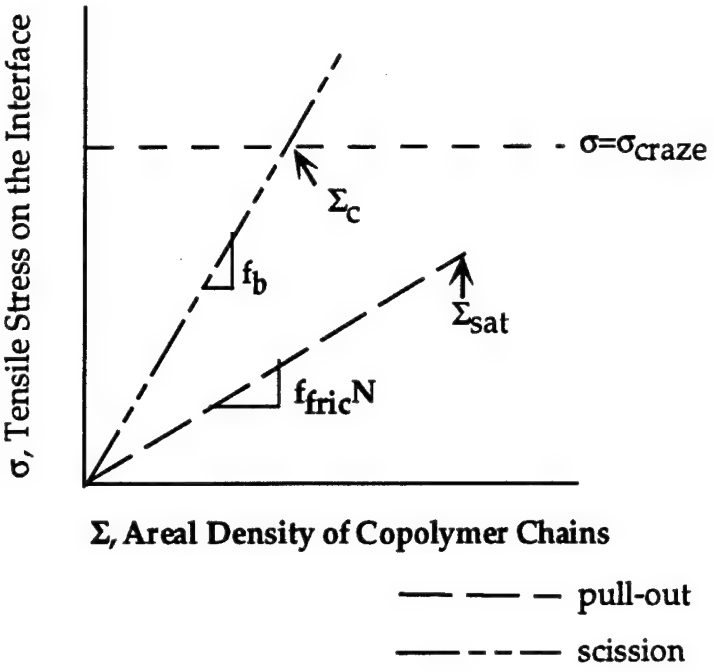

Figure 2.2. Failure Mechanism Map for Compatibilized Interfaces.

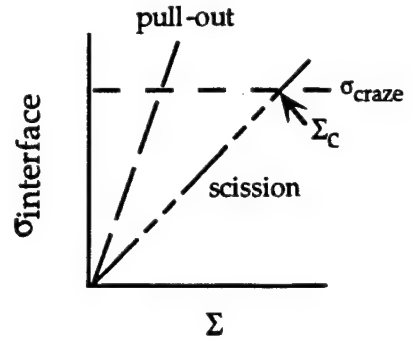

Failure by chain scission.

$N >> N_e$

$f_b < f_{fric}N$

Transition to crazing at Σ_c.

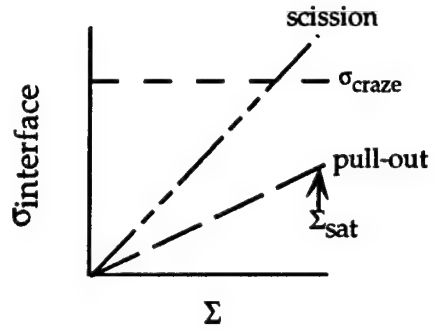

Failure by chain pull-out.

$N << N_e$

$f_{fric}N < f_b$

No crazing regime.

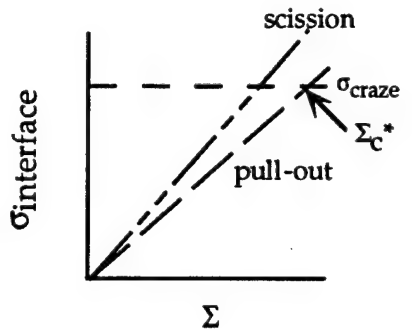

Failure by chain pull-out.

$N \sim N_e$

$f_{fric}N < f_b$

Transition to crazing at Σ_c^*.

Figure 2.3. Changes in the Failure Mechanism Map for various values of N.

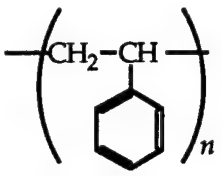

Polystyrene

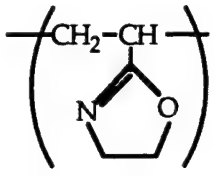

Vinyl Oxazoline

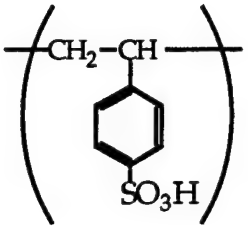

Styrene sulfonic acid

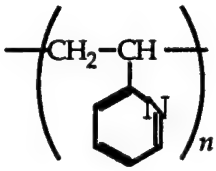

Poly(2-vinyl pyridine)

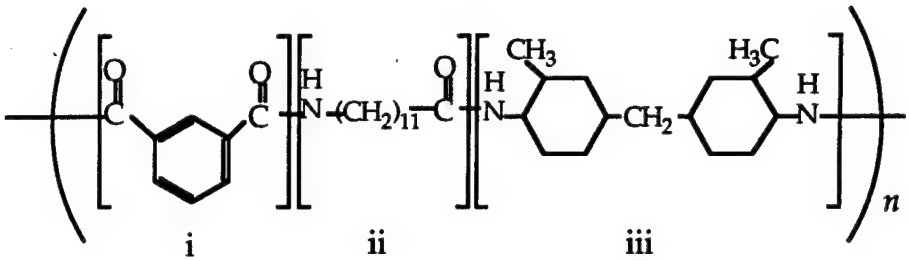

i ii iii

Amorphous Nylon

Figure 3.1. Monomer structures.

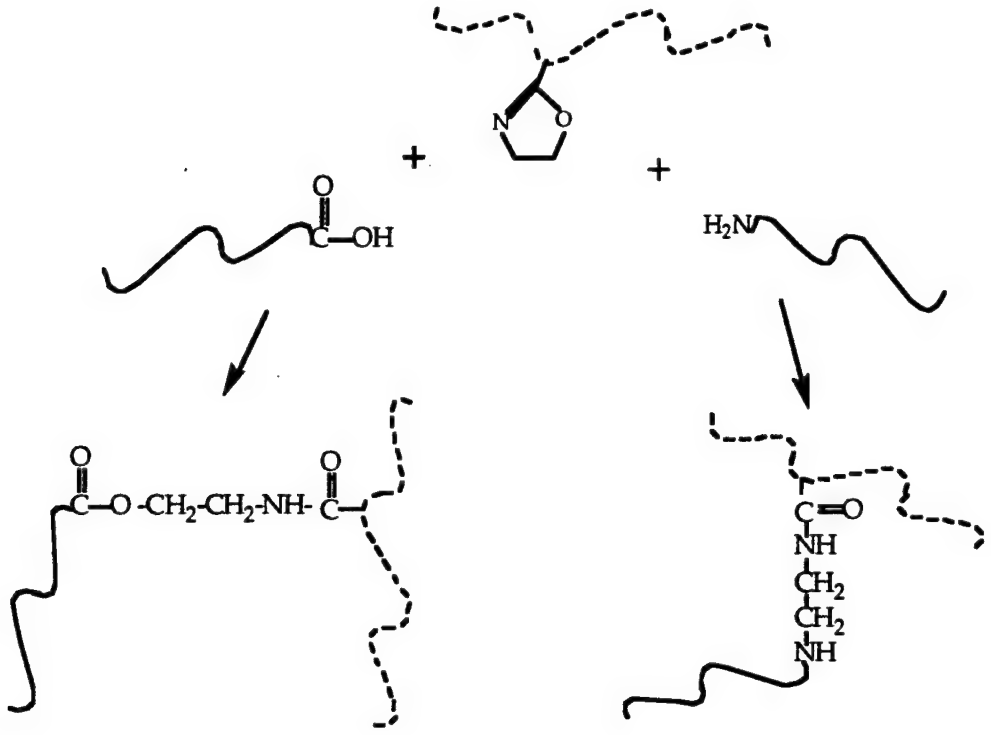

Figure 3.2. Schematic representation of reactions between vinyl oxazoline and aPA endgroups.

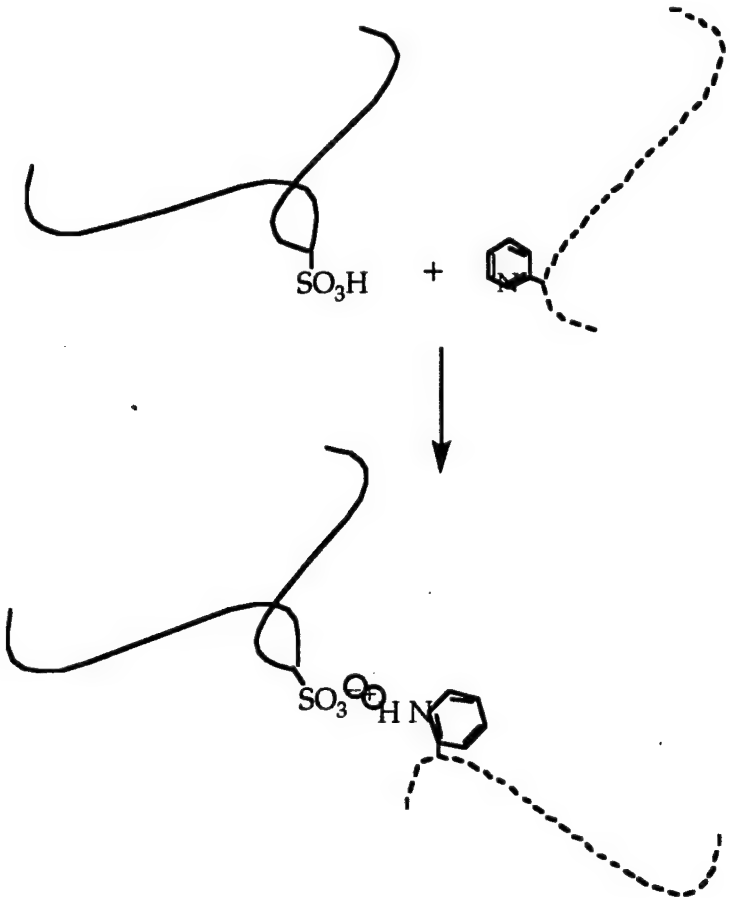

Figure 3.3. Ionic bonding between pyridine and sulfonic acid.

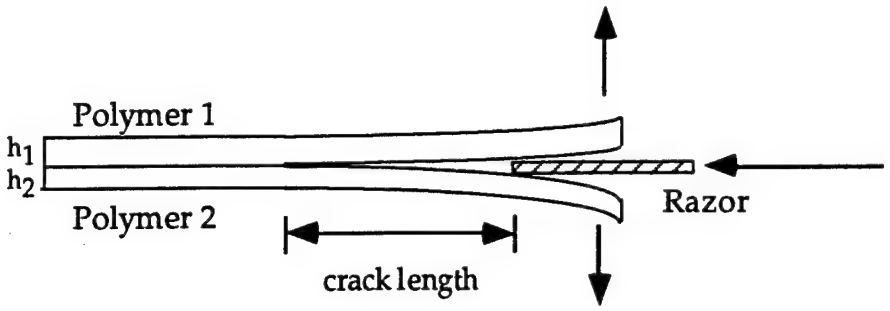

Figure 3.4. Schematic representation of the ADCB test.

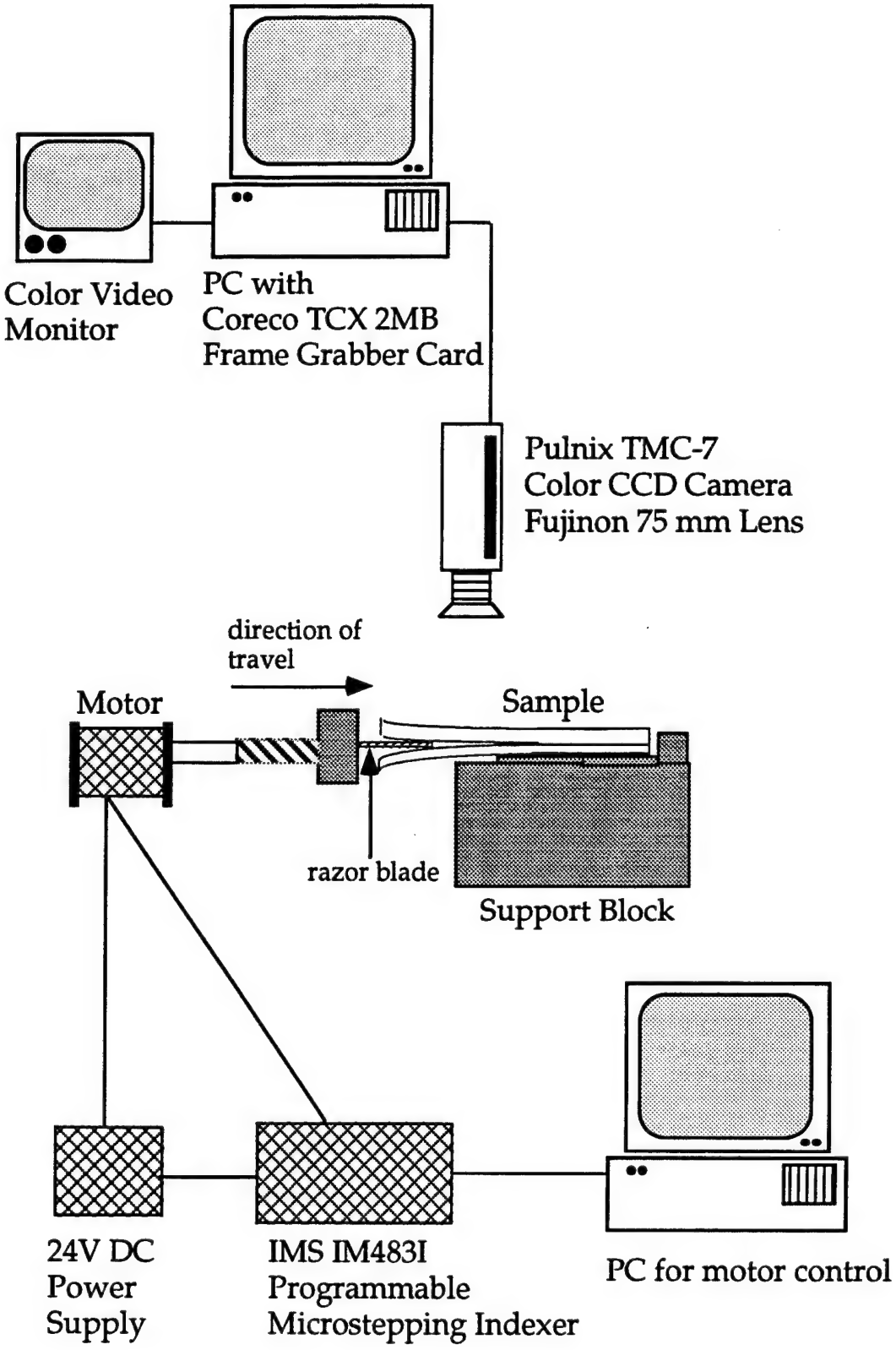

Figure 3.5. Schematic representation of the data collection system.

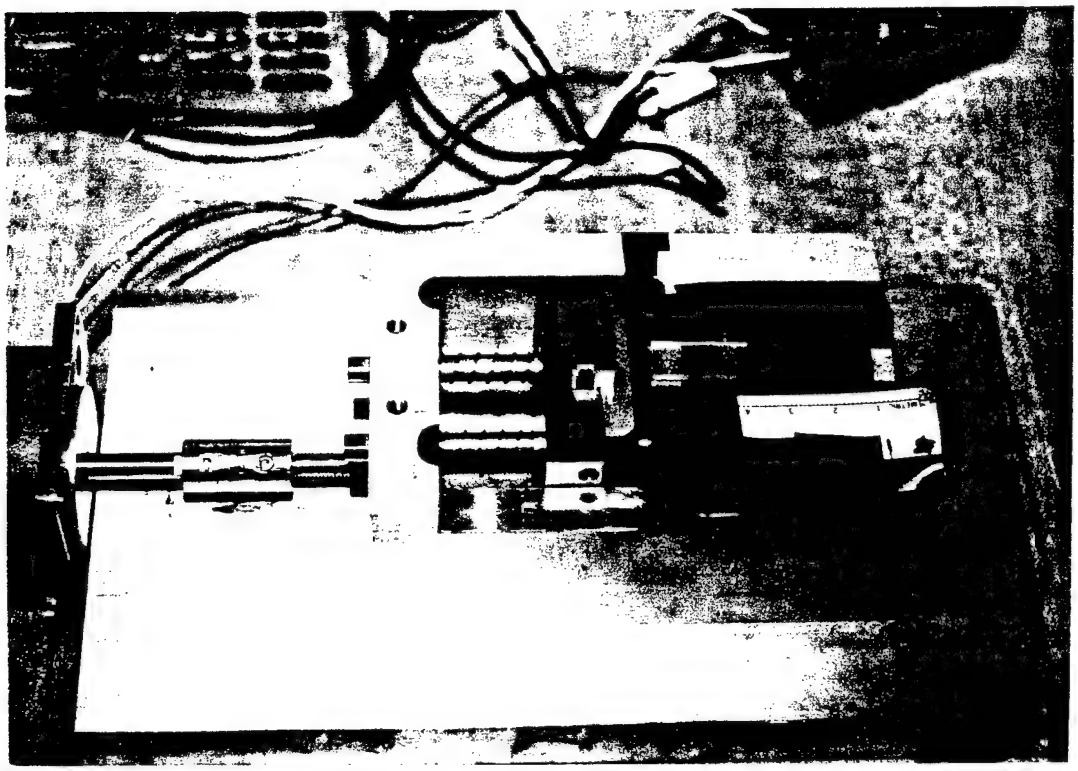

Figure 3.6. The support block and sample positioning.

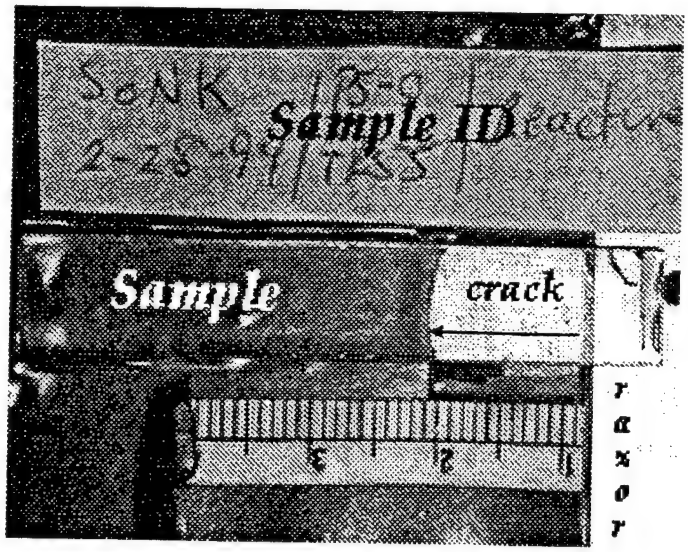

Figure 3.7. Example video data from an interfacial fracture test.

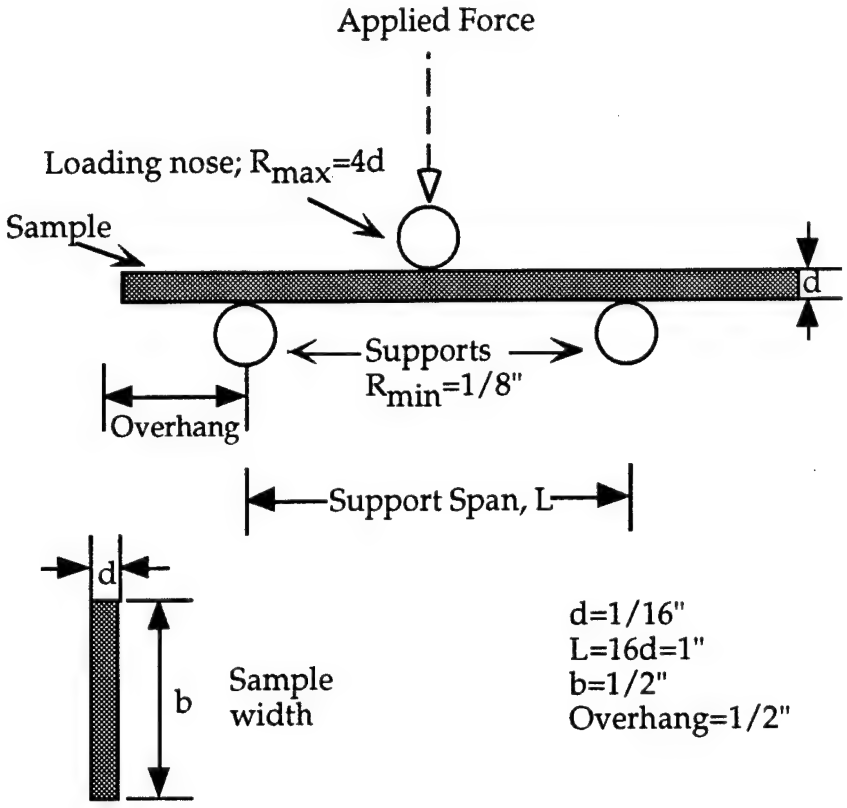

Figure 3.8. Geometry and dimensions of the 3 point bending test.

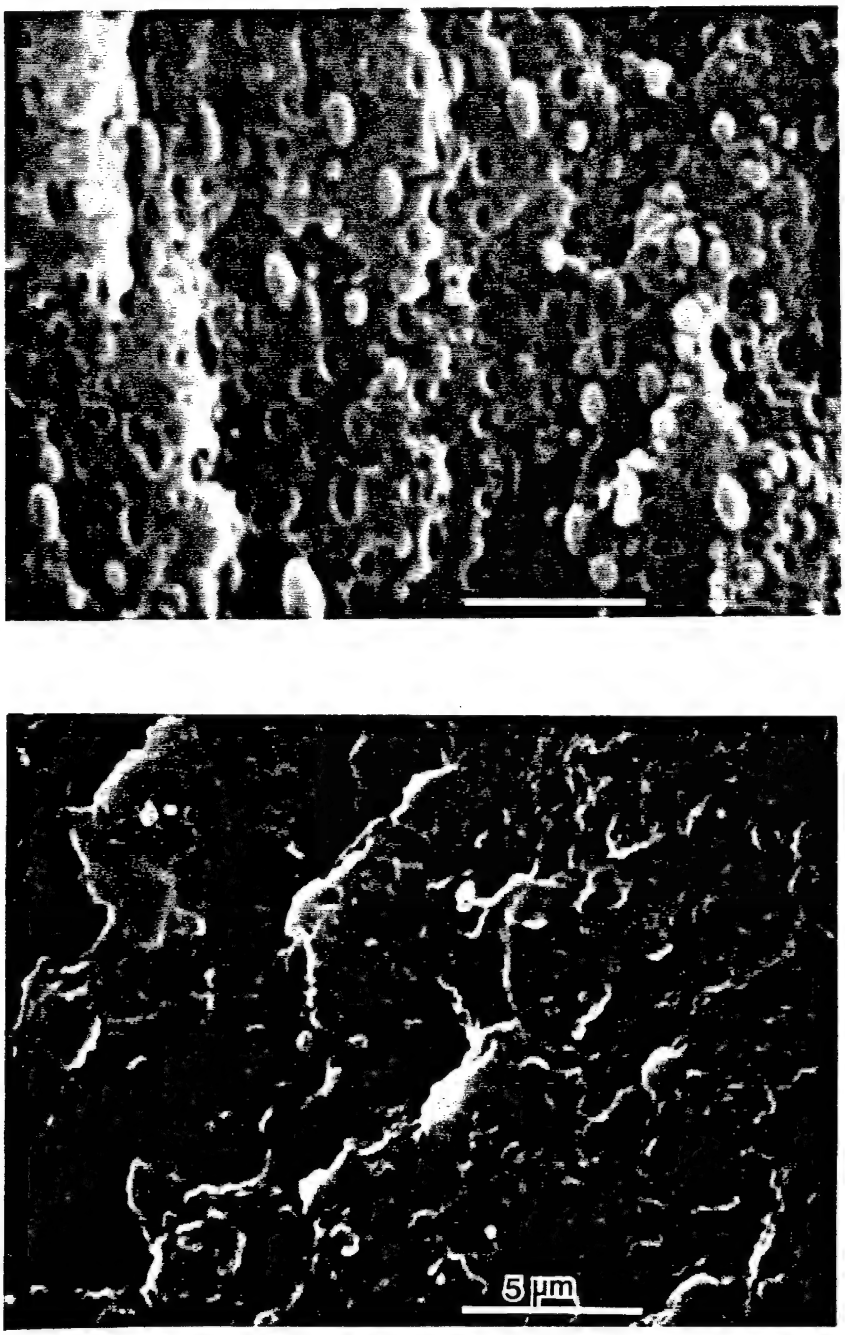

Figure 4.1. Microstructure of a) 20PS/80aPA and b) 20PS-ox/80aPA blends. (Scanning electron micrographs, x5000)

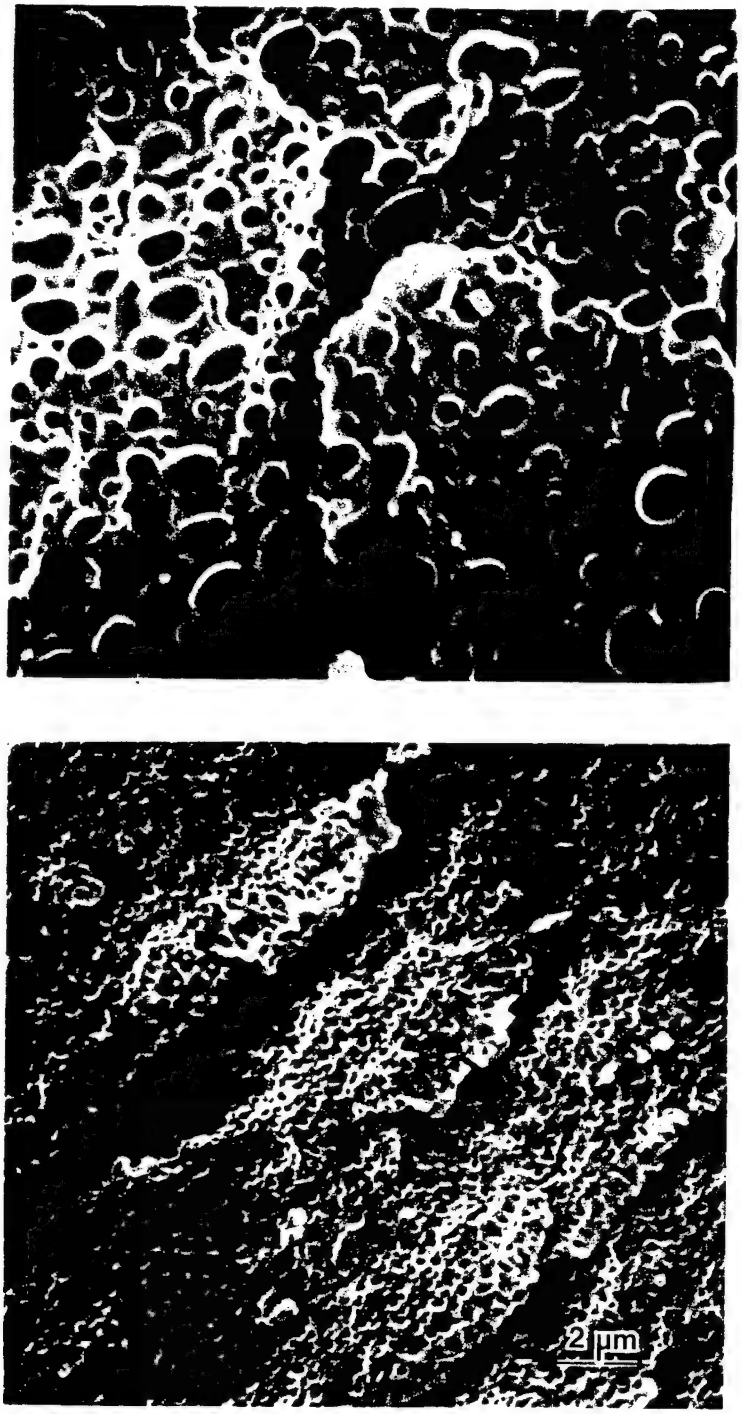

Figure 4.2. Microstructure of a) 20PS/80aPA and b) 20PS-ox/80aPA blends, etched in toluene to remove PS particles. (Scanning electron micrographs, x5000)

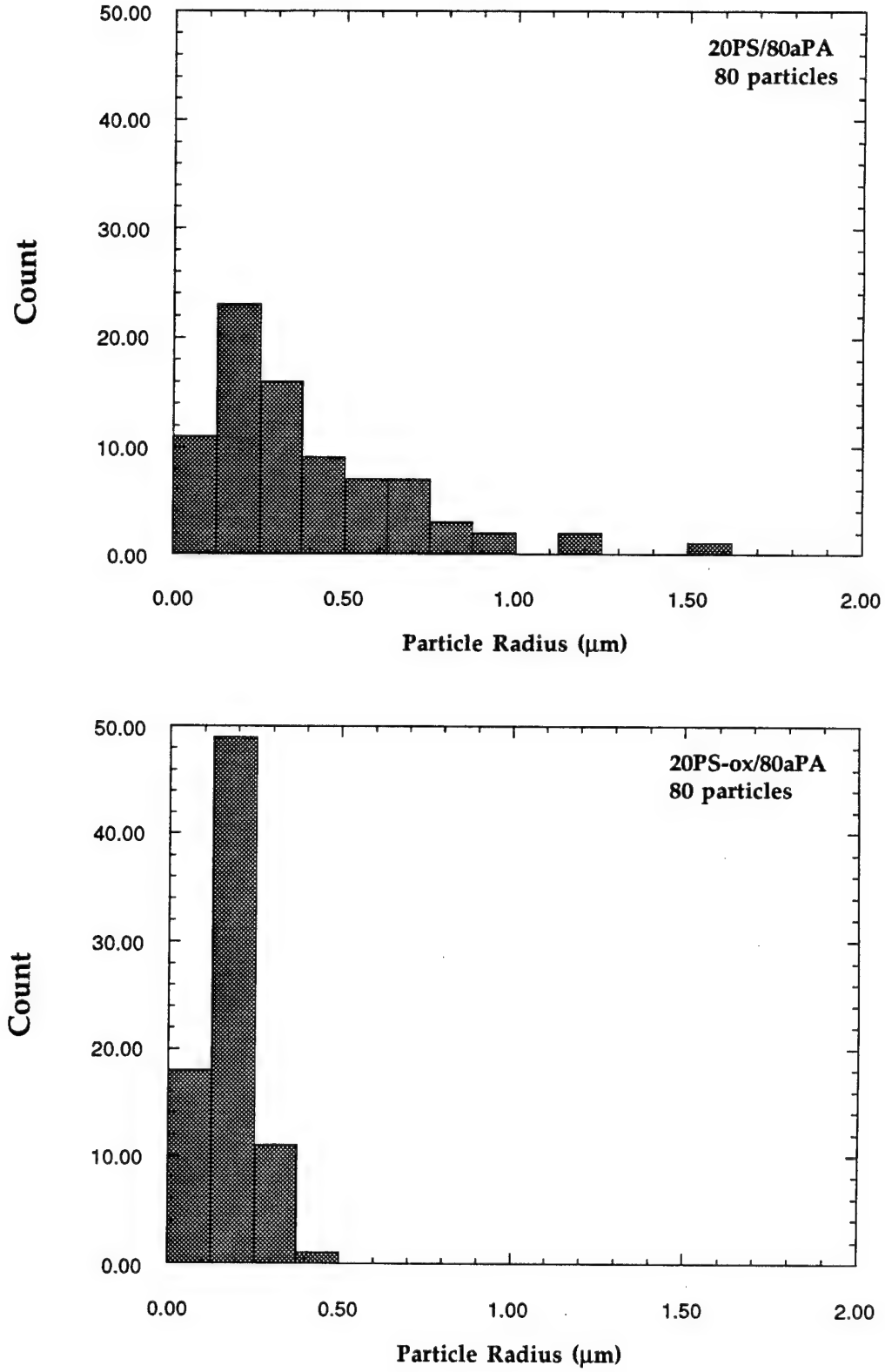

Figure 4.3. Particle size distributions in PS/aPA melt blends.

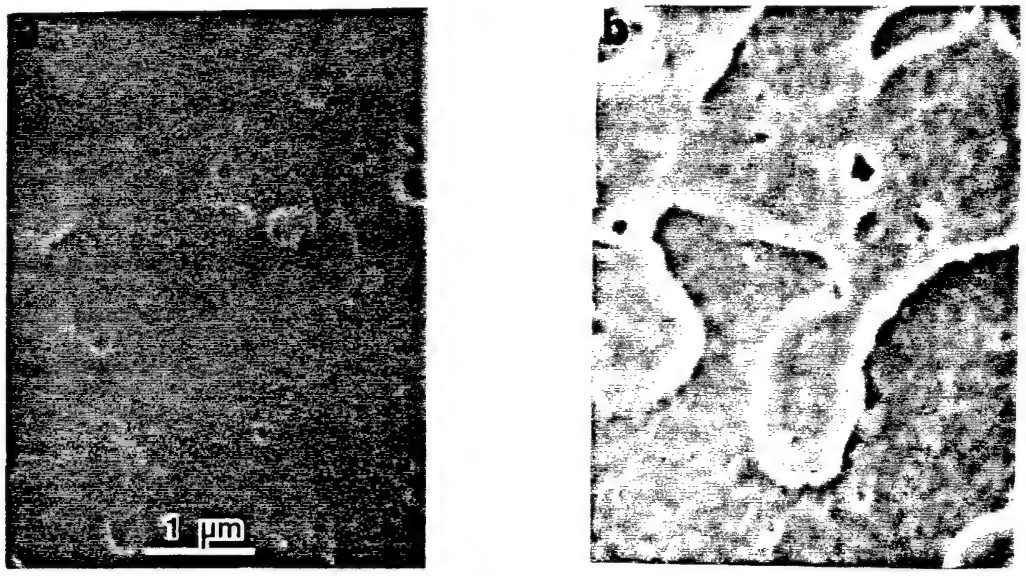

Figure 4.4. Microstructures of a) 1PS/99aPA and b)1PS-ox/99aPA blends, etched in toluene to remove PS particles. (Scanning electron micrographs, x15,000)

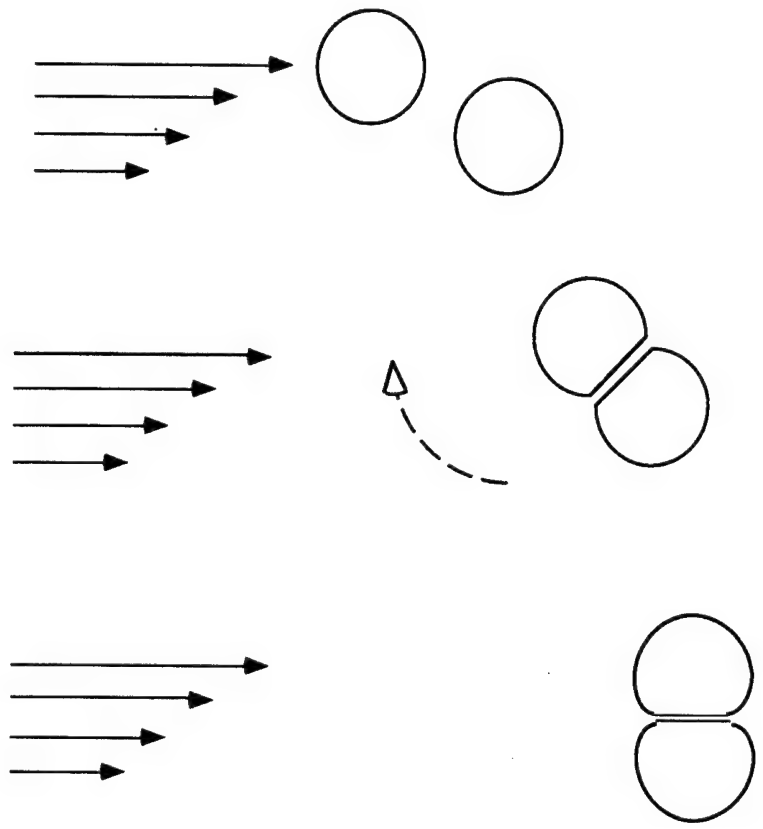

Figure 4.5. Geometry of an interacting pair of droplets.
Initial approach, top. Collision and rotation, middle. Bottom, final position. The upper droplet may move past the lower one, or the pair may coalesce.

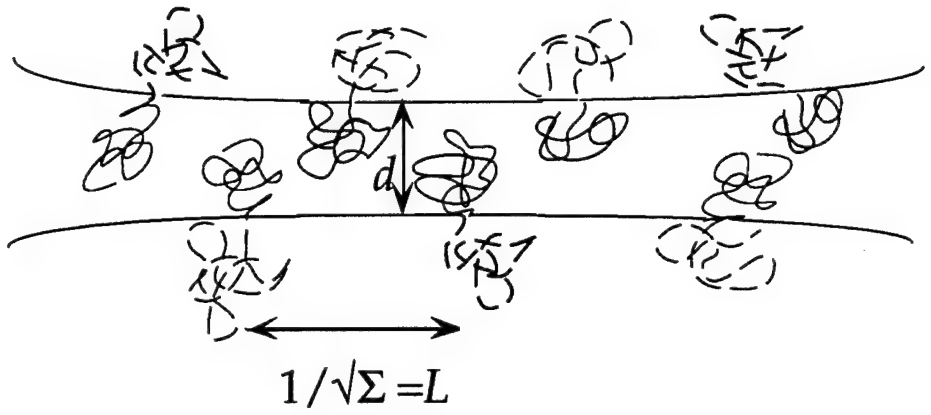

Figure 4.6. Schematic of the contact area between two compatibilized particle surfaces.

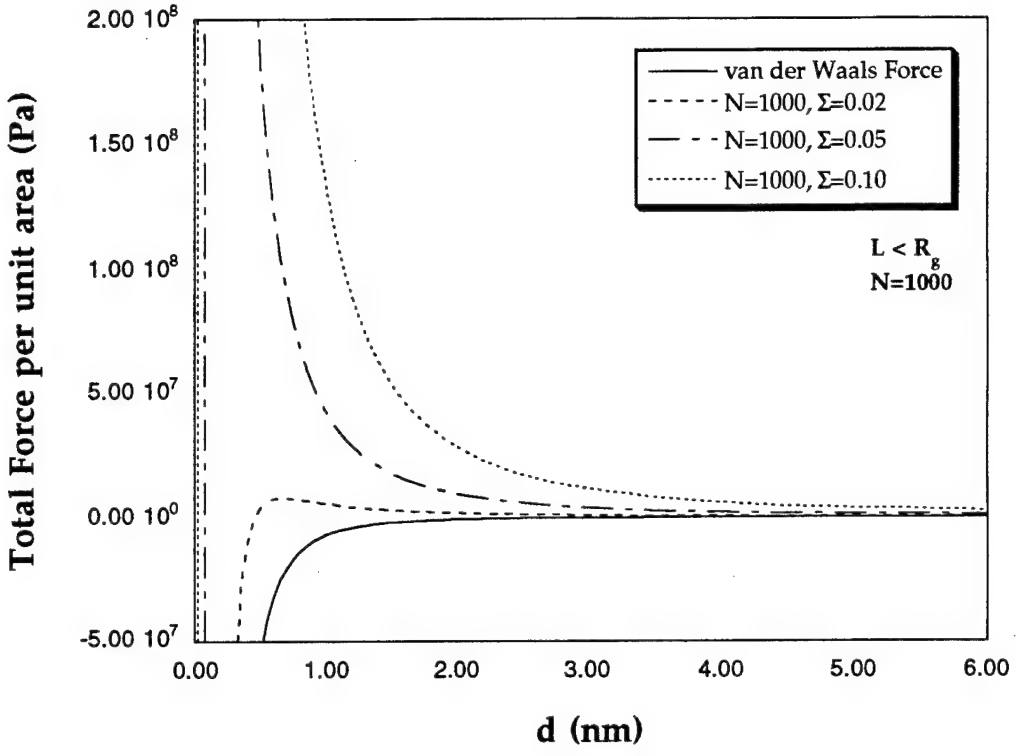

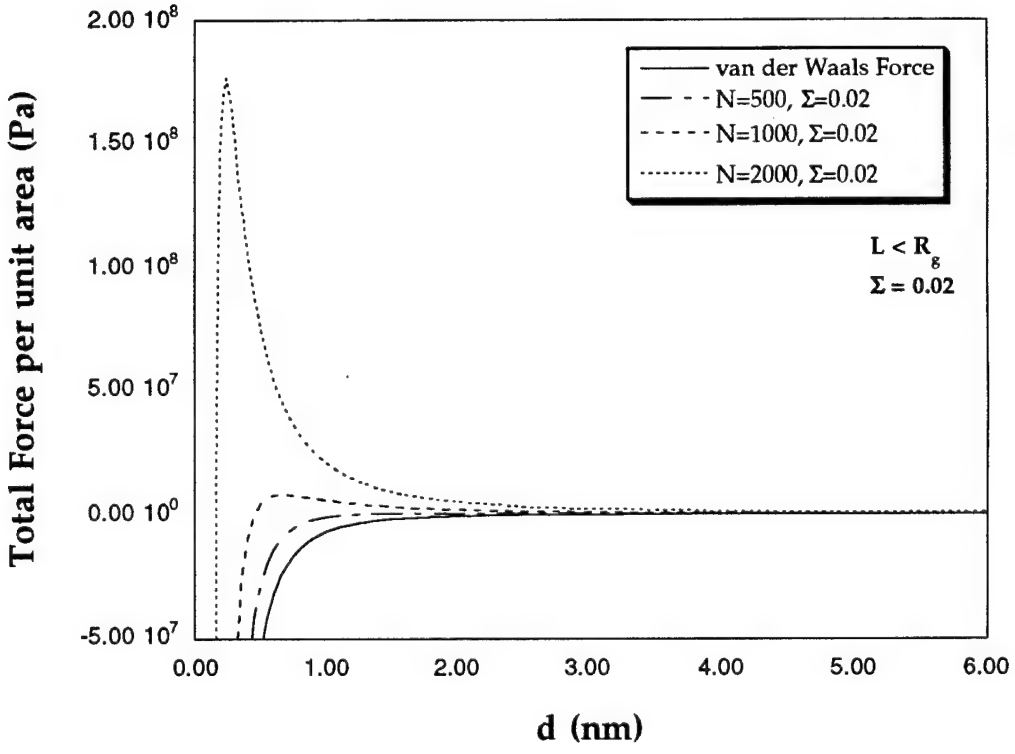

Figure 4.7. Surface forces versus surface separation. High grafting density.

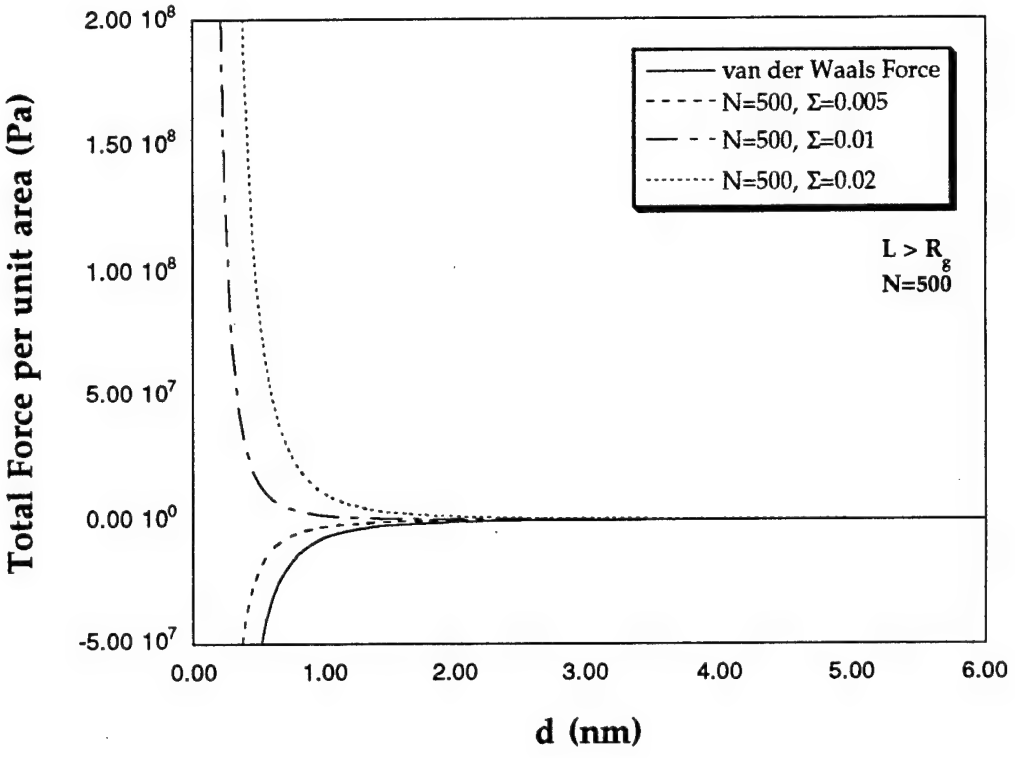

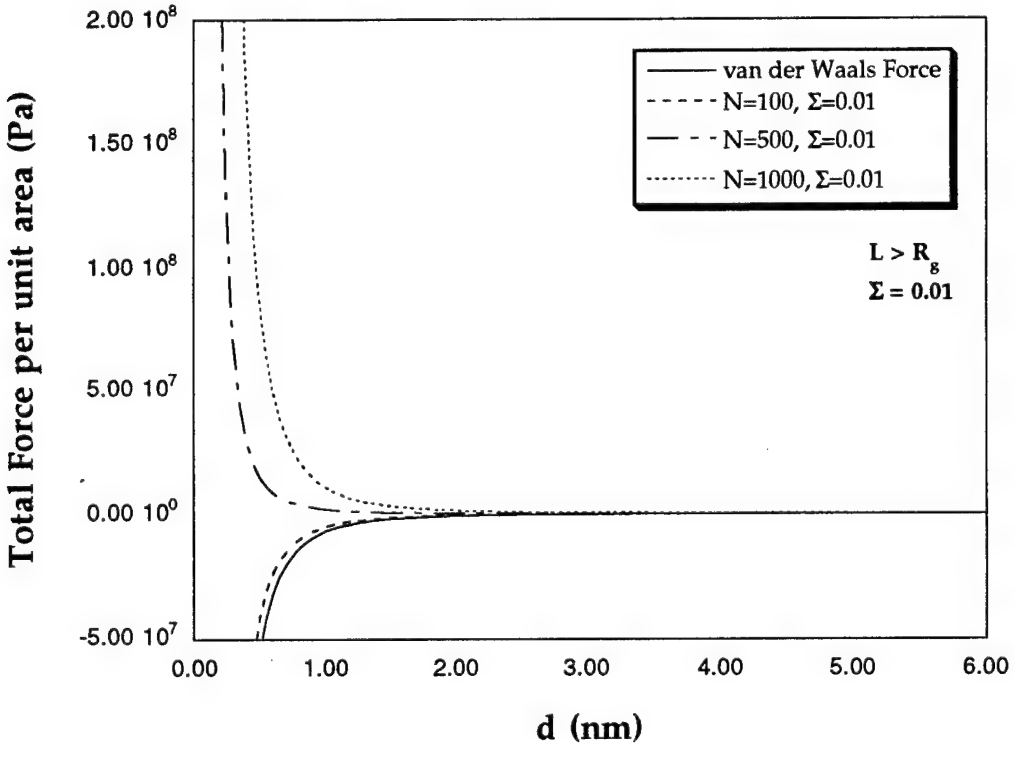

Figure 4.8. Surface force versus surface separation. Low grafting density.

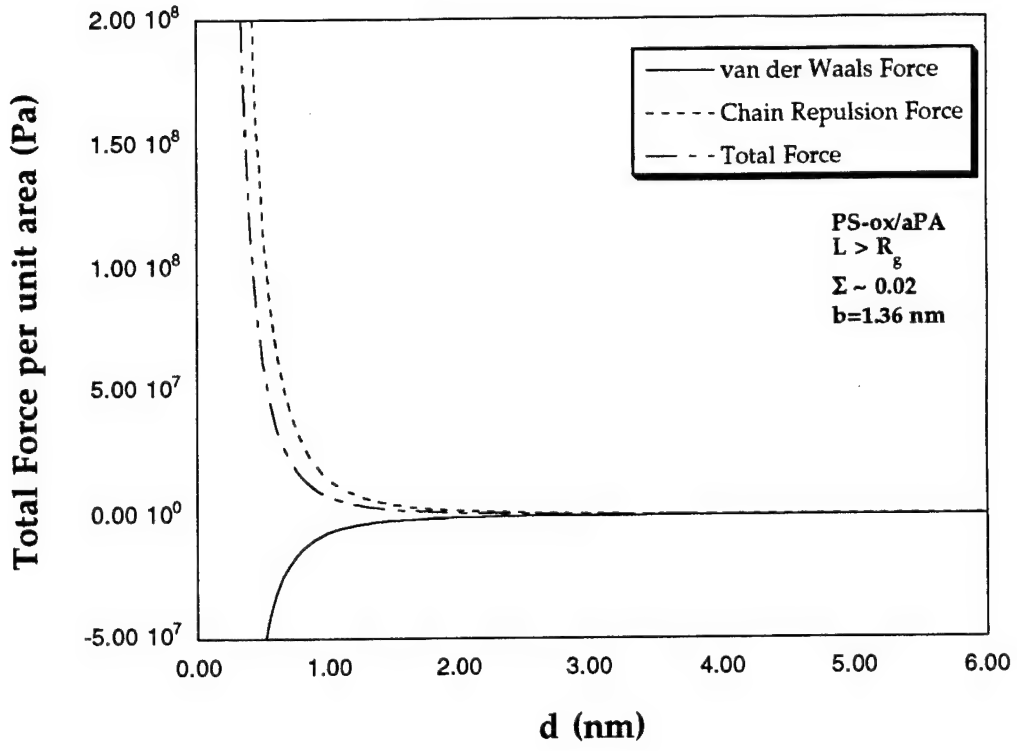

Figure 4.9. Surface force versus surface separation. $\Sigma = \Sigma_{PS\text{-}ox/aPA} = 0.02$, $N = N_{aPA} \sim 110$, $b = b_{Nylon\ 12} = 1.36$ nm.

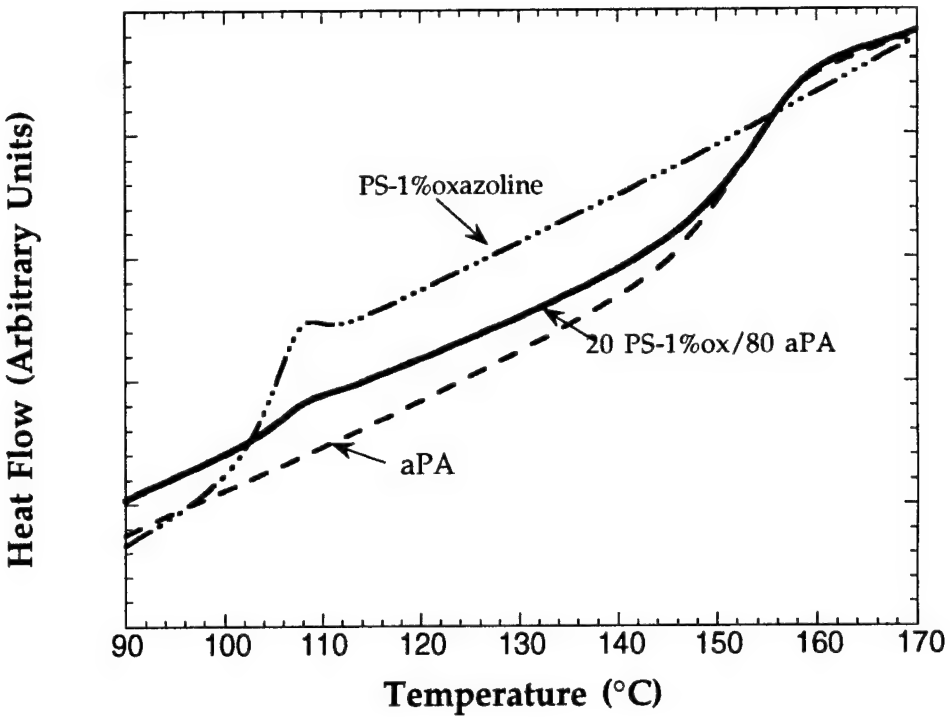

Figure 4.10. Differential scanning calorimetry of the 20 PS-ox/80 aPA blend, PS-ox and aPA.

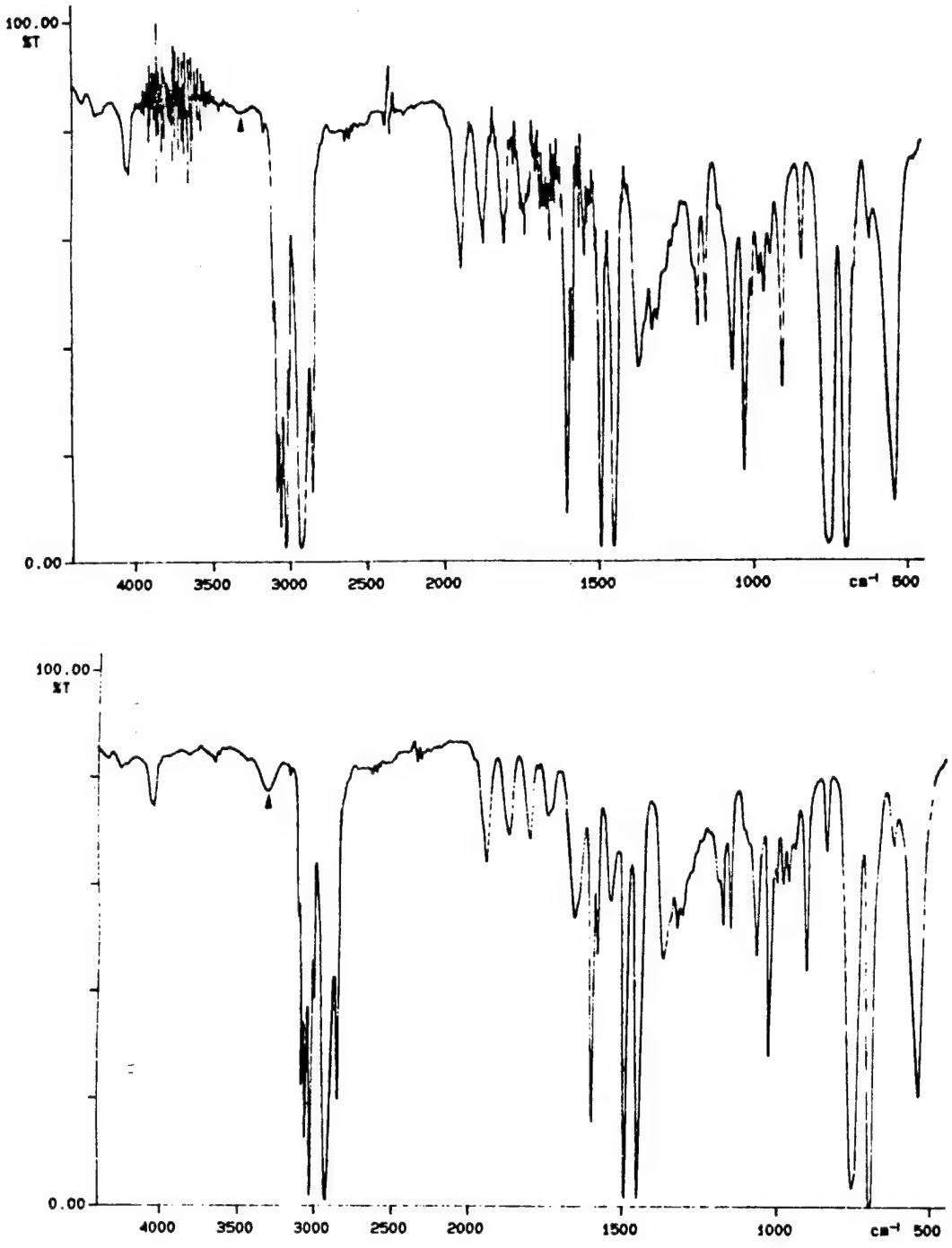

Figure 4.11. FTIR spectroscopic scan of a) PS and b) PS-ox extracts from 20% blends in aPA. Arrow indicates peak associated with residual aPA.

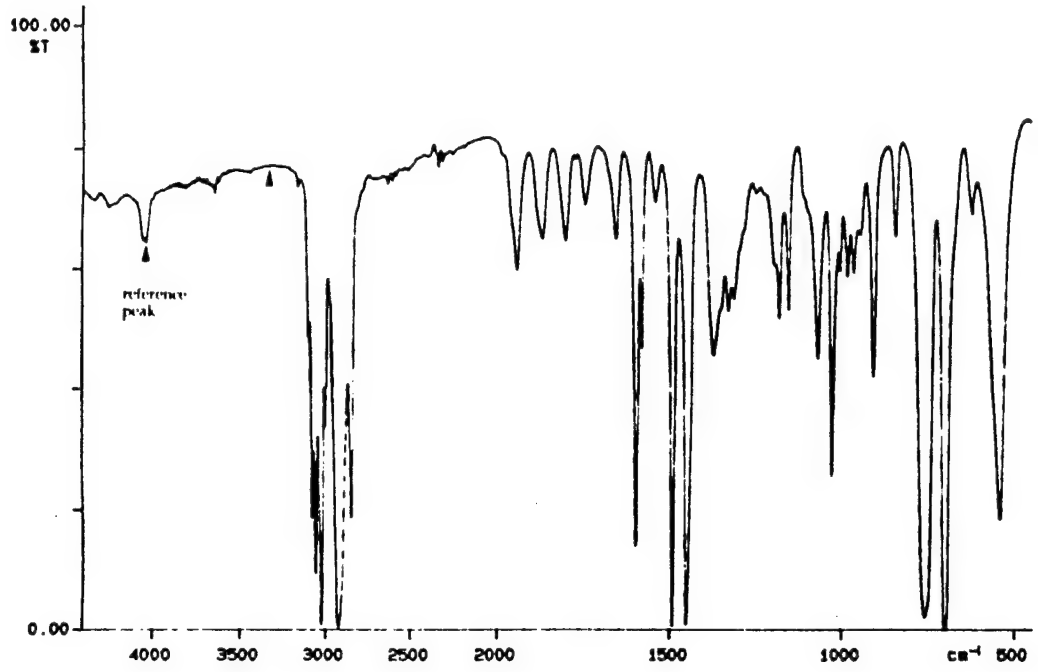

Figure 4.12. FTIR spectroscopic scan of pure PS-ox.

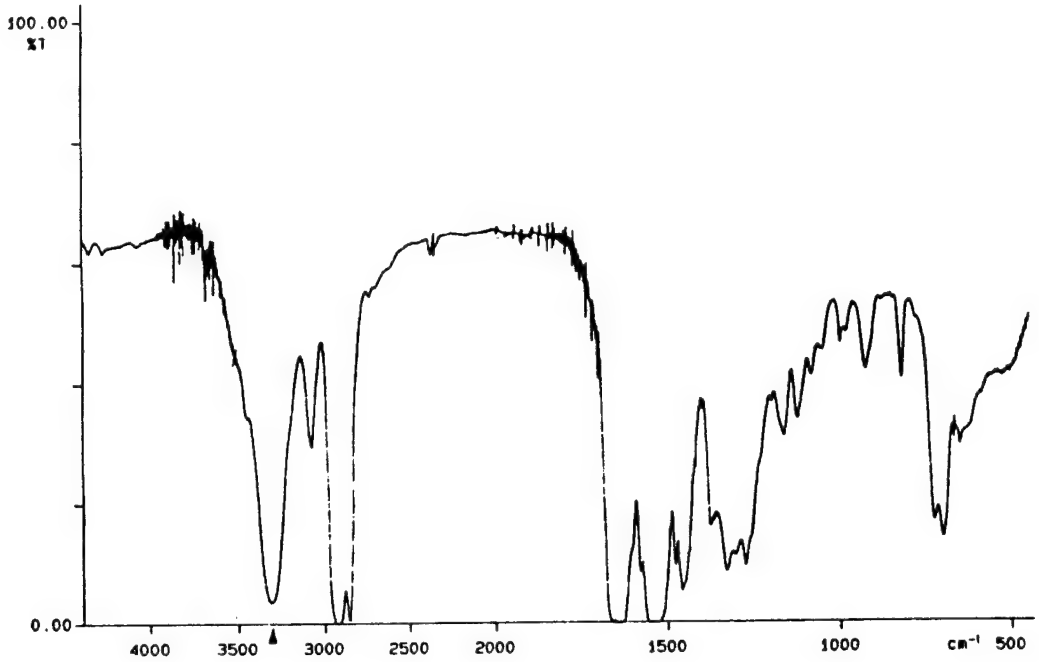

Figure 4.13. FTIR spectroscopic scan of pure aPA.

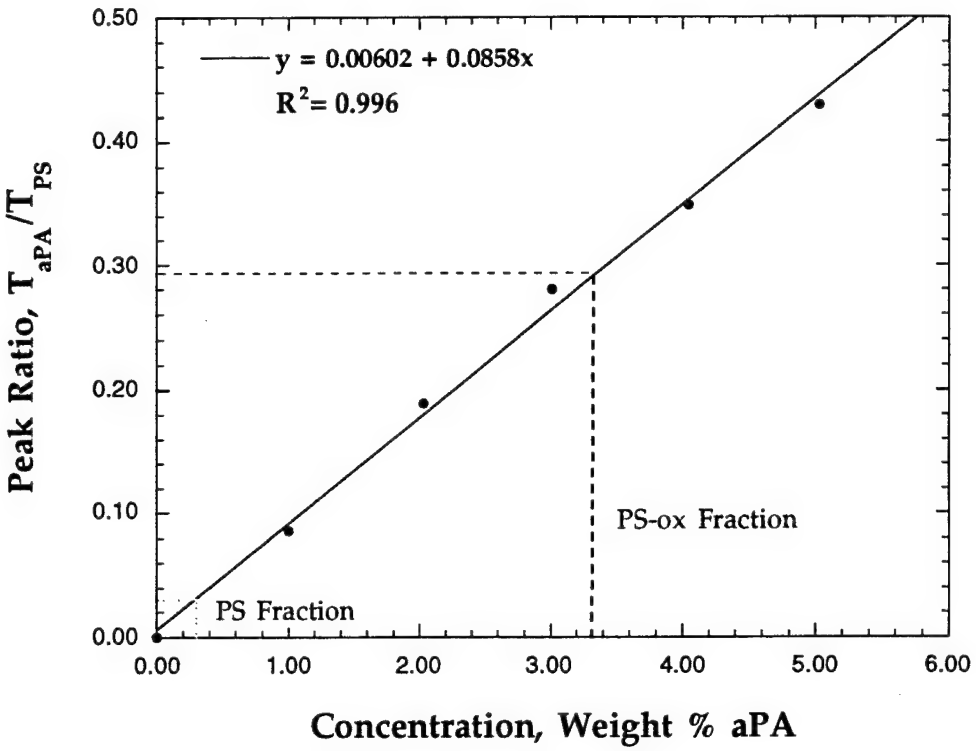

Figure 4.14. Calibration curve for PS/aPA blends. Dashed lines indicate method of obtaining aPA concentration in PS fractions extracted from 20:80 melt blends.

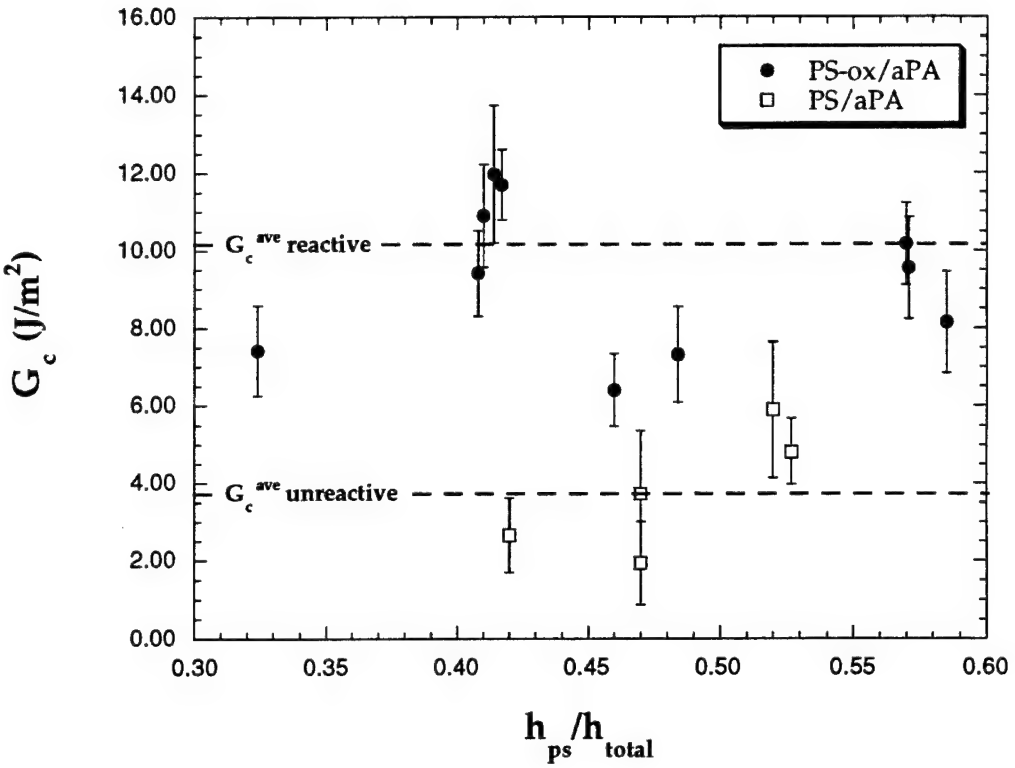

Figure 4.15. Critical energy release rate for interfacial fracture versus the ratio of ps beamthickness to total beam thickness.

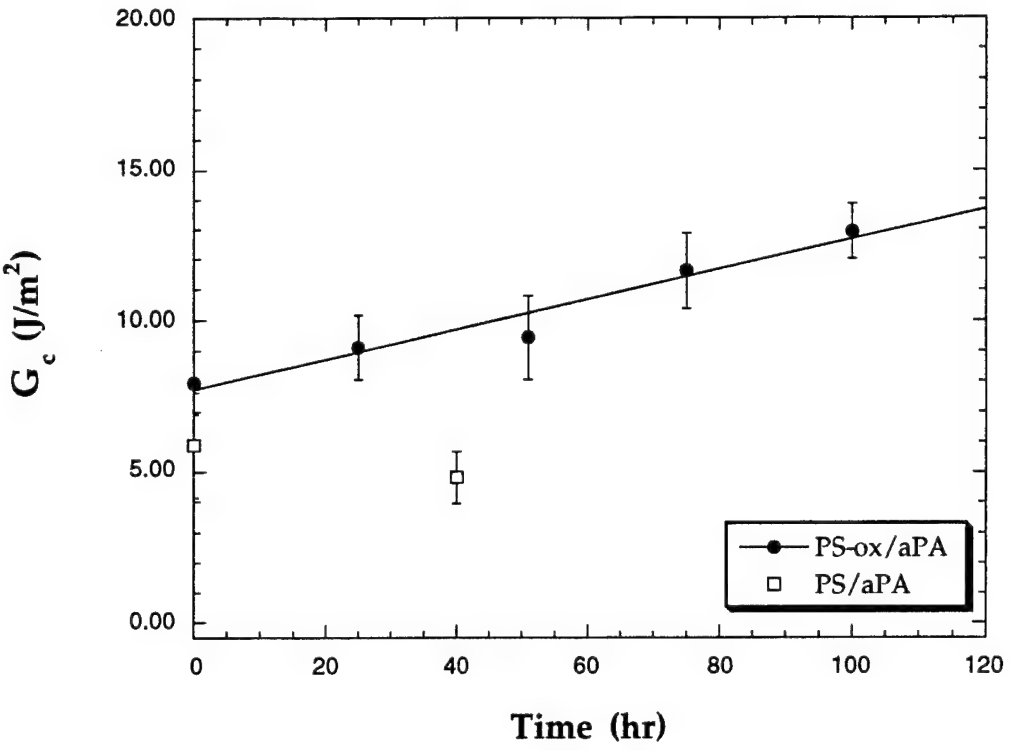

Figure 4.16. Critical energy release rate for interfacial failure versus reaction time at 150°c.

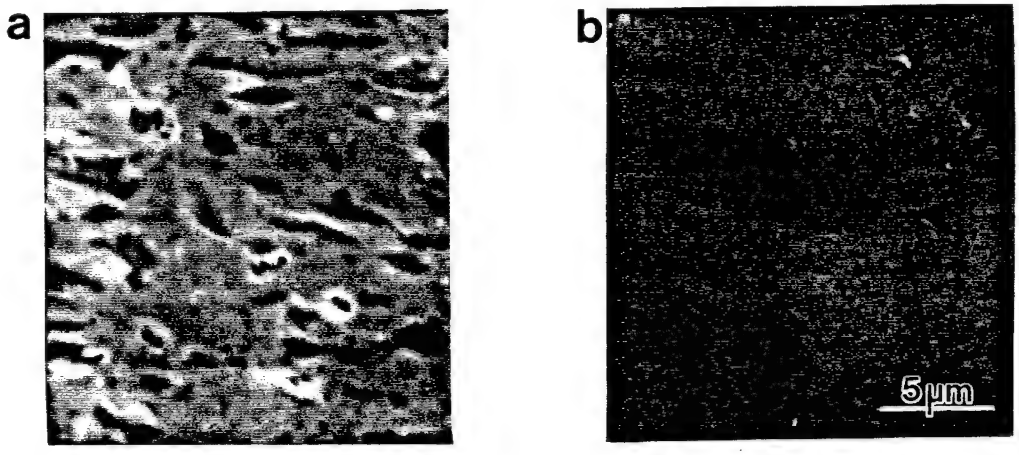

Figure 5.1. Microstructure of a) 20PS/80 P2VP and b) 20PS-1.67SO_3H/80P2VP blends. (Backscattered electron image, 3000x. Samples have been stained with iodine vapor. The lighter phase is P2VP.)

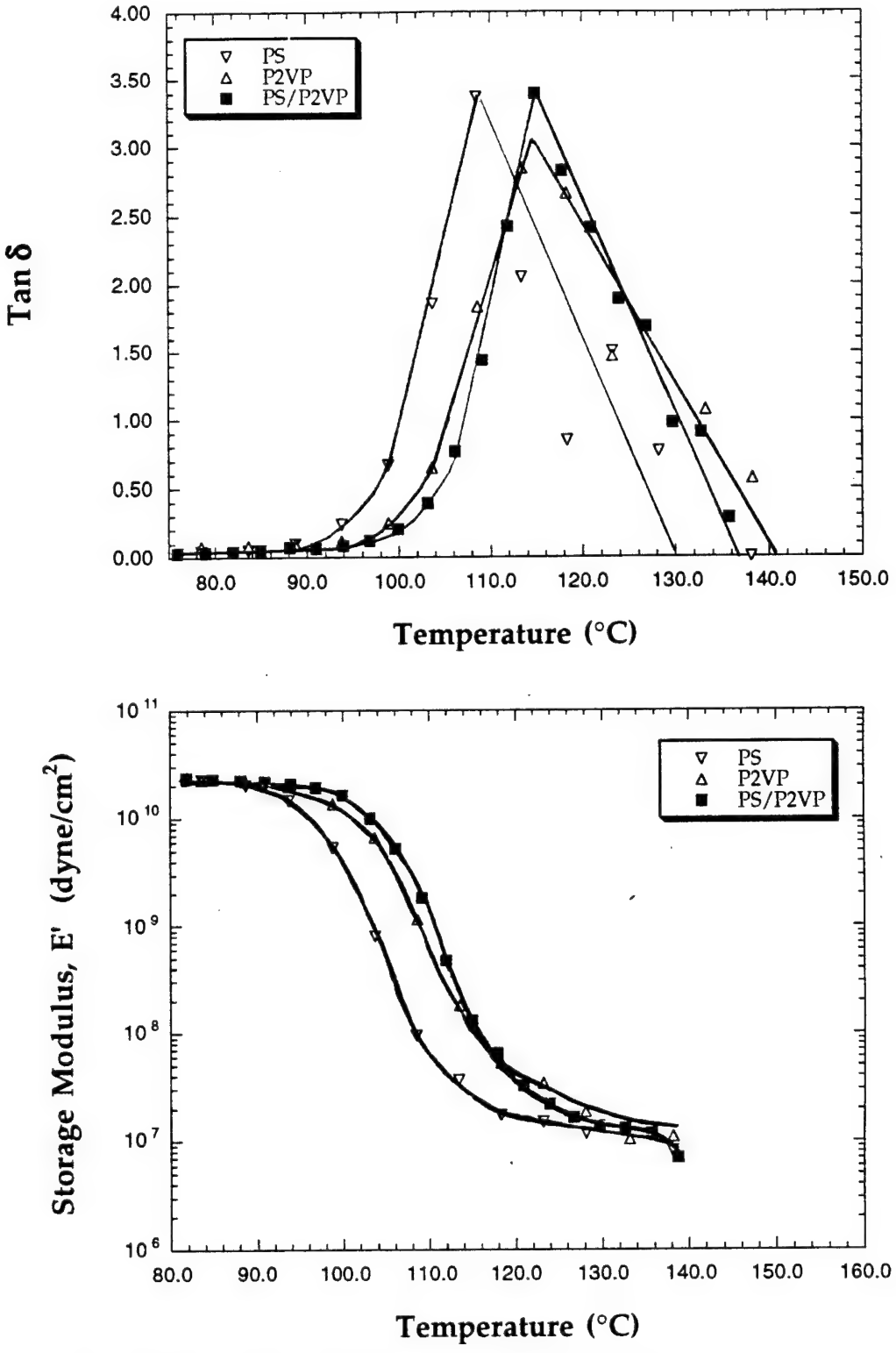

Figure 5.2. DMA of PS, P2VP and the 50:50 blend.

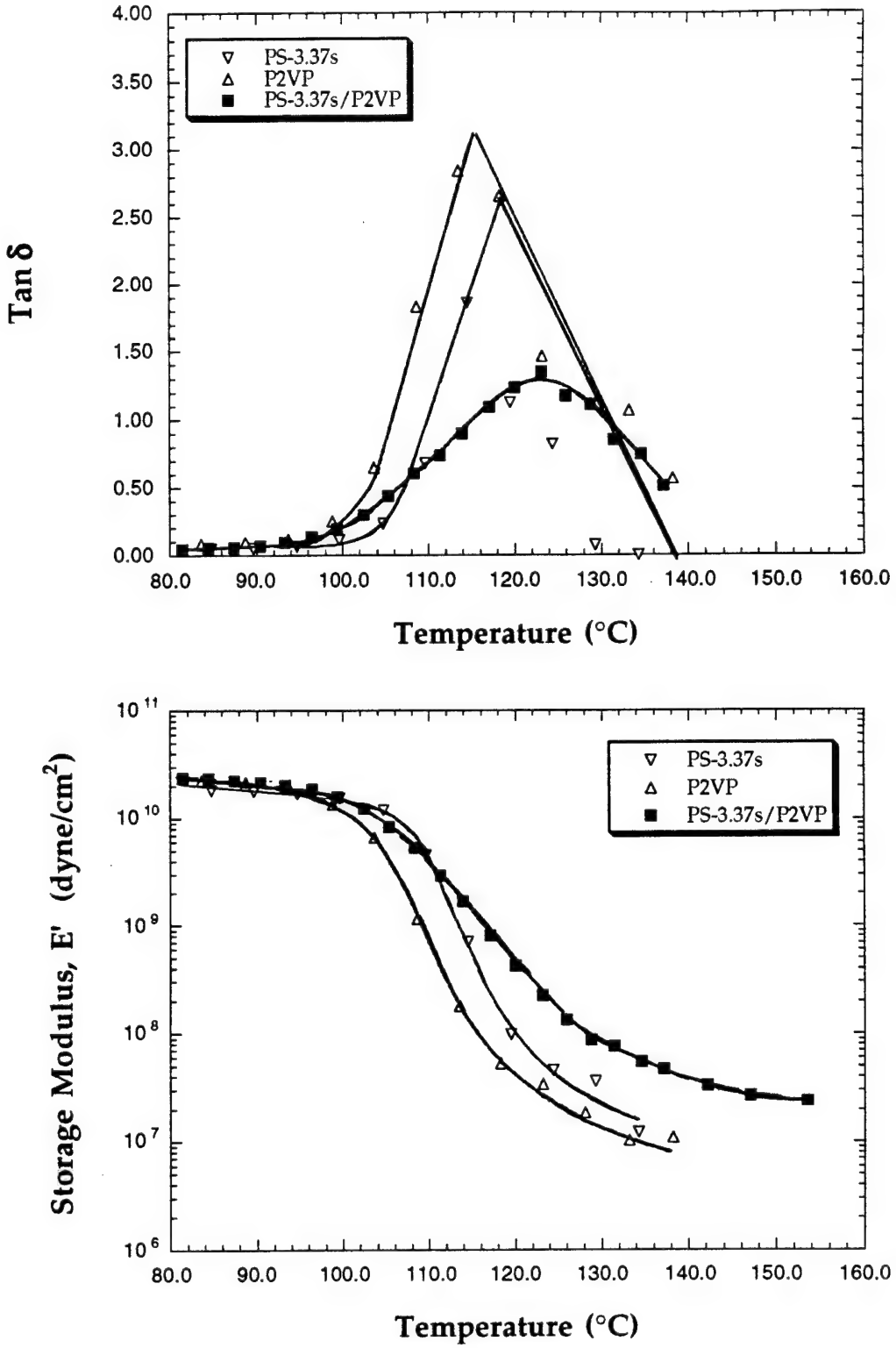

Figure 5.3. DMA of PS-3.37SO_3H, P2VP and the 50:50 blend.

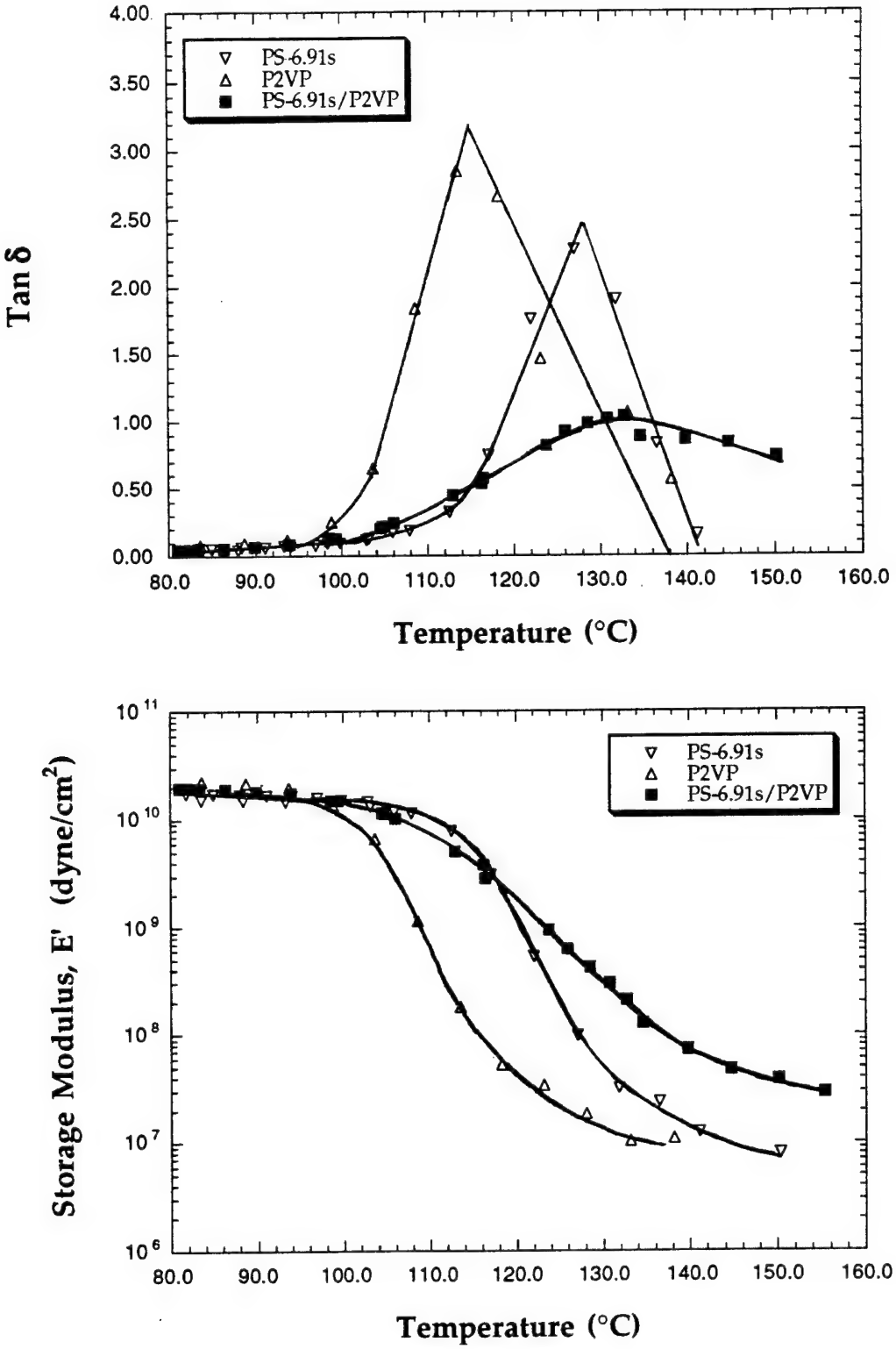

Figure 5.4. DMA of PS-6.91SO3H, P2VP and the 50:50 blend.

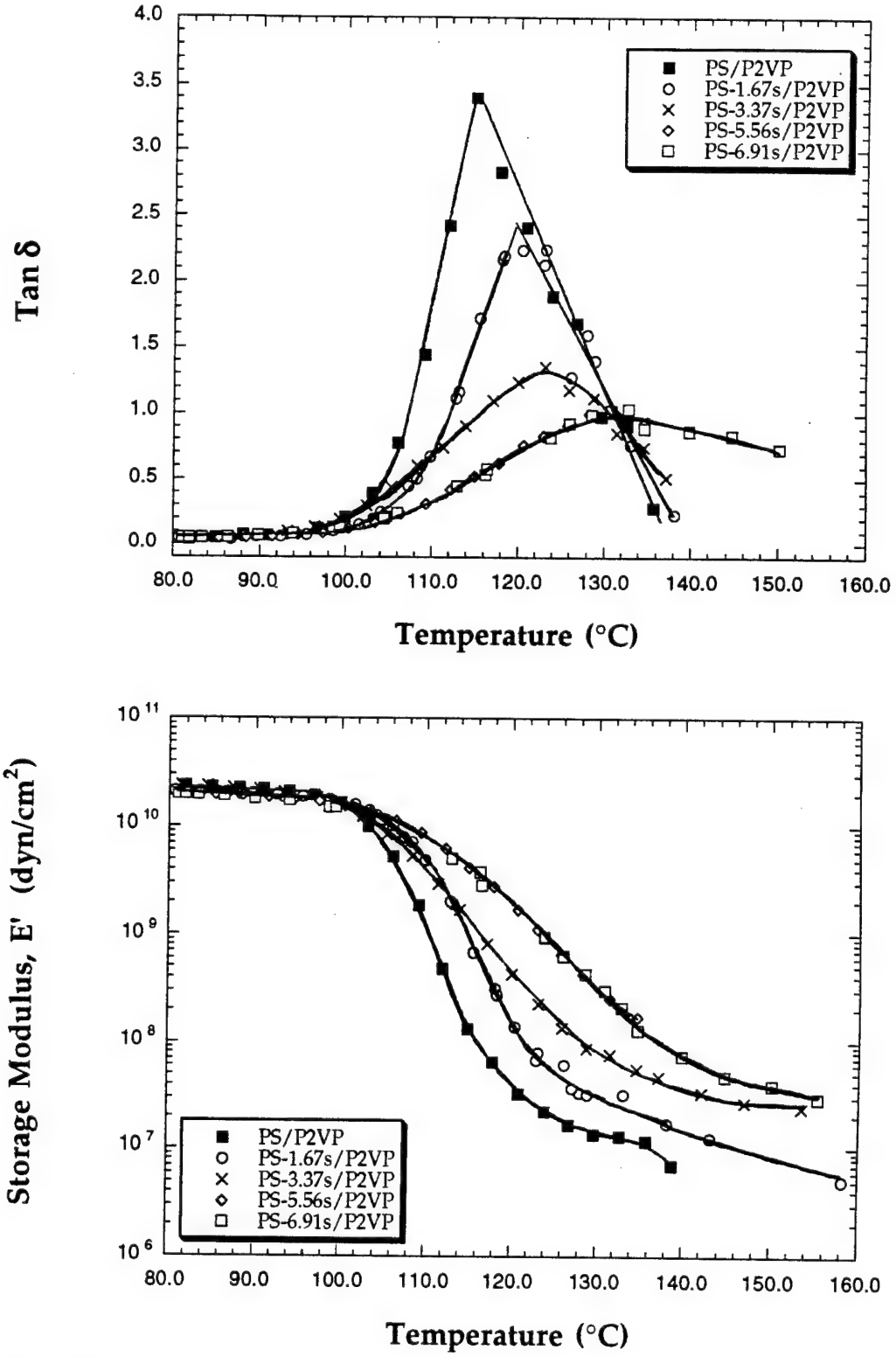

Figure 5.5. Dynamic mechanical spectra of 50:50 sPS/P2VP blends.

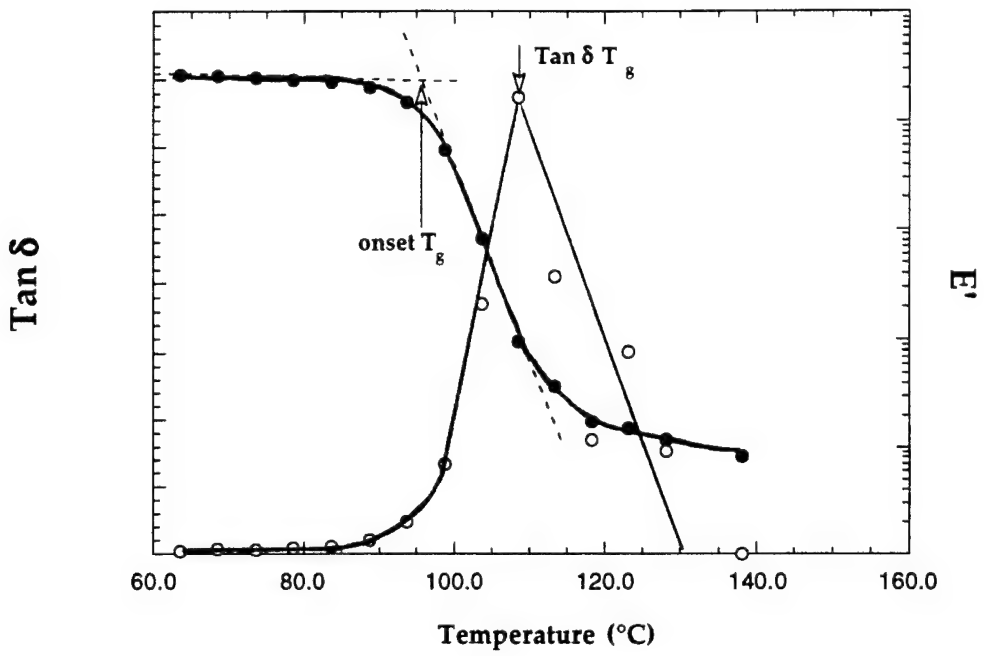

Figure 5.6. Determination of the glass transition temperature by the onset method and from the Tan δ peak.

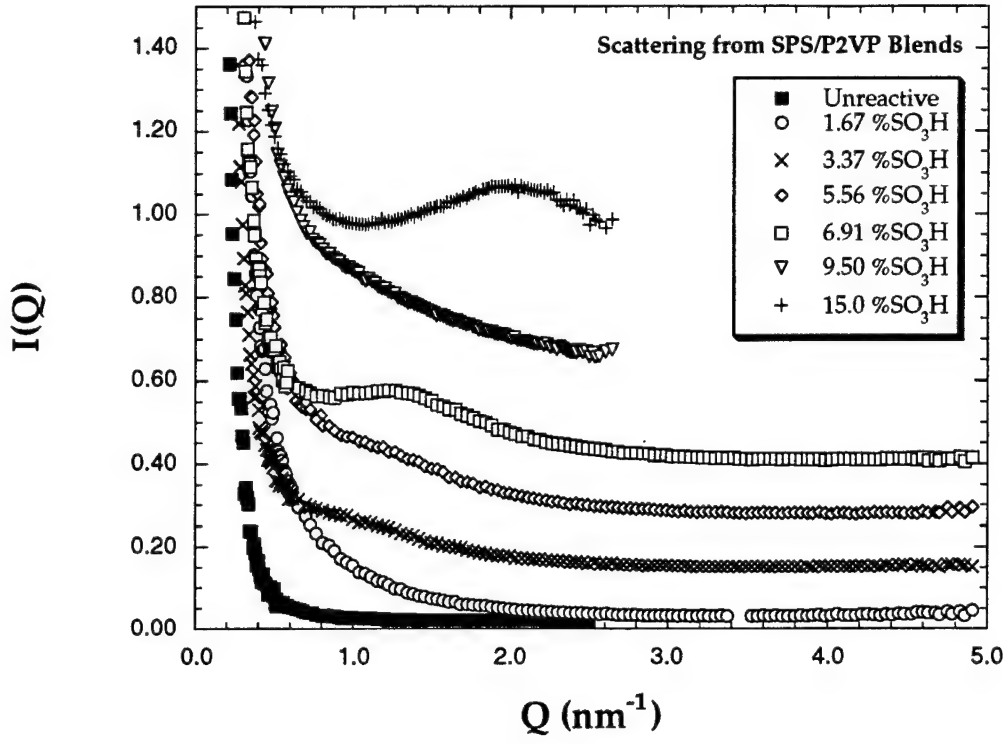

Figure 5.7. Small angle X-ray scattering from sPS/P2VP Blends. The curves have been vertically shifted for clarity.

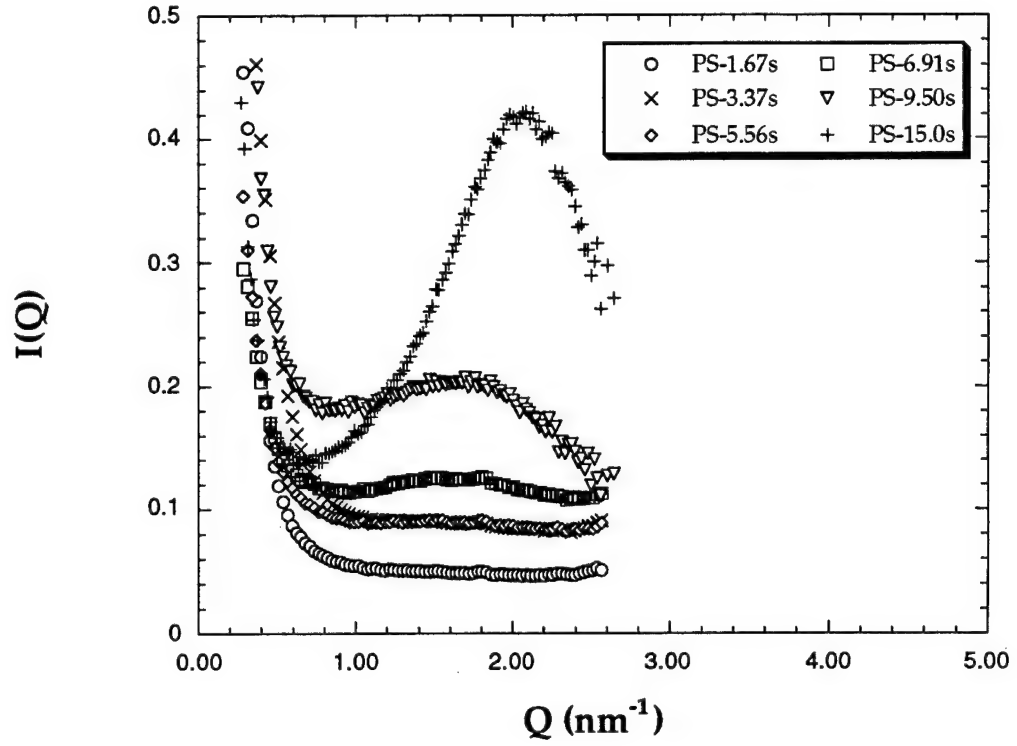

Figure 5.8. Small angle scattering from sulfonated polystyrenes. (Note: The vertical scale has been reduced to accentuate the scattering maxima.)

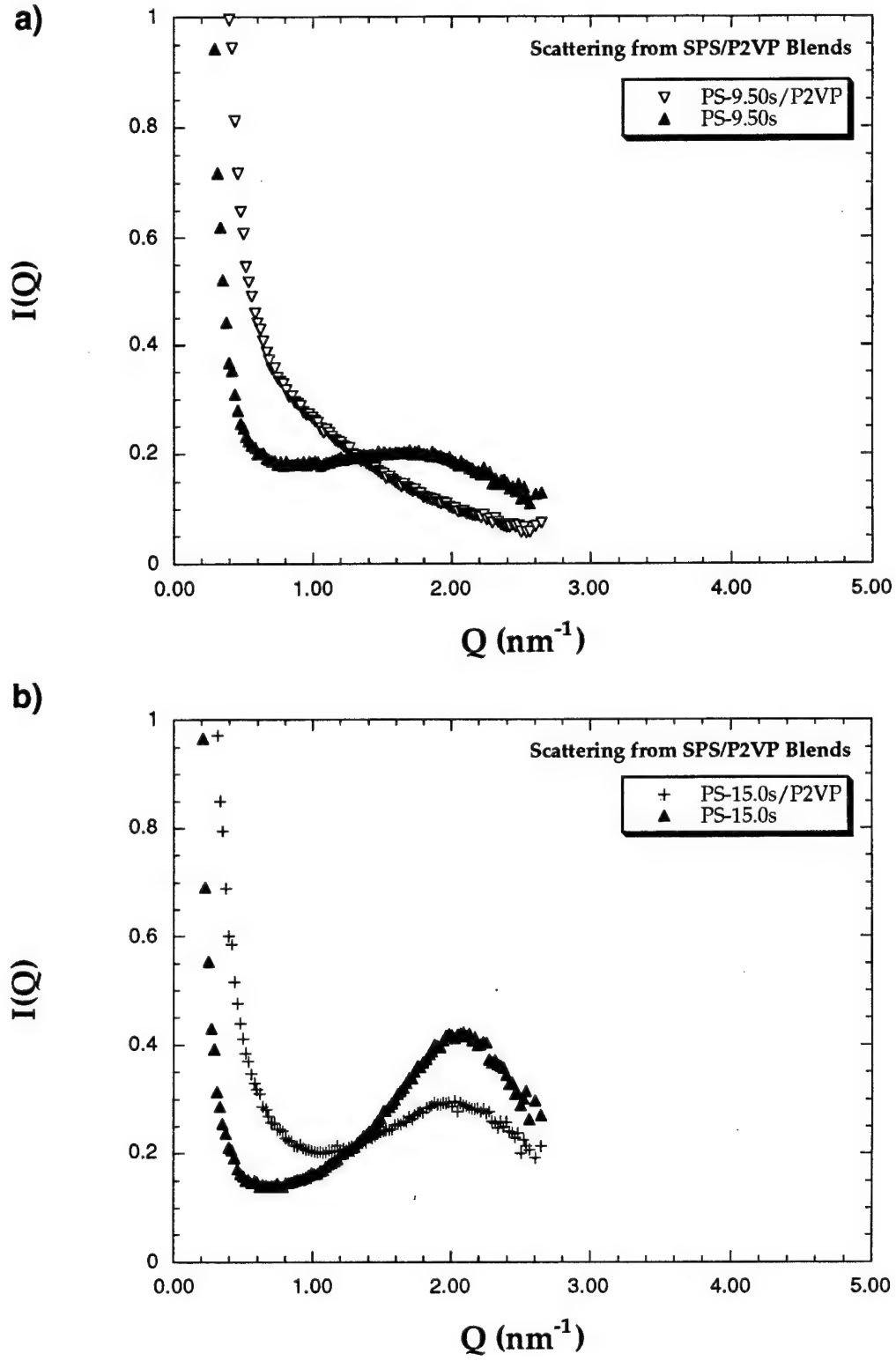

Figure 5.9. Scattering from sPS and sPS/P2VP blends.

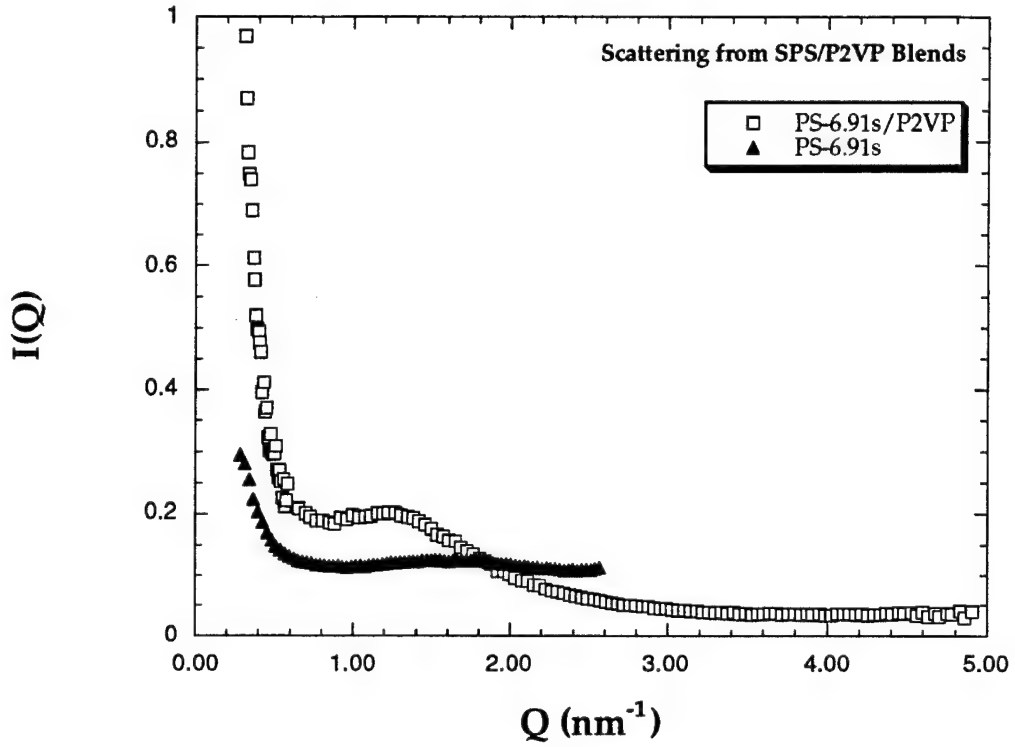

Figure 5.10. Scattering from PS-6.91SO_3H and the PS-6.91SO_3H /P2VP Blend.

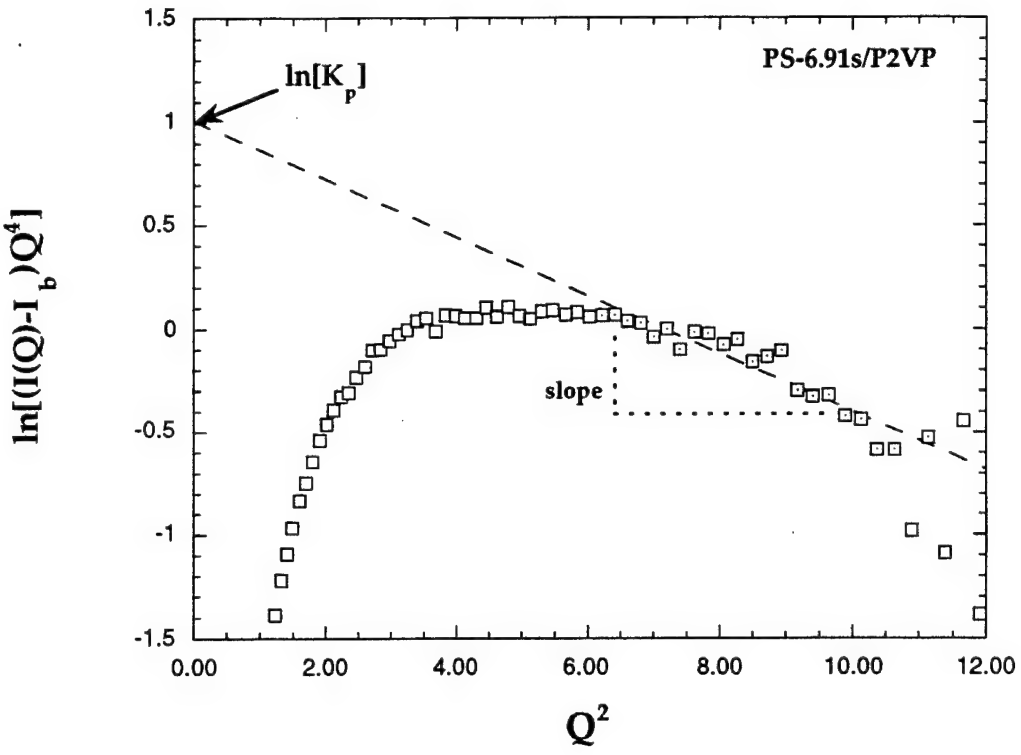

Figure 5.11. Porod plot for PS-6.91SO_3H/P2VP Blend. Background intensity (I_b) has been subtracted from the measured intensity I(Q).

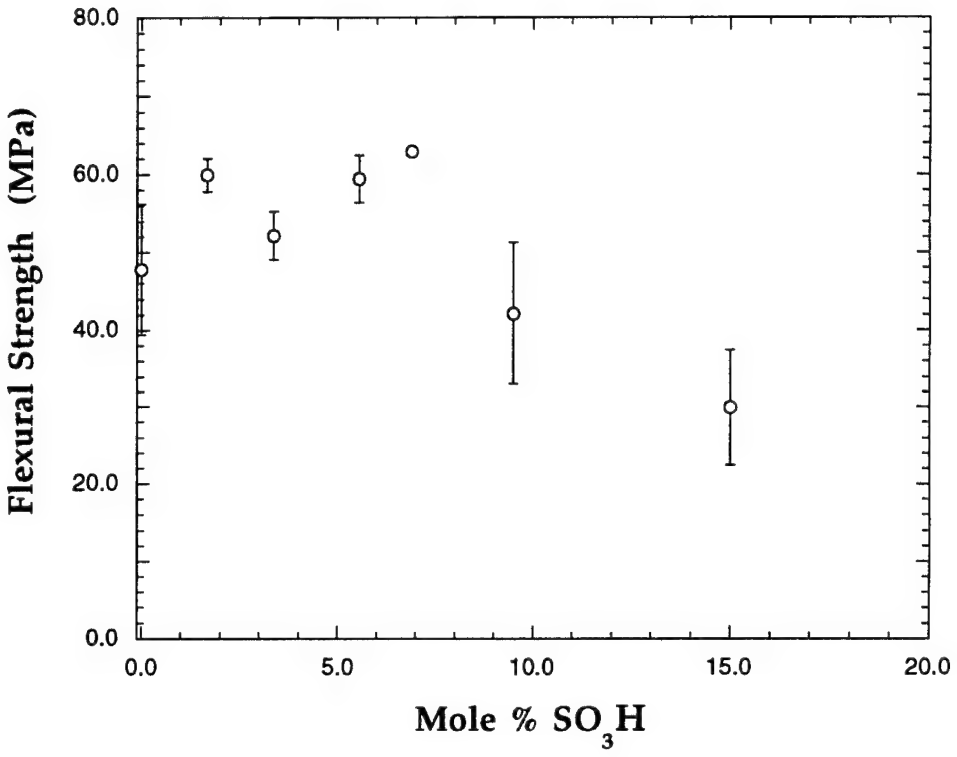

Figure 5.12. Flexural strength of sPS as a function of sulfonic acid content.

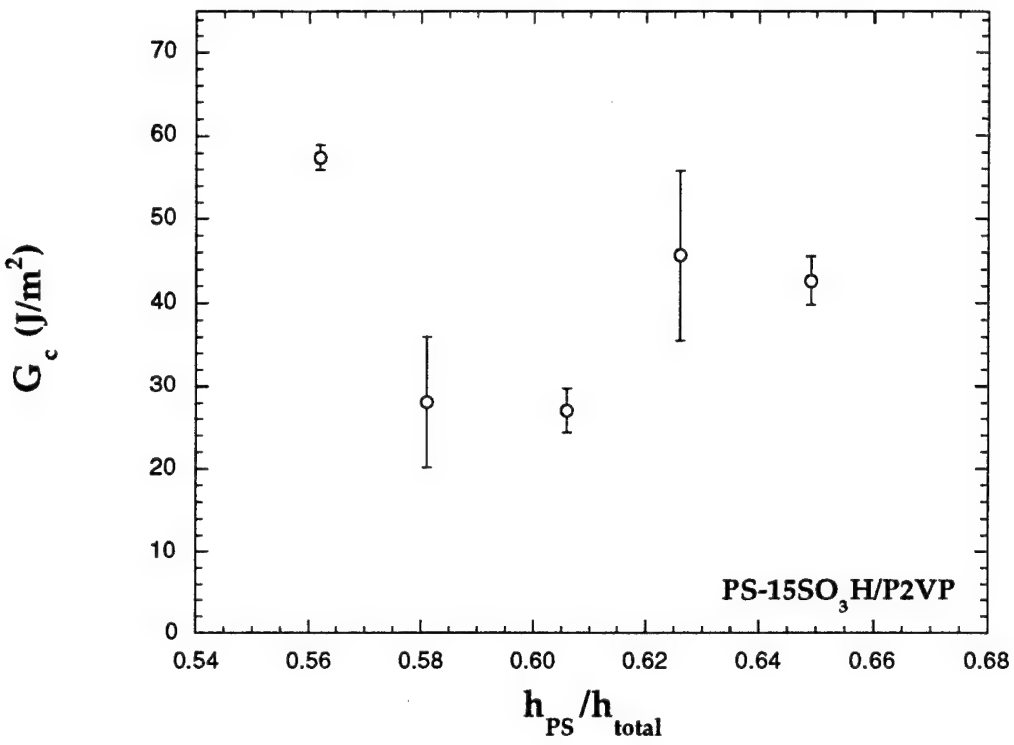

Figure 5.13. Toughness versus beam thickness ratio for the PS-15.0SO_3H/P2VP interface.

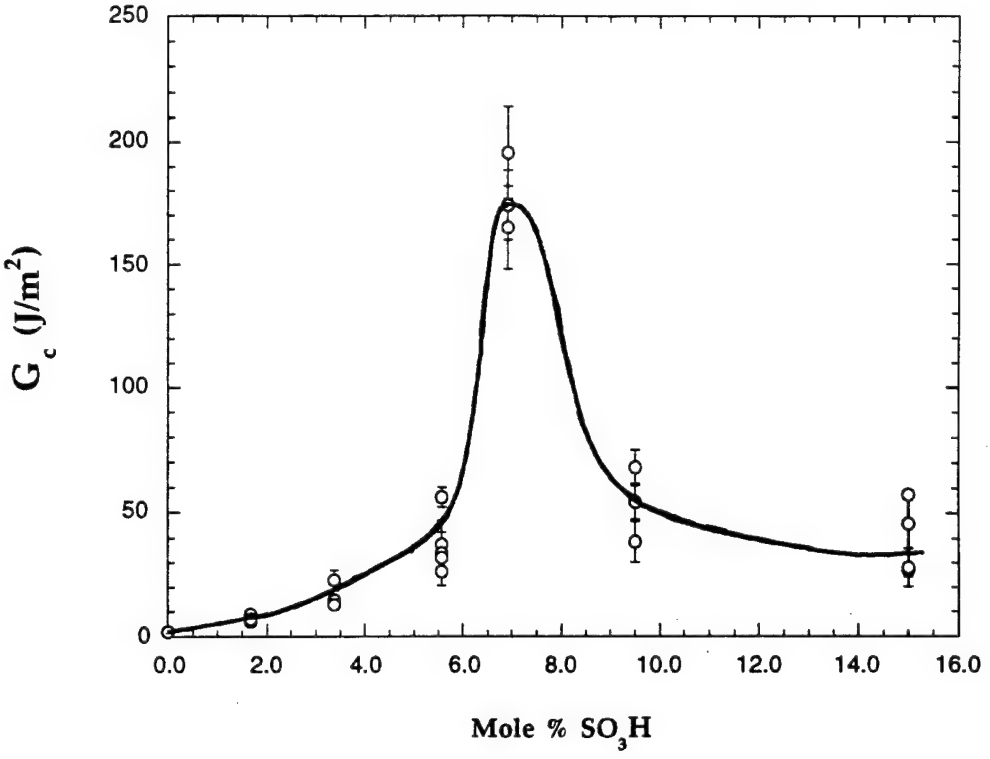

Figure 5.14. Toughness of the sPS/P2VP interface as a function of reactivity. Higher molecular weight P2VP-PS. Bonding time: 60 minutes.

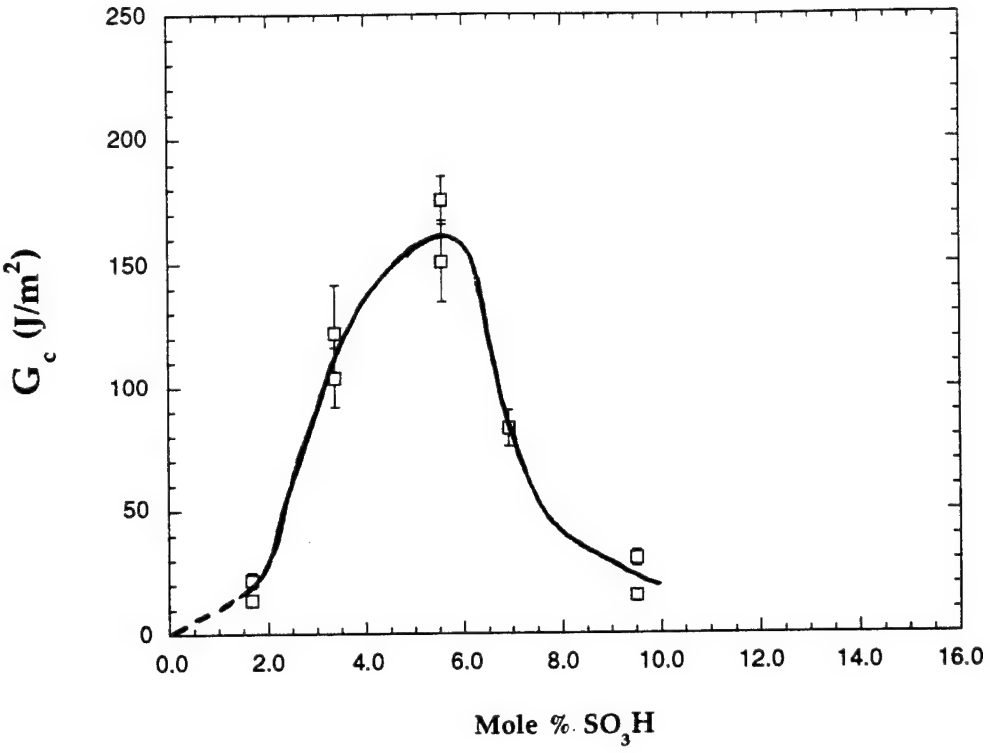

Figure 5.15. Toughness of the sPS/P2VP interface as a function of reactivity. Lower molecular weight P2VP-R. Bonding time: 6 minutes.

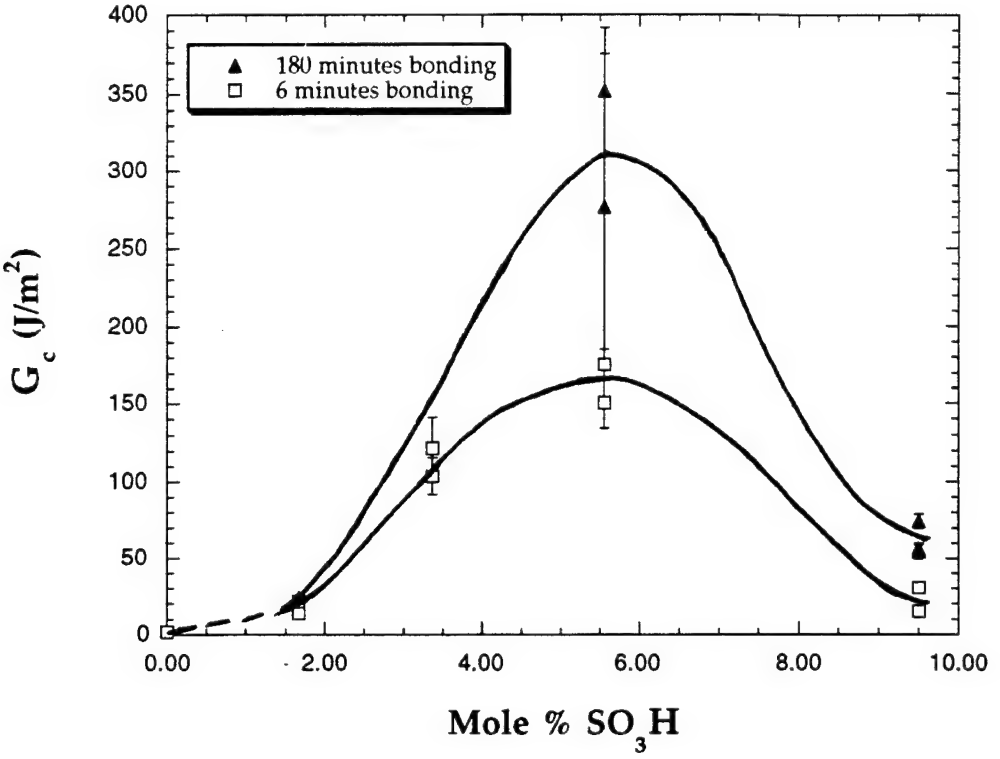

Figure 5.16. Influence of bonding conditions on the interfacial toughness of sPS/P2VP-R interfaces.

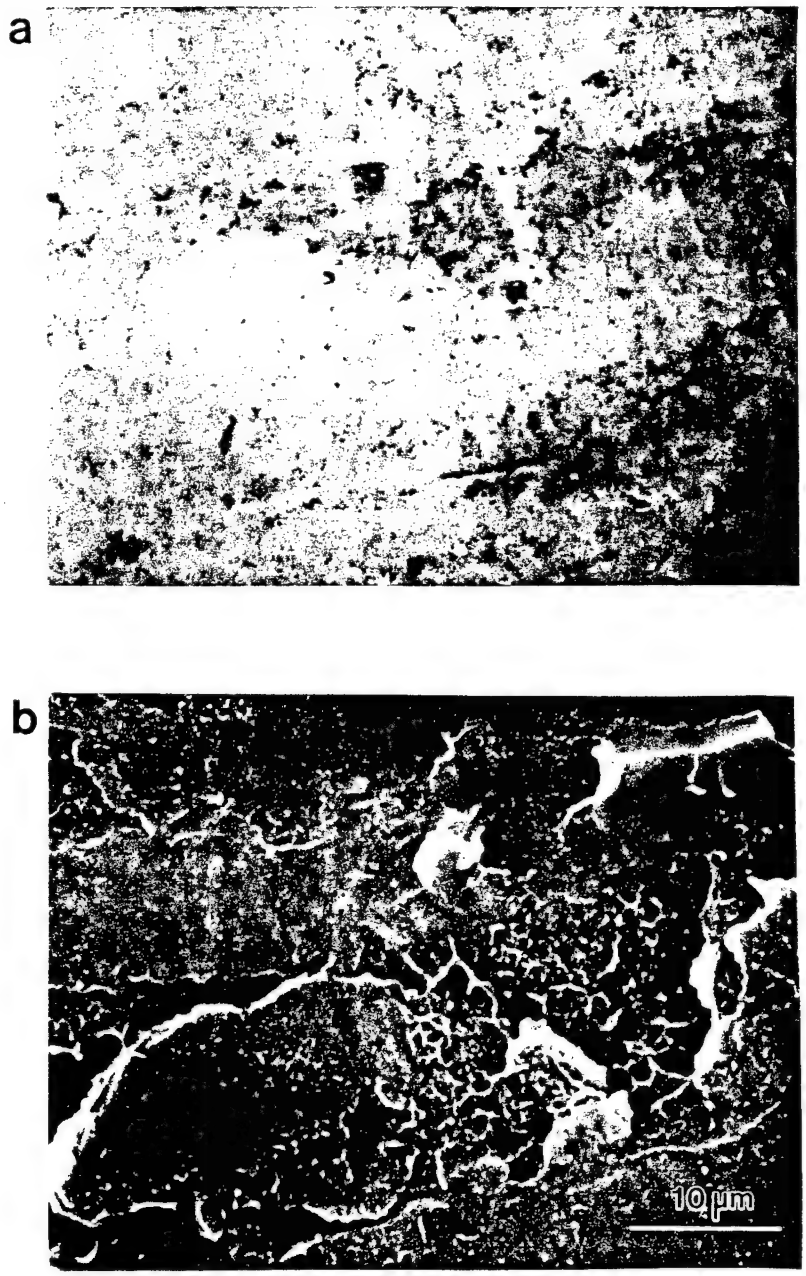

Figure 5.17. SPS fracture surfaces from a) a PS-1.67SO_3H/P2VP interface, G_c~8 J/m^2, b) a PS-6.91SO_3H/P2VP interface, G_c~150 J/m^2. (Scanning electron micrographs, x2000.)

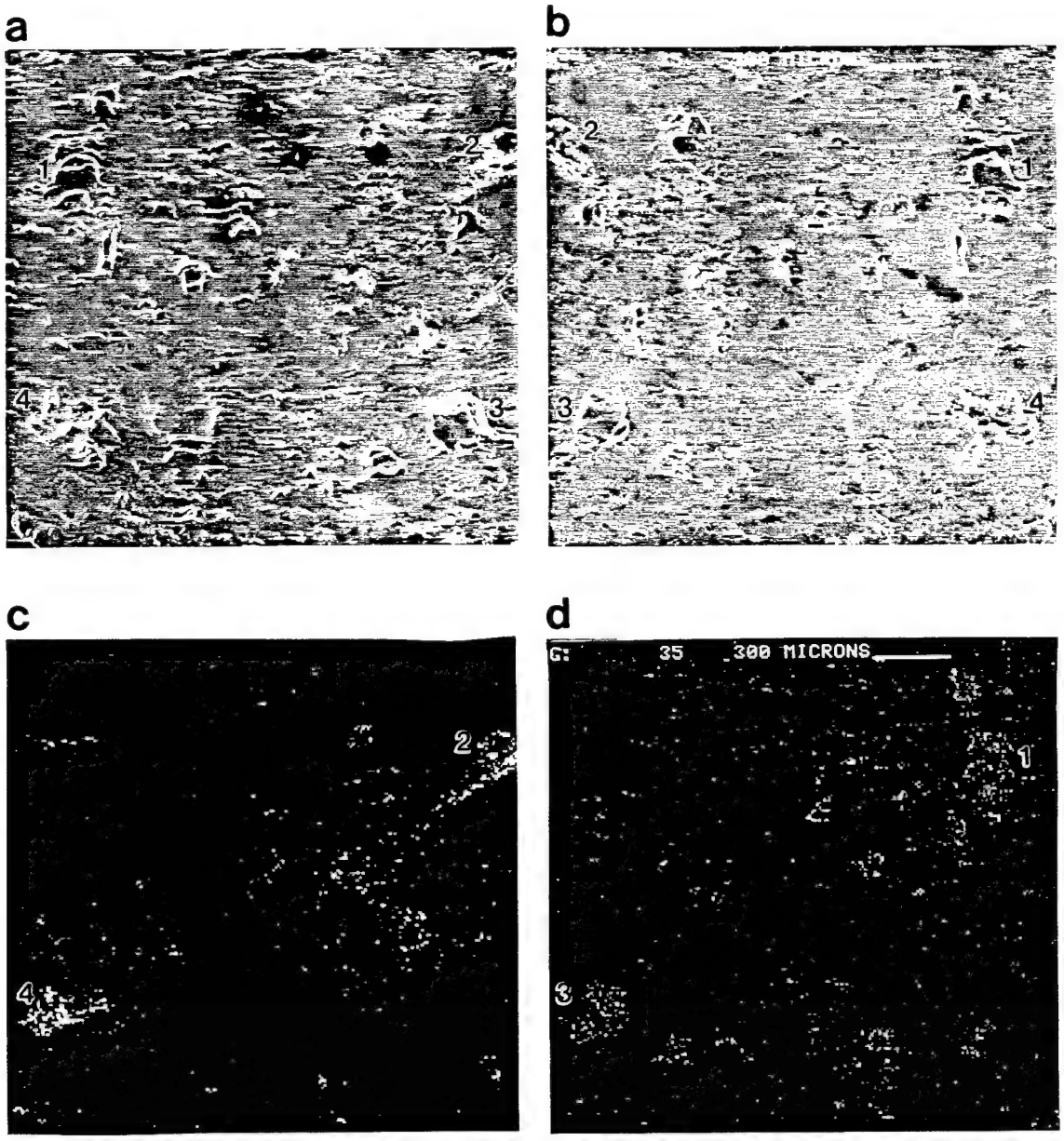

Figure 5.18. Matching fracture surfaces from a PS-6.91SO_3H/P2VP interface and the corresponding elemental x-ray maps: a) sPS surface, b) P2VP surface, c) iodine map of the sPS surface, d) sulfur map of the P2VP surface. (Scanning electron micrographs, x35.)

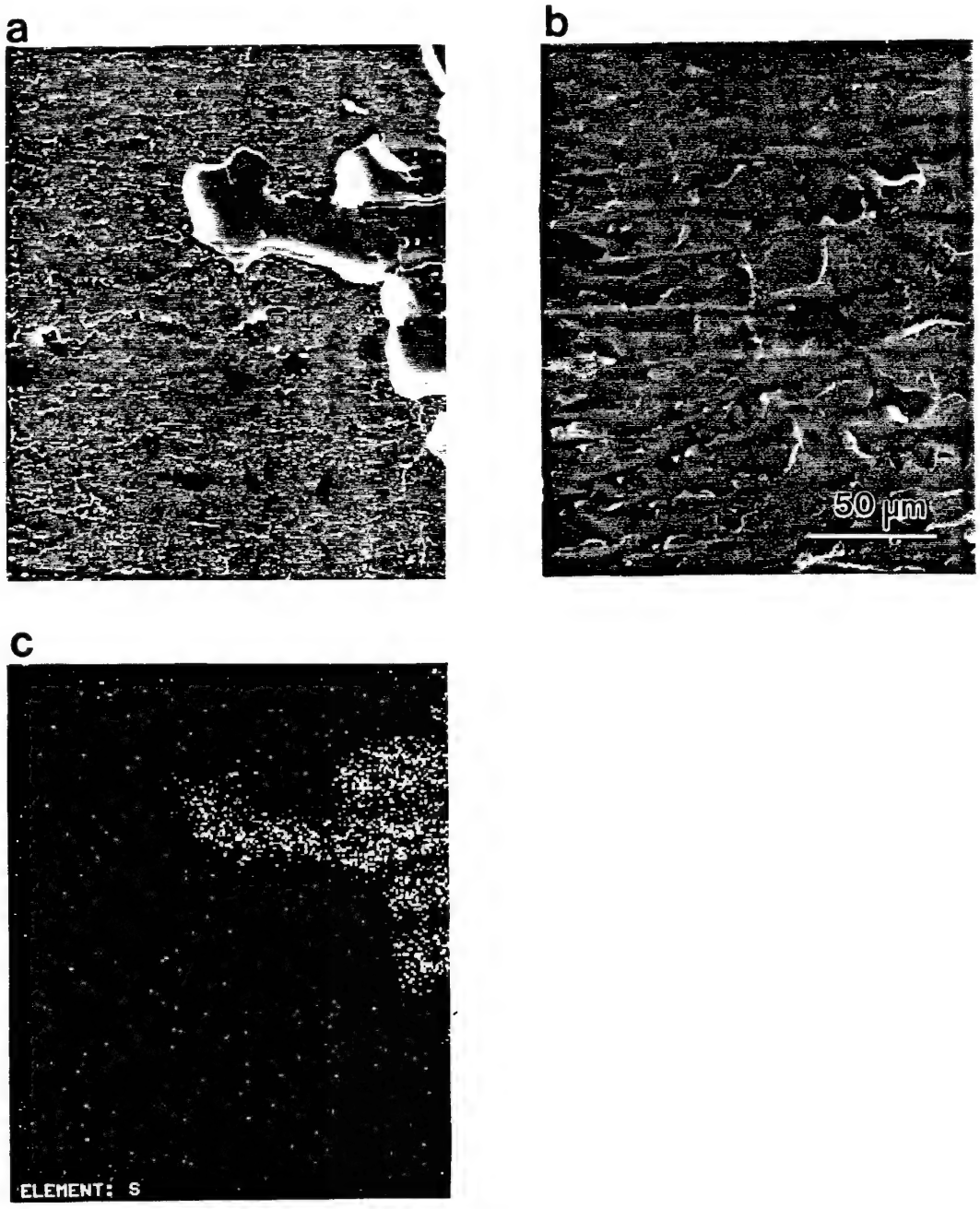

Figure 5.19. P2VP fracture surfaces from a) a PS-15.0SO_3H/P2VP interface, b) a PS-6.91SO_3H/P2VP interface. Part c) is the sulfur map corresponding to part a) illustrating an area where the crack has wandered into the sPS beam. (Scanning electron micrographs, x 350.)

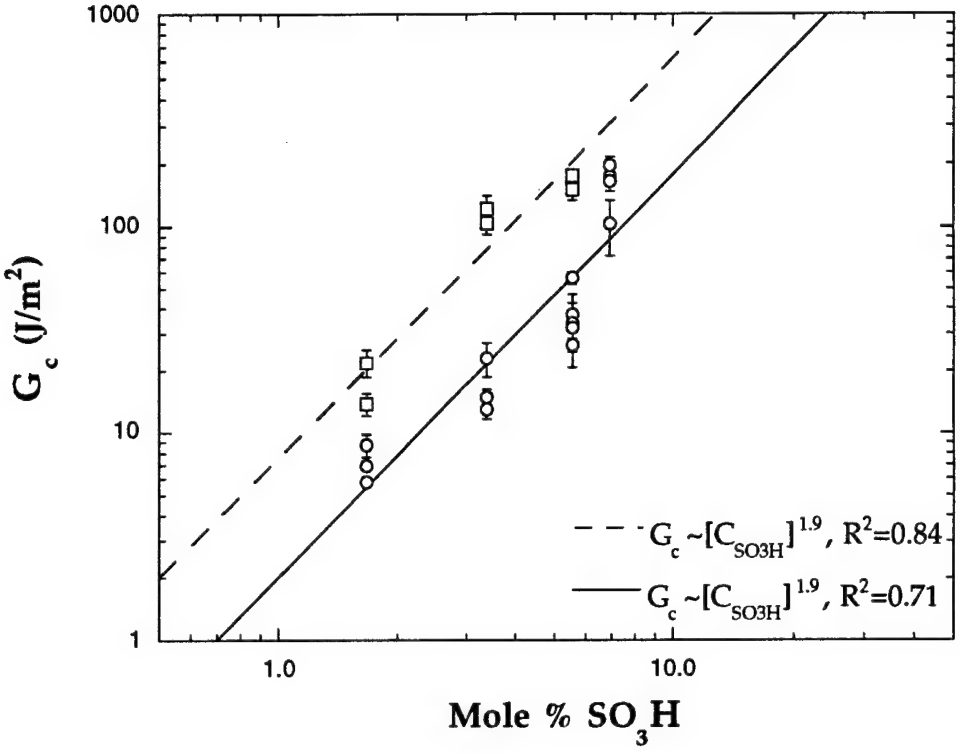

Figure 5.20. Power law scaling of G_C with reactivity.

Low Grafting Density:
Grafted chains entangle with the bulk.

Higher Grafting Density:
Grafted chains entangle with
the bulk and with each other.

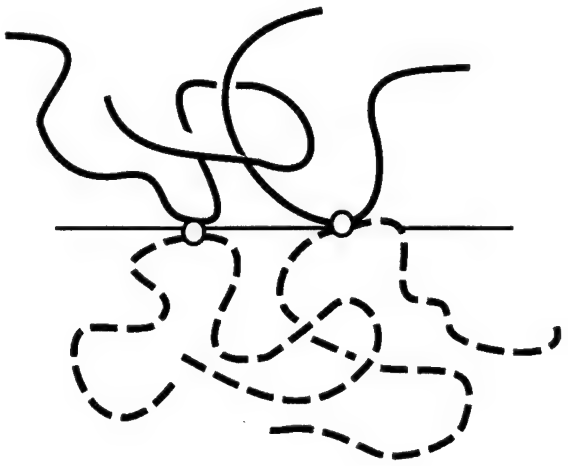

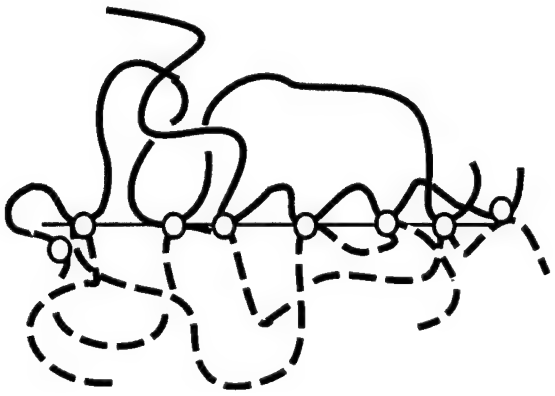

Multiple Grafting:
Grafted chains form a dense
interfacial layer.

Figure 5.21. Schematic illustration of interfacial copolymer geometry at a reactive sPS/P2VP interface.

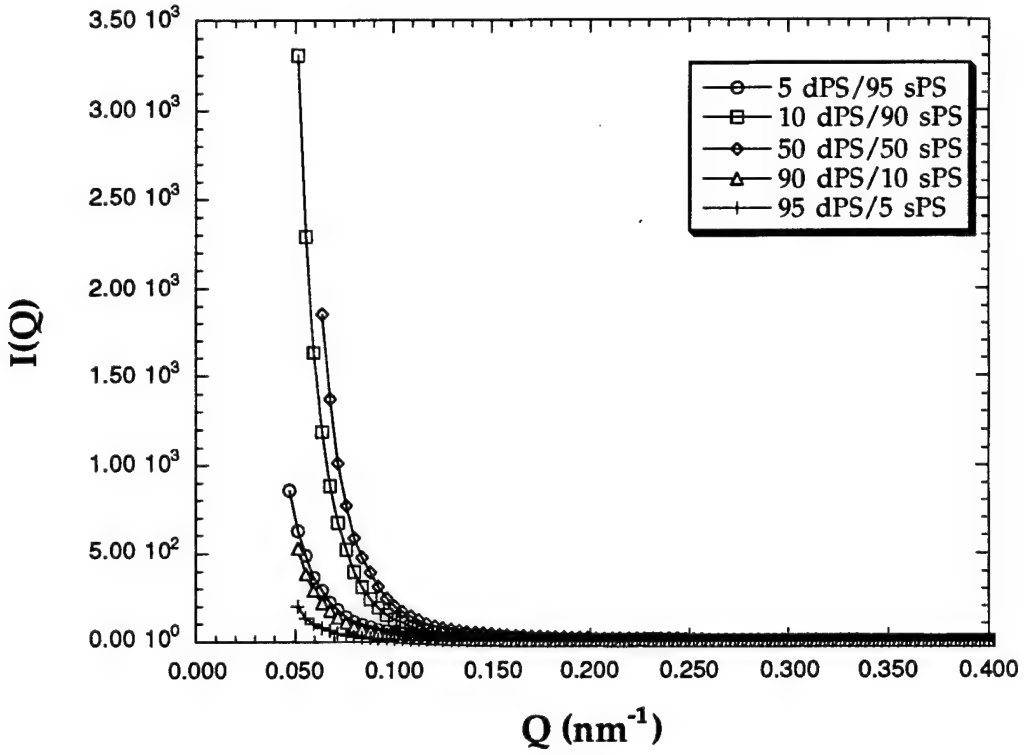

Figure 5.22. Scattered intensity versus scattering vector for dPS/PS-1.67SO_3H blends.

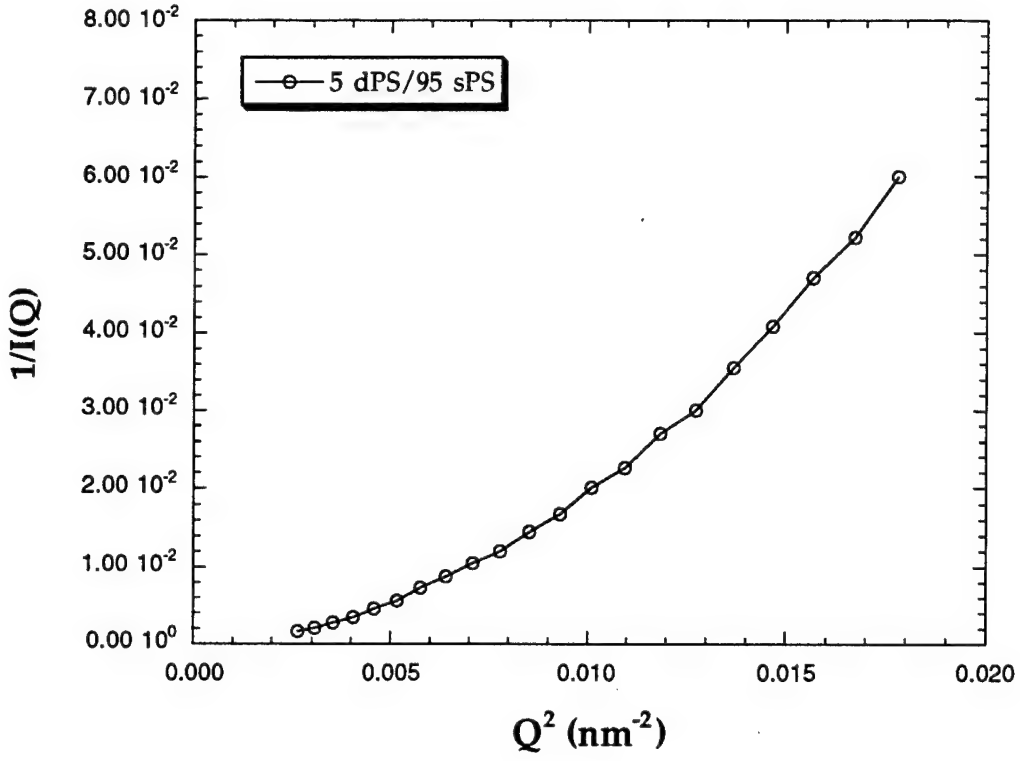

Figure 5.23. Orstein-Zernike plot of scattering from the 5dPS/95PS-1.67SO_3H blend.

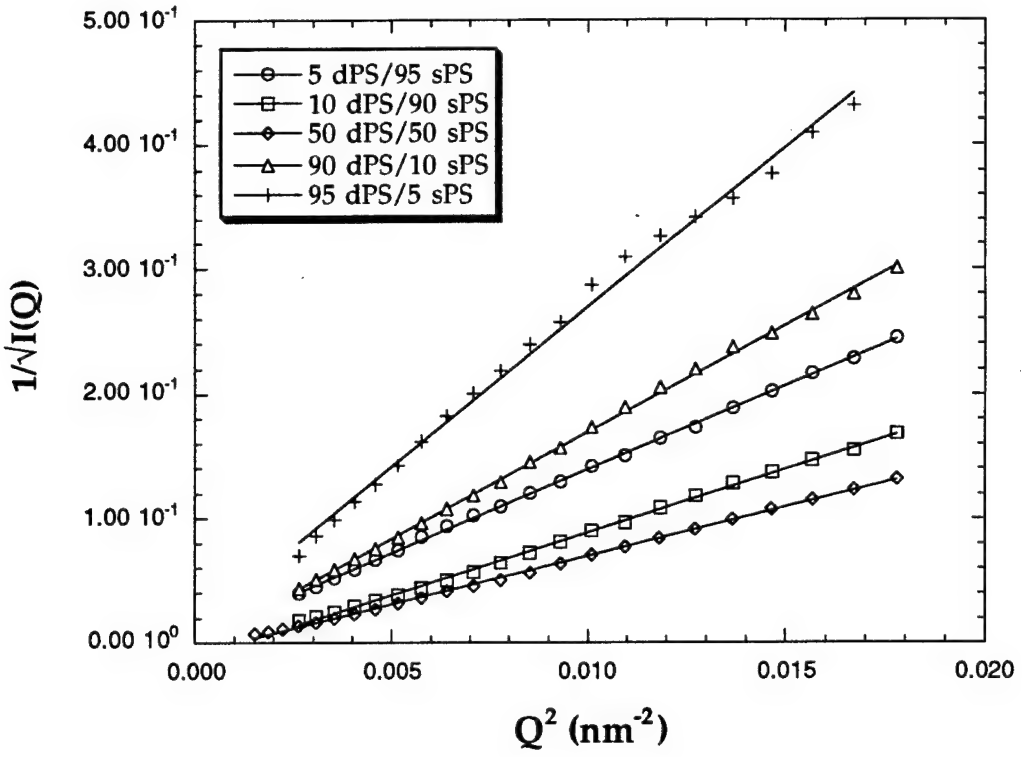

Figure 5.24. Debye plot of scattering from dPS/PS-1.67SO_3H blends.

APPENDIX F: Tables

Table 3-I. Polymer properties.

Polymer	Supplier	M_w	M_w/M_n	T_g (°C)	Reactivity
Polystyrene	Aldrich	315,000	3.25	100	None
Polystyrene	Dow	212,000	2.36	99	None
Polystyrene-oxazoline	Scientific Polymer Products	230,000	2.55	107	1.18 mole % vinyl oxazoline
Deuterated Polystyrene	Polymer Laboratories	188,000 210,000	1.02 1.02	~100	None
Sulfonated Polystyrene	Exxon Research & Engineering	212,000	2.36	105-140	styrene-sulfonic acid ≥15.0 mole %
Transparent Nylon (Grilamid TR55)	EMS-American Grilon	62,500*	2.12*	155	endgroups: ~1.78 mole %
Poly(2-vinyl pyridine)	Polysciences	200,000	****	95	100% vinyl pyridine

* From reference 79.

Table 3-II. Rheological properties.

Sample	M_W (g/mole)	Melt Index [83]	Temperature	Torque (10 minutes)	Torque Ratio PS/aPA
PS-ox	230,000	7g/min @200 °C	200-208 °C	462.5	0.168
PS (Aldrich)	315,000	~3g/min @ 200 °C	200-208°C	612.5	0.223
PS *	190,000	21g/min @ 200 °C	200-208°C	275	0.100
Styron 666	212,000	8g/min @200 °C	198-206°C	425	0.155
GRILAMID TR55 (aPA)	62,500	25g/min @ 265 °C	220-228°C	2750	1.000

* purchased from Scientific Polymer Products

Table 3-III. Flexural properties.

Polymer (Supplier)	Flexural Strength (MPa)	Flexural Modulus (GPa)
PS (Aldrich)	48.4 ± 8.0	3.4 ± 0.44
PS-ox (Sp^2)	47.9 ± 5.2	3.4 ± 0.20
aPA (EMS)	********	2.4 ± 0.11
PS (Dow Styron)	49.1	3.5 ±0.12
sPS	51.8 ± 12.0	3.5 ± 0.25
P2VP (Polysciences)	76.7 ± 0.47	4.3 ± 0.11

Table 4-I. Characteristics of the Particle Size Distributions in 20:80 Melt Blends.

Blend Identification	Mean Particle Radius (μm)	Median Particle Radius (μm)	Standard Deviation (μm)
PS-ox/aPA	0.18	0.18	0.07
PS/aPA	0.46	0.32	0.78

Table 4-II. Bimaterial Beam Joining Conditions and Interfacial Fracture Toughness between PS-ox and aPA.

Joining Temperature (°C)	Joining Time (hours)	G_c (J/m^2)
165.5 ± 5.5	1.0	9.41 ± 1.1
176.7	0.25	9.33 ± 0.69
176.7	1.0	10.2 ± 1.1
185.0	1.0	12.0 ± 1.8
190.6	0.25	6.58 ± 0.55

Table 5-I. Glass transitions of sPS/P2VP Solution Blends.

Material	T_g onset (°C)	T_g Tan δ (°C)	T_g (0)$^{calc.}$ (°C)	T_g(x)$^{calc.}$ (°C)
PS	97	108	*****	*****
P2VP	100	113	*****	*****
PS-1.67s	107	118	****	****
PS-3.37s	107	114	****	****
PS-5.56s	112	125	****	****
PS-6.91s	113	127	****	****
PS/P2VP	103	114	111	****
PS-1.67s/P2VP	106	120	116	122
PS-3.37s/P2VP	102	118	114	127
PS-5.56s/P2VP	107	128	119	142
PS-6.91s/P2VP	104	132	120	149

Table 5-II. Characteristics of the SAXS peak from sPS/P2VP Solution Blends.

Blend	Feature	Q_{Peak} (nm^{-1})	Feature Size (nm)	Accessible Size Range (nm)
PS/P2VP	none	*****	*****	~1.5-150
PS-1.67SO_3H/P2VP	none	*****	*****	~1.5-150
PS-3.37SO_3H/P2VP	shoulder	< 0.9	> 7.0	~1.5-150
PS-5.56SO_3H/P2VP	shoulder	< 1.0	> 6.5	~1.5-150
PS-6.91SO_3H/P2VP	peak	1.25	5.0	~1.5-150
PS-9.50SO_3H/P2VP	none	*****	*****	~2.5-140
PS-15.0SO_3H/P2VP	peak	2.05	3.1	~2.5-140

Table 5-III. Interfacial Width of sPS/P2VP Solution Blends.

Blend	σ (nm)	$\frac{\sigma_{reactive}}{\sigma_{unreactive}}$
PS/P2VP	0.043	1
PS-1.67SO_3H/P2VP	0.076	1.8
PS-3.37SO_3H/P2VP	0.083	1.9
PS-5.56SO_3H/P2VP	0.076	1.8
PS-6.91SO_3H/P2VP	0.060	1.4

Table 5-IV. Correlation Length from dPS/PS-1.67SO_3H Blends.

Blend	Correlation Length, a (nm)
5 dPS/95 PS-1.67SO_3H	40
10 dPS/90 PS-1.67SO_3H	105
50 dPS/50 PS-1.67SO_3H	*******
90 dPS/10 PS-1.67SO_3H	50
95 dPS/5 PS-1.67SO_3H	45

References

1 Olabisi, Olagoke, Robeson, Lloyd M. and Shaw, Montgomery T. Polymer -Polymer Miscibility, (New York: Academic Press), 1979.

2 Fox, Daniel W. and Allen, Richard B. "Compatibility," Encyl. Polym. Sci. Eng., 2nd ed. (New York: John Wiley & Sons), Vol. 12, 1987, 759-775.

3 Briber, Robert M. *Lecture Notes-Introduction to Polymer Physics*, University of Maryland, College Park, Fall, 1992.

4 Flory, Paul J. Principles of Polymer Chemistry, (Ithaca, NY: Cornell University Press), 1953.

5 Gaylord, Norman G. "Compatibilizing Agents: Structure and Function in Polyblends," *J. Macromol. Sci. Chem.*, A26, 1989, 1211-1229.

6 Utracki, L. A. and Shi, Z. H. "Development of Polymer Blend Morphology During Compounding in a Twin-Screw Extruder. Part I: Droplet Dispersion and Coalescence--A Review," *Polym. Eng. Sci.* 32, 1992, 1824-1833, and references cited therein.

7 Favis, B. D. and Therrien, D., "Factors influencing structure formation and phase size in an immiscible polymer blend of polycarbonate and polypropylene prepared by twin-screw extrusion," *Polymer*, 32, 1991, 1474-1481.

8 White, James L, and Min, Kyonsuku, " Development of Polymer Blend Phase Morphology During Processing," *Makromol. Chem., Macromol. Symp.*, 16, 1988, 19-39.

9 Wu, Souheng, "Formation of Dispersed Phase in Incompatible Polymer Blends: Interfacial and Rheological Effects," *Polym. Eng. and Sci.*, 27, 1987, 335-343.

10 Willis, J. M., Favis, B. D. and Lunt, J. "Reactive Processing of Polystyrene-co-maleic anhydride/Elastomer Blends: Processing-Morphology-Property Relationships," *Polym. Eng. Sci.*, 30, 1990, 1073-1084.

11 Taylor, G. I. , *Proceedings of the Royal Society of London*, Ser. A146, 1934, 501.

12 Helfand, Eugene and Tagami, Yukiko, "Theory of the Interface Between Immiscible Polymers," *Polym. Lett.*, 9, 1971, 741-746.

13 Helfand, Eugene and Sapse, Anne Marie, "Theory of Unsymmetric Polymer-Polymer Interfaces," *J. Chem. Phys.*, 62, 1975, 1327-1331.

14 Sanchez, Isaac C., "Bulk and Interface Thermodynamics of Polymer Alloys," *Ann. Rev. Mater. Sci.*, 19, 1983, 387-412.

15 Leibler, Ludwik, "Emulsifying Effects of Block Copolymers in Incompatible Polymer Blends," *Makromol. Chem., Macromol. Symp.*, 16, 1988, 1-17.

16 Sundararaj, Uttandaraman and Macosko, C. W., "Morphology

Development during Polymer Blending," *Polym. Preprints, Japan (English Edition)*, 41, 1992, E-753.

17 Favis, B. D. and Willis, J. M., "Phase Size/Composition Dependence in Immiscible Blends: Experimental and Theoretical Considerations," *J. Polym. Sci., Polym. Phys.*, 28, 1990, 2259-2269.

18 Paul, D. R., Barlow, J. W. and Keskkula, H., "Polymer Blends," Encyl. Polym. Sci. Eng., 2nd ed. (New York: John Wiley & Sons), Vol. 12, 1987, 399-461.

19 Teyssié, Ph., Fayt, R. and Jérôme, "Study and Control of Polymer Blends Morphology and Related Properties," *Makromol. Chem., Macromol. Symp.*, 16, 1988, 41-56.

20 Wu, Souheng, "Phase Structure and Adhesion in Polymer Blends: A Criterion for Rubber Toughening," *Polymer*, 26, 1985, 1855-1862.

21 Liu, N. C. and Baker, W. E., "The Separate Roles of Phase Structure and Interfacial Adhesion in Toughening a Brittle Polymer," *Polym. Eng. Sci.*, 32, 1992, 1695-1702.

22 Brown, H. R. "A Molecular Interpretation of the Toughness of Glassy Polymers," *Macromolecules*, 24, 1991, 2752-2756.

23 Washiyama, Junichiro et. al., "Chain Pullout Failure of Polymer Interfaces," *Macromolecules*, 27, 1994, 2019-2024.

24 Xu, D. B. et. al., "A micromechanical model of crack growth along polymer interfaces," *Mech. Mater.*, 11, 1991, 257-268.

25 Creton, Constantino, et. al., "Failure Mechanisms of Polymer Interfaces Reinforced with Block Copolymers," *Macromolecules*, 25, 1992, 3075-3088.

26 Ji, Hong and de Gennes, P. -G., "Adhesion via Connector Molecules: The Many-Stitch Problem," *Macromolecules*, 26, 1993, 520-525.

27 Raphael, E. and de Gennes, P. -G., "Rubber-Rubber Adhesion with Connector Molecules," *J. Phys. Chem.*, 96, 1992, 4002-4007.

28 de Gennes, P. G., "Weak Adhesive Junctions," *J. Phys. France*, 50, 1989, 2551-2562.

29 Liu, N. C. and Baker, W. E., "Reactive Polymers for Blend Compatibilization," *Adv. Polym. Tech.*, 11, 1992, 249-262.

30 Brown, S. Bruce, " Review of Reactive Extrusion Processes," in Reactive Extrusion: Principles and Practice, M. Xanthos, ed. (New York: Oxford University Press), 1992, 75-199.

31 Xanthos, M. and Dagli, S. S., "Compatibilization of Polymer Blends by Reactive Processing," *Polym. Eng. Sci.*, 31, 1991, 929-935.

32 Brown, S. Bruce, "Chemical Processes Applied to Reactive Extrusion of

Polymers," *Ann. Rev. Mater. Sci.*, 21, 1991, 409-435.

33 Liang, Zhizhong and Williams, H. Leverne, "Dynamic Mechanical Properties of Polypropylene-Polyamide Blends: Effect of Compatibilization," *J. Appl. Polym. Sci.*, 44, 1992, 699-717.

34 Chang, Feng-Chih and Hwu, Yih-Chyun, "Styrene Maleic Anhydride and Styrene Glycidyl Methacrylate Copolymers as *In Situ* Reactive Compatibilizers of Polystyrene/Nylon 6,6 Blends," *Polym. Eng. Sci.*, 31, 1991, 1509-1519.

35 Triacca, V. J. et. al., "Reactive compatibilization of blends of nylon 6 and ABS materials," *Polymer*, 32, 1991, 1401-1413.

36 Saleem, M. and Baker, W. E., "*In Situ* Reactive Compatibilization in Polymer Blends: Effects of Functional Group Concentrations," *J. Appl. Polym. Sci.*, 39, 1990, 655-678.

37 Fowler, M. W. and Baker, W. E., "Rubber Toughening of Polystyrene Through Reactive Blending," *Polym. Eng. Sci.*, 28, 1988, 1427-1433.

38 MacKnight, W. J. et. al., "Binary Alloys of Nylon 6 and Ethylene-Methacrylic Acid Copolymers: Morphological, Thermal and Mechanical Analysis," *Polym. Eng. Sci.*, 25, 1985, 1124-1134.

39 Douglas, Elliot P., Kazuo, Sakurai and MacKnight, William J., "Thermal Analysis and Optical Microscopy of Modified Polystyrene/Poly(ethyl acrylate) Blends Containing Specific Interactions," *Macromolecules*, 24, 1991,

6776-6781.

40 Angola, Juan C., et. al., "Compatibilizer-aided Toughening in Polymer Blends Consisting of Brittle Polymer Particles Dispersed in a Ductile Polymer Matrix," *J. Polym. Sci., Polym. Phys.*, 26, 1988, 807-816.

41 Liu, N. C., Baker, W.E. and Russell, K. E., "Functionalization of Polyethylenes and Their Use in Reactive Blending," *J. Appl. Polym. Sci.*, 41, 1990, 2285-2300.

42 Song, Zhiqiang and Baker, Warren E., "*In Situ* Compatibilization of Polystyrene/Polyethylene Blends using Amino-Methacrylate-Grafted Polyethylene," *J. Appl. Polym. Sci.*, 44, 1992, 2167-2177.

43 Zhang, Xinsheng, Natansohn, Almeria and Eisenberg, Adi, "Intermolecular Cross-Polarization Studies of the Miscibility Enhancement of PS/PMMA Blends through Ionic Interactions," *Macromolecules*, 23, 1990, 412-416.

44 Sakurai, Kazuo, Douglas, Elliot P. and MacKnight, William J., "Spectroscopic Study of an Ionic Blend Made from the Acid Form of Sulfonated Polystyrene and Poly[ethyl acrylate-co-(4-vinyl pyridine)]," *Macromolecules*, 25, 1992, 4506-4510.

45 Baker, W. E. and Saleem, M., "Polystyrene-Polyethylene Melt Blends Obtained Through Reactive Mixing Process," *Polym. Eng. Sci.*, 27, 1987, 1634-1641.

46 Baker, W. E. and Saleem, M, "Coupling of Reactive Polystyrene and Polyethylene in Melts," *Polymer*, 28, 1987, 2057-2062.

47 Sundararaj, Uttandaraman, Macosko, C W., Nakayama, A. and Inoue, T., "Milligrams to Kilograms: An Evaluation of Mixers for Reactive Polymer Blending," submitted to *Polym. Eng. Sci.*

48 Sullivan, M. J. and Weiss, R. A., "Characterization of Blends of an Amorphous Polyamide with Lightly Sulfonated Polystyrene Ionomers," *Polym. Eng. Sci.*, 32, 1992, 517-523.

49 Yukioka, Satoshi and Inoue, Takashi, "Ellipsometric analysis on the *in situ* reactive compatibilization of immiscible polymer blends," *Polymer*, 35, 1994, 1182-1186.

50 Chen, Cheng Chung et. al., "An Investigation of Instability of Phase Morphology of Blends of Nylons with Polyethylenes and Polystyrenes and Effects of Compatibilizing Agents," *Polym. Eng. Sci.*, 28, 1988, 69-80

51 Liu, N. C. and Baker, W. E., "Basic Functionalization of Polypropylene and the Role of Interfacial Chemical Bonding in its Toughening," *Polymer*, 35, 1994, 989.

52 " Ions in Polymers", Advances in Chemistry No. 187, (Washington, D. C.: American Chemical Society), 1980.

53 Lu, Xinya and Weiss, R. A., "Development of Miscible Blends of Polyamide-

6 and Manganese Sulfonated Polystyrene Using Specific Interactions," *Macromolecules*, 24, 1991, 4379-4385.

54 Lu, Xinya and Weiss, R. A., "Specific Interactions and Ionic Aggregation in Miscible Blends of Nylon-6 and Zinc Sulfonated Polystyrene Ionomer," *Macromolecules*, 25, 1992, 6185-6189.

55 Gao, Zhisheng et. al., "Blends of Polyamide-6 and Sulfonated Polystyrene. A Solid-State NMR Study," *Macromolecules*, 25, 1992, 6460-6465.

56 Kwei, T. K. et. al., "Solid-State NMR Analysis of Blends of Nylon 6 and Zinc Salts of Sulfonated Polystyrene Ionomers," *Macromolecules*, 26, 1993, 6583-6588.

57 Agarwal, P. K. et. al.,"Polymer Blend Complexes Based on Coordination Chemistry," *J. Polym. Sci., Polym. Phys.*, 25, 1987, 839-854.

58 Register, R. A. et. al., "Morphology and Cation Local Structure in a Blend of Copper-neutralized Carboxy-terminated Polybutadiene and Poly(styrene-co-4-vinyl pyridine)," *J. Polym. Sci., Polym. Phys.*, 27, 1989, 1911-1925.

59 Zhang, Xinsheng and Eisenberg, Adi, "NMR and Dynamic Mechanical Studies of Miscibility Enhancement via Ionic Interactions in Polystyrene/poly(ethyl Acrylate) Blends," *J. Polym. Sci., Polym. Phys.*, 28, 1990, 1841-1857.

60 Charlier, Pascal et. al., "Viscoelastic Properties of Immiscible Telechelic

Polymer Blends: Effect of Acid-Base Interactions," *Macromolecules*, 25, 1992, 2651-2656.

61 Eisenberg, A., Smith, P. and Zhou, Z.-L., "Compatibilization of the Polystyrene/Poly(Ethyl Acrylate) and Polystyrene/Polyisoprene Systems through Ionic Interactions," *Polym. Eng. Sci.*, 22, 1982, 1117-1121.

62 Huglin, Malcom B. and Rego, Jose M., "Study of polymer blends based on poly(vinyl pyridines) and acidic polymers," *Polymer*, 31, 1990, 1269-1276.

63 Huglin, Malcom B., Rego, Jose M. and Gooda, Shaban R., "Comments on Thermal Transitions in Some Polyelectrolyte Complexes," *Macromolecules*, 23, 1990, 5359-5361.

64 Liu, N. C. and Baker, W. E., "Morphology Control and Impact Toughening of Polypropylene/Rubber Blends," *PMSE Preprints*, 67, 1992, 305-306.

65 Creton, C., Brown, H. R. and Deline, V. R., "Influence of Chain Entanglements on the Failure Modes in Block Copolymer Toughened Interfaces," *Macromolecules*, 27, 1994, 1774-1780.

66 Brown, H. R. et. al., "Effects of a Diblock Copolymer on Adhesion between Immiscible Polymers. 1. PS-PMMA Copolymer between PS and PMMA," *Macromolecules*, 26, 1993, 4155-4163.

67 Char, K, Brown, H. R. and Deline, V. R., "Effects of a Diblock Copolymer on Adhesion between Immiscible Polymers. 2. PS-PMMA Copolymer between

PPO and PMMA," *Macromolecules*, 26, 1993, 4164-4170.

68 Washiyama, Junichiro, Creton, Constantino and Kramer, Edward J.," TEM Fracture Studies of Polymer Interfaces," *Macromolecules*, 25, 1992, 4751-4758.

69 Creton, Constantino, Kramer, Edward J. and Hadziioannou, Georges, "Critical Molecular Weight for Block Copolymer Reinforcement of Interfaces in a Two-Phase Polymer Blend," *Macromolecules*, 24, 1991, 1846-1853.

70 Reichert, Werner F. and Brown, Hugh R., "Effect of a polystyrene-polyisoprene diblock layer on the adhesion between polystyrene and polyisoprene," *Polymer*, 34, 1993, 2289-2296.

71 Brown, Hugh R., "Effects of Chain Pull-out on Adhesion of Elastomers," *Macromolecules*, 26, 1993, 1666-1670.

72 Brown, H. R., "Mixed-mode effects on the toughness of polymer interfaces," *J. Mater. Sci.*, 25, 1990, 2791-2794.

73 Brown, H. R., "Effect of a Diblock Copolymer on the Adhesion between Incompatible Polymers," *Macromolecules*, 22, 1989, 2259-2260.

74 Cho, K., Brown, H. R. and Miller, D. C.,"Effect of a Block Copolymer on the Adhesion Between Incompatible Polymers. I. Symmetric Tests," *J. Polym. Sci., Polym. Phys.*, 28, 1990, 1699-1718.

75 Brown, Hugh R., Hui, Chung-Yuen and Raphaël, Elie,"Interplay between

Intermolecular Interactions and Chain Pullout in the Adhesion of Elastomers," *Macromolecules*, 27, 1994, 608-609.

76 Washiyama, Junichiro, Kramer, Edward J. and Hui, Chung-Yuen,"Fracture Mechanisms of Polymer Interfaces Reinforced with Block Copolymers: Transition from Chain Pullout to Crazing," *Macromolecules*, 26, 1993, 2928-2934.

77 Hui, C.-Y. et. al., "Micromechanics of Crack Growth into a Craze in a Polymer Glass", *Macromolecules*, 25, 1992, 3948-3955.

78 Makowski, H. S., Lundberg, R. D. and Singhal, G. H., "Flexible Polymeric Compositions Comprising a Normally Plastic Polymer Sulfonated to about 0.2 to about 10 Mole % Sulfonate." US Patent No. 3 870 841, 1975.

79 Ellis, Thomas S., "Influence of Structure on Phase Behavior of Polyamide Blends," *Macromolecules*, 24, 1991, 3845-3852.

80 Lundberg, R. D. and Makowski, H. S., "A Comparison of Sulfonate and Carboxylate Ionomers," Ions in Polymers. Advances in Chemistry Series #187, A. Eisenberg, ed., 1980, 20-36.

81 Freakly, P. K. and Wan Idris, W. Y.,"Visualization of Flow During the Processing of Rubber in an Internal Mixer," *Rubber Chem. Tech.*, 52, 1979, 134-145.

82 For a discussion of the relation between torque and viscosity for polymers processed in a Banbury mixer see Goodrich, Judson E. and Porter, Roger S., "A

Rheological Interpretation of Torque-Rheometer Data," *Polym. Eng. Sci.*, 7, 1967, 45-51.

83 Note: Melt index is a standardized measure of flow properties, which is inversely related to the viscosity. See ASTM D1238, "Standard Test Method for Flow Rates of Thermoplastics by Extrusion Plastometer," ASTM 1993 Annual Book of Standards, Vol. 8.01.(Phila.,PA: ASTM).

84 Fitzgerald, J. J. and Weiss, R. A., "Synthesis, Properties, and Structure of Sulfonate Ionomers," *J. Macromol. Sci., Rev. Macromol. Chem. Phys.*, C28, 1988, 99-185.

85 Aronson, S. and Wilensky, S. B., "Complex Formation in 2-Polyvinylpyridine-Iodine Solutions," *J. Polym. Sci., Polym. Chem.*, 26, 1988, 1259-1262.

86 Hendricks, R. W., "The ORNL 10-Meter Small-Angle X-Ray Scattering Camera," *J. Appl. Crystallogr.*, 11, 1978, 15-30.

87 Barnes, J. and Mopsik, F., "Small Angle X-Ray Characterization of Polymers," *SPE ANTEC Proc.*, 1988, 1178-1181.

88 Hammouda, B., Krueger, S. and Glinka, C. J., *J. Nat. Inst. Std.*, 98, 1993, 31.

89 Kanninen, M. F., "An augmented double cantilever beam model for studying crack propagation and arrest," *Int. J. Fracture*, 9, 1973, 83-92.

90 Brown, H. R., "The Adhesion Between Polymers," *Annu. Rev. Mater. Sci.*, 21, 1991, 463-489.

91 Rice, J. R., "Elastic Fracture Mechanics Concepts for Interfacial Cracks," *J. Appl. Mech.*, 55, 1988, 98-103.

92 Hutchinson, J. W. and Suo, Z., "Mixed Mode Cracking in Layered Materials," *Adv. Appl. Mech.*, 29, 1991, 64-191.

93 Evans, A. G. et. al., "The Fracture Energy of Bimaterial Interfaces," *Metall. Trans. A*, 21A, 1990, 2419-2429.

94 Suo, Zhigang and Hutchinson, John W., "Interface crack between two elastic layers," *Int. J. Fracture*, 43, 1990, 1-18.

95 Xiao, F., Hui, C.-Y. and Kramer, E. J., "Analysis of a mixed mode fracture specimen: the asymmetric double cantilever beam," *J. Mater. Sci.*, 28. 1993, 5620-5629.

96 "Standard Test Methods for Flexural Properties of Unreinforced Plastics and Electrical Insulating Materials," *American Society for Testing and Materials*, ASTM D790-90, 8.01, 1991, 272-281.

97 Portions of the blending and FTIR studies were performed in conjunction with Mr. Shih-Quan Tai.

98 Elmendorp, J. J. and van der Vegt, " A Study on Polymer Blending

Microrheology: Part IV. The Influence of Coalescence on Blend Morphology Origination," *Polym. Eng. Sci.*, 26, 1986, 1332-1338.

99 Israelachvili, Jacob. Intermolecular & Surface Forces, (New York: Academic Press), 1992.

100 de Gennes, P. G., "Polymers at an Interface; A Simplified View", *Adv. Colloid Inter. Sci.*, 27, 1987, 189-209.

101 See also Milner, S. T., Witten, T. A. and Cates, M. E., "Theory of Grafted Polymer Brushes", *Macromolecules*, 21, 1988, 2610-2619.

102 Equations (4-3) are derived from Equations (15) in Dolan, A. K. and Edwards, F. S., "Theory of the stabilization of colloids by adsorbed polymer", *Proc. R. Soc. Lond. A*, 337, 1974, 509-516.

103 Moore, Eugene R., ed. "Styrene Polymers", Encyl. Polym. Sci. Eng., (New York: John Wiley & Sons), Vol. 16, 1989, 1-246.

104 "Grilamid TR55 Transparent Nylons," Material Data Sheet supplied by EMS-American Grilon, Inc., Sumter, SC, 29151-1717.

105 Brandrup, J. and Immergut, E. H., eds. Polymer Handbook, (New York: John Wiley & Sons), 1989.

106 Frump, John A., "Oxazolines. Their Preparation, Reactions, and Applications," *Chem. Rev.*, 71, 1971, 483-505.

107 Nishikubo, Tudatomi, Iiawa, Takashi and Tokairin, Atsushi, "Addition Reactions of Poly(2-vinyl-2-oxazoline)s with Thiols and Carboxylic Acids," *Makromol. Chem., Rapid Commun.*, 2, 1981, 91-94.

108 Conley, Robert T. Infrared Spectrosopy, (Boston: Allyn and Bacon, Inc.), 1966.

109 Koenig, Jack L. Spectroscopy of Polymers, (Washington, D. C.: American Chemical Society), 1992.

110 Ferry, John D., Viscoelastic Properties of Polymers, (New York: John Wiley & Sons), 1980.

111 Weiss, R. A., Agarwal, P. K., and Lundberg, R. D., "Control of Ionic Interactions in Sulfonated Polystyrene Ionomers by the Use of Alkyl-Substituted Ammonium Counterions," *J. Appl. Polym. Sci.*, 29, 1984, 2719-2734.

112 Smith, P. and Eisenberg, A., "Infrared Spectrosopy Study of Blends of Poly(styrene-co-styrenesulfonic acid) with Poly(styrene-co-(4-vinyl pyridine))," *Macromolecules*, 27, 1994, 545-552.

113 Kaplan, Donald S., "Structure Property Relationships in Copolymers to Composites: Molecular Interpretation of the Glass Transition Phenomena," *J. Appl. Polym. Sci.*, 20, 1976, 2615-2629.

114 MacKnight, W. J., Karasz, F. E. and Fries, J. R., "Solid State Transition

Behavior of Blends," in Polymer Blends, Vol. 1.,(New York: Academic Press), 1978.

115 Rodriguez, Ferdinand. Principles of Polymer Systems, (New York: Hemisphere Publishing Corp.), 1982.

116 Sperling, L. H. Introduction to Physical Polymer Science, (New York: John Wiley & Sons), 1986.

117 DiMarzio, E. A., "On the Second Order Transition of a Rubber," *J. Res. Nat. Bur. Stand.*, 68A, 1964, 611-617.

118 Schneider, Hans Adam, and DiMarzio, Edmund A., "The glass transition temperature of polymer blends," *Polymer*, 33, 1992, 3453-3461.

119 Fitzgerald, J. and Weiss, R. A., "Synthesis, Properties, and Structure of Sulfonate Ionomers," *J. Macromol. Sci., Macromol. Rev. Chem. Phys.*, C28, 1988, 99-185.

120 Tant, Martin R. and Wilkes, Garth L., "An Overview of the Viscous and Viscoelastic Behavior of Ionomers in Bulk and Solution," *J. Macromol. Sci., Macromol. Rev. Chem. Phys.*, C28, 1988, 1-63.

121 Lundberg, Robert D., "Ionic Polymers," Encyl. Polym. Sci. Eng., 2nd ed. (New York: John Wiley & Sons), Vol. 8, 1987, 393-423.

122 Pineri, Micheal and Eisenberg, Adi, eds. Structure and Properties of

Ionomers, (Boston: D. Reidel Publishing Company), 1986.

123 Holliday, L., ed. Ionic Polymers, (New York: John Wiley & Sons), 1975.

124 Douglas, Elliot P., Waddon, Alan J. and MacKnight, Wiliam J., "Viscoelastic and Morphological Study of Ionic Aggregates in Ionomers and Ionomer Blends," *Macromolecules*, 27, 1994, 4344.4352.

125 Von Hippel, A. ed. Dielectric Materials and Applications (New York: John Wiley & Sons), 1954.

126 Koberstein, J. T., Morra, B. and Stein, R. S., "The Determination of Diffuse-Boundary Thicknesses of Polymers by Small-Angle X-ray Scattering," *J. Appl. Cryst.*, 13, 1980, 34-45.

127 Feigin, L. A. and Svergun, D. I. Structure Analysis by Small-Angle X-Ray and Neutron Scattering (New York: Plenum Press), 1987.

128 Tyagi, D., McGrath, J. E. and Wilkes, G. L., "Small Angle X-ray Studies of Siloxane-urea Segmented Copolymers," *Polym. Eng. Sci.*, 26, 1986, 1371-1398.

129 Dai, Kevin H. and Kramer, Edward J.,"Determining the temperature-dependent Flory interaction parameter for strongly interacting immiscible polymers from block copolymer segregation measurements," *Polymer*, 35, 1994, 157-161.

130 Kramer, Edward J.,"Microscopic and Molecular Fundamentals of

Crazing," *Adv. Polym. Sci.*, 52/53, 1988, 1-56.

131 Kausch, H.-H. Polymer Fracture, 2nd. ed., (New York: Springer-Verlag), 1987, Chapter 5.

132 Molnar, A. and Eisenberg, A., "Compatibilization of Nylon 6 and Polystyrene through the Functionalization of Polystyrene," *Polym. Comm.*, 32, 1991, 370-373.

133 Bellinger, M., Sauer, J. A. and Hara, M., "Tensile Fracture Properties of Sulfonated Polystyrene Ionomers. 1. Effect of Ion Content," *Macromolecules*, 27, 1994, 1407-1412.

134 Hara, Masanori and Jar, Pean-Yue, "Deformation and Fracture of Ionomers under Simple Tension. 1. Sulfonated Polystyrene Film from THF Solution," *Macromolecules*, 21, 1988, 3187-3190.

135 DiMarzio, Edmund A., "Proper Accounting of Confirmations of a Polymer Near a Surface," *J. Chem. Phys.*, 42, 1965, 2101-2106.

136 Guiselin, O., "Irreversible Adsorption of a Concentrated Polymer Solution," *Europhysics Lett.*, 17, 1992, 225-230.

137 Aubouy, Miguel and Raphael, Elie., "Structure of an Irreversibly Adsorbed Polymer Layer Immersed in a Solution of Mobile Chains," *Macromolecules*, 24, 1994, 5182-5186.

138 Feller, William. An Introduction to Probability Theory and Its Applications, (New York: John Wiley & Sons, Inc.), 1957, Chapter 3.

139 DiMarzio, Edmund and McCrackin, Frank L.,"One Dimensional Model of Polymer Adsorption," *J. Chem. Phys,*, 43, 1965, 539-547.

140 Schull, K. R. and Kramer, E. J., " Mean-Field Theory of Polymer Interfaces in the Presence of Block Copolymers", *Macromolecules*, 23, 1990, 4769-4779.

141 Hseih, Dong-Tsai and Peiffer, Dennis G.,"Miscibility and immiscibility in functionalized associating polymer systems: polystyrene-poly(phenylene oxide) blends," *Polymer*, 33, 1992, 1210-1217.

142 de Gennes, Pierre-Gilles. Scaling Concepts in Polymer Physics,(Ithaca, NY: Cornell University Press), 1979, Chap. IV, IX.

143 Han, Charles C., et. al., "Temperature, composition and molecular-weight dependence of the binary interaction parameter of polystyrene/poly(vinyl methyl ether) blends," *Polymer*, 29, 1988, 2002.

144 Hoseman, R. and Bagchi, S. N. Direct Analysis of Diffraction by Matter, (New York: Interscience Publishers, Inc.), 1962.

145 Fernandez, A. M., Wignall, G. D., and Sperling, L. H. Multicomponent Polymer Materials, D. R. Paul and L. H. Sperling, eds. (Washington, D.C.: American Chemical Society), 1986.

146 Higgins, Julia S., and Stein, Richard S., "Recent Developments in Polymer Applications of Small-Angle Neutron, X-Ray and Light Scattering," *J. Appl. Cryst.*, 11, 1978, 346-375.

147 Alexander, Leroy E. X-Ray Diffraction Methods in Polymer Science, (Huntington, NY: Robert E. Kreiger Publishing Company), 1979, 296.

148 ten Brinke, Gerrit, Karasz, Frank E., and MacKnight, William J., " Phase Behavior in Copolymer Blends: Poly(2,6-dimethyl-1,4-phenylene oxide) and Halogen-Substituted Styrene Copolymers", *Macromolecules*, 16, 1983, 1827-1832.

149 Kambour, Roger P., Bendler, John T., and Bopp, Richard C., " Phase Behavior of Polystyrene, Poly(2,6-dimethyl-1,4-phenylene oxide), and Their Brominated Derivatives" *Macromolecules*, 16, 1983, 753-757.

150 Bauer, Barry J., "Equilibrium Phase Compositions of Heterogeneous Copolymers,"*Polym. Eng. Sci.*,25, 1985,1081-1087.

151 Nesarikar, A., Olvera de la Cruz, M., and Crist, B., "Phase Transitions in random copolymers," *J.Chem. Phys.*, 98, 1993, 7385-7397.

152 Fredrickson, Glenn H., and Liebler, Ludwik., "Nematic to Isotropic Transition in Chemically Disordered or Multicomponent Liquid-Crystalline Polymers," *Macromolecules*, 23, 1990, 531-539.

153 Bates, F. S., Wignall, G. D.,"Isotope-Induced Quantum-Phase Transitions

in the Liquid State," *Phys. Rev. Lett.*, 57, 1986, 1429-1432.